FABRICATION AND EXPERIMENTAL CHARACTERIZATION OF ECCENTRICALLY LAYERED SCATTERERS IN 2-D PHONONIC MATERIALS

by

DISNA PRIYADARSANI SAMARAKOON

B.S., University of Moratuwa, Sri Lanka, 2005

A THESIS

submitted in partial fulfillment of the requirements for the degree

MASTER OF SCIENCE

Department of Mechanical and Nuclear Engineering
College of Engineering

KANSAS STATE UNIVERSITY
Manhattan, Kansas

2010

Approved by:

Major Professor
Liang Wu Cai

Abstract

The study on artificially created materials has much evidence of naval properties. Phononic Crystals (PCs) are new class of artificially constructed materials. They have a large number of scattering inclusions that are embedded in a homogeneous host material. These scatterers are arranged in periodic lattice structures. The scatterers and host materials are usually either solids or fluids. Phononic materials are useful due to their ability to hinder the existence of certain frequencies over which the propagation of elastic and acoustic waves are forbidden. The formation of phononic band gaps (PBGs) in PCs is determined by the material properties and the geometry of the periodic lattice structures. Some PCs have full band gaps [14, 55] while others have partial band gaps [35]. Although the study of PCs is an attractive area for many researchers, the investigations on PCs are just emerging.

The aim of the thesis is to study on perform fabrication and experimental characterization of 2-D PCs having eccentrically layered scatterers. In addition, the influence of the eccentricity of the layered scatterers on the amplitude spectrums are experimentally observed. Hence, the main objective in this work is to characterize the influence of the eccentricity orientation angles on the transmitted amplitude spectra. The layered scatterers were created by inserting the paraffin-coated stainless steel rods into the cavities. Two sets of stainless steel rod diameters (2 *mm* and 2.5 *mm*) were used. The eccentricity orientation angles of scatterers were changed from 0 degree to 90 degrees at the increment of 22.5 degrees. Ultrasonic waves were introduced into the test pieces to observe the propagated waves through the material. The ultrasonic Through Transmission Test (TTT) followed by signal processing techniques was employed to produce the transmitted spectra of PCs. The frequency dependent amplitude spectrums were observed at the chosen frequency ranges with the help of MATLAB and Fast Fourier Transformation (FFT) function. The results show that the geometry and the material parameters change the attenuation of amplitudes by hindering the wave propagation. This leads PC as a good candidate for a sound barrier for controlling the wave propagation or vibrations within the chosen frequency ranges.

Keywords: Phononic Crystal/s (PC or PCs); Phononic Band Gap/s (PBG or PBGs); Through Transmission Test (TTT), Fast Fourier Transformation (FFT), Square array, Triangular array, Amplitude spectrum/ Spectra, Eccentrically layered scatterers

Table of Contents

List of Figures

List of Tables

Acknowledgements

Here I would like to thank everyone who supported me to make this thesis including my major advisor, Dr. Liang Wu Cai, and my supervisory committee Dr. Sameer I. Madanshetty , Dr. Jack Xin. for serving as one of my M.Sc. committee members. Thanks also go to Mr. Eric Wagner and Mr. Jeffrey Hicks for helping me to fabricate test pieces. I would like to thank my great friends in my office and MNE department who helped me in various ways whenever I needed their assistance. My deepest gratitude goes to my family for their encouragements and understanding. Finally a special thank goes to my husband for strengthening me to get through some difficulties in my studies and life.

CHAPTER 1 - Background of Phononic Materials

1.1 Introduction

Phononic Crystals (PCs) are new class of artificially constructed materials. They are created by embedding a large number of scatterers in homogeneous host materials having periodic lattice structures. The host materials are usually either solid or fluid. Phononic materials are able to prevent the propagation of acoustic or elastic waves at certain frequencies within the material. As a result, the study of PCs is an attractive area for many researchers over the last two decades. Band gaps in which the propagation of waves are forbidden at certain frequencies are called Phononic Band Gaps (PBGs). The creation of PBGs has much evidence of naval properties.

The formation of PBGs in PCs is determined by material properties and geometry of the periodic lattice structures. Some PCs have absolute or full band gaps [14, 55], while others have partial band gaps [35]. Band gaps are called absolute band gaps, if the wave propagation in any direction is restricted within the material. Materials with partial band gaps restrict the wave propagation only in certain directions. Some materials can be distinguished by their band structure related properties [40, 46]. Similarities exist in the electron waves in ordinary electronic crystals and the electromagnetic waves in photonic crystals. Likewise, similarities exist in elastic waves of both phononic and photonic materials. Band related properties of electronic, photonic, and phononic materials are shown in Table 1-1.

Table 1-1: Comparison of band related material properties [33, 40]

Property	Electronic crystal	Photonic crystal	Phononic crystal
Material	Crystalline solid	Consists of at least two dielectric materials	Constitute of at least two elastic materials
Parameter(s)	Atomic numbers	E/M permittivity, permeability	Mass density, sound speed
Lattice constant	1-5 °A (microscopic)	0.1 μm - 1 cm (macroscopic)	$\geq 0.1\ \mu m$ (macroscopic)
Wave type	Electrons	EM (photons)	Vibration or sound (phonons)
Polarization	Spin	Transverse	Shear, compression
Spectral region	Radio waves, Microwaves, Optical,	Microwaves, Optical	$\omega \leq 1$GHz

	X-rays		

According to Table 1-1, one can observe that the electromagnetic waves in photonic crystals possess only transverse displacements. In semi-conductor materials, the electrons occupy only certain energy gaps. Although the physical behaviors of phononic and photonic crystals are different, the origination of band gaps in both materials are similar. The band gaps in photonic crystals depend only on refractive index, which is the measure of speed of a substance with respect to light. Different refractive indices can be observed in photonic crystals as they composed of different dielectric materials. As a result, they are able to pass light waves only within a certain frequency range. Similarly, PCs are comprised of different refractive indices due to artificially embedded solid or fluid materials. In addition to different refractive indices, the PCs can have large mass density variations. They may also have different elastic or sub-elastic constants within periodically distributed structures. Consequently, PCs show a large velocity contrast and a strong combination of longitudinal and transverse waves. The sound waves in elastic solid support both longitudinal and transverse speeds. Conversely, acoustic waves in fluid propagate at a single longitudinal speed.

As a result of two wave speeds, the propagation and excitation of waves through solid PCs can change dramatically. These materials can control sound waves from low (audio) to high (THz) frequency ranges. Based on the frequency of operation, PCs are categorized into the following three classes [47, 52]: sonic (1 Hz – 20 kHz), ultrasonic (20 kHz – 1GHz), and hypersonic ($\geq$1GHz). In comparison with the photonic crystals, phononic crystals are difficult to model accurately. The multiple-scattering theories, which are originally applicable for the electronic structure, have been used to model phononic or photonic crystals [49, 2, 32, 40].

However, the investigations on PCs are just emerging. Further research is required for PC fundamentals that govern their behaviors as well as their potential applications. The main goal of this thesis is to study on 2-D eccentrically layered scatterers in homogeneous aluminum, Teflon, and LDPE hosts. The remainder of this chapter is organized as follows: The important possible applications of phononic materials are introduced in section 1.2. In section 1.3, the experimental and theoretical evidence of absolute and partial PBGs in 2-D PCs are reviewed briefly. Moreover, various theoretical methods to compute PBGs are also discussed in the same section. The goals of the thesis are explained further in section 1.4. Subsequently, thesis organization is presented in the last section of this chapter.

1.2 Applications

The important property of phononic materials is their ability to hinder the wave propagation at certain frequencies within the material. This feature is called acoustic or elastic band gaps depending on the medium where it is propagated. The elastic or acoustic band gaps make PCs potential candidates for developing new applications and materials. Since the major prospect of PCs is to control sound waves, they are useful in applications such as acoustic filters, improvements in noise control in the design of transducers, and signal processors [44]. Carefully designed PCs with accurately calculated band structures leads novel properties in the structure.

1.2.1 Sound and Vibration Management

The sound plays a vital role in the communication and information transfer systems. Also, the sound is important as a creative aspect to demonstrate music and rhythm. Audible range for a human's ear is from 20 Hz to 20 kHz. If PCs are constructed with appropriate lattice constants in the audible frequency range, they act as barriers for the sound transmission. Sculpture (refer to Figure 1-1), by Eusebio Sempere exhibited at the Juan March Foundation in Madrid is such an example for a sound barrier [42].

Figure 1-1: Sculpture, by Eusebio Sempere in Madrid [42]

After being motivated by the band structures in the sculpture [42], M. S. Kushwaha [37] carried out a computational work on infinite square arrays of rigid cylinders constructed in air. A stop band was uncovered in the frequency range between 200 Hz and 23 kHz. This computation

was based on the assumption that the rigid cylinders cannot penetrate sound waves and propagation of waves occur only through surrounding air.

The low frequency applications of phononic crystals are called sonic crystals. B. C. Gupta *et al.* [7] numerically computed multiple-scattering theories based on focusing effect of sonic crystals formed by arranging rigid cylinders in the air. The lattice parameters, filling fractions, acoustic frequencies, and the shapes of the sonic crystals considered as the variables in the computation. Later, 2-D sonic crystals were effectively investigated to use as acoustic barriers [52]. Hypersonic PCs are difficult to construct due to their small lattice parameters. The wave length in such materials is analogous to that of light. In 2005, T. Gorishny and coworkers [47] explained the application of hypersonic PCs to control the lattice vibrations at very high frequencies.

1.2.2 Wave Guides and Filters

Guiding and confining the acoustic waves have been studied theoretically and experimentally by several groups. Anything introduced into the band gap as a defect would change the generation of vibration, sound, or phonons. The elastic waves can either be localized or propagated along the point defect or linear defect within the band gap [1, 2, 31, 40, 4, 44, 54]. Khelif *et al.* [2, 4, 3] carried out an experimental and theoretical research on trapping and guiding acoustic waves across defect modes. In this investigation, 2-D phononic crystals were consisted of steel cylinders immersed in water. Linear defect modes were introduced into the wave guide by removing one or more steel cylinders from the structure. The elastic wave equation was computed and the results were compared with the experimental measurements. A full band gap of decreasing bandwidth was observed as the increased inter-cavity separation [4]. Following the marked success in their former work [2], the same research team investigated the guiding and bending of 2-D PCs experimentally and theoretically.

Pennec *et al.* [54] investigated the filtering and the multiplexing capabilities within the band gap of 2-D phononic crystals. The wave guides were made within the band gap by removing a chosen layer of cylinders. The lattice parameter of the 2-D square arrays was selected as 5 *mm* and the measurements were performed by varying the diameters of the hollow steel cylinders. The longitudinal and transverse velocities of the steel were taken as 5,825 *m*/*s* and 3,226 *m*/*s*. When the spectrum was examined by changing radii of cylinders in the air, a band gap

was observed in the frequency range 110 kHz - 215 kHz. Also, the presence of two narrow pass bands observed at the frequencies 161 kHz and 194 kHz [54] within the gap. In 2009, the filtering properties of PCs were investigated by J. Wang *et al.* [22].

1.2.3 Negative-Refraction

Negative-refraction occurs due to the multiple scattering at solid-air interface of PCs. Generally, the speed of the sound depends on the refractive indices of the respective media where the wave is traveled. When a sound wave incident onto a PC, two components of waves can be observed at solid-air interfaces. One component travels normal to the interface while the other travels parallel to the surface. The negative-refraction occurs in PCs, if the direction of the wave component parallel to the surface is reversed while the direction of normal component is unchanged. Ke *et al.* [39] observed the negative-refraction in 2-D phononic crystals consisted of triangular array stainless steel rods in water. In this study, focusing properties of a flat crystal was also investigated [39]. In 2008, Sukhovich *et al.* [6], experimentally demonstrated and L. Y. Wu *et al*. theoretically explored the existence of negative-refraction [29]. More recently (2010), C. Y. Huang and coworkers [11] fabricated Lamb wave resonators using 2-D PCs.

1.2.4 Thermal Tuning

Investigations on thermal tuning of ferroelectric ceramic-epoxy composite PCs in the ultrasonic range was carried out by K. L. Jim and coworkers [30]. This investigation was based on tuning the band structure of the composites made of Barium Strontium Titanate-epoxy around the Curie temperature. This led many applications such as non-destructive testing, medical diagnoses and imaging.

1.3 Evidence of Phononic Band Gaps (PBGs)

It is important and essential to recall appropriate studies on PCs to date in the literature. Numerous research efforts show that the complete or partial band gaps are mostly occur in 2-D or 3-D PCs. In 1993, Kushwaha *et al.* [2, 33] reported the first theoretical investigation on acoustic band structure in PCs. The computed band gaps for elastic composite structures were composed of parallel metallic rods arranged hexagonally in host elastic media. Elastic composite materials demonstrated to give rise for the formation of band gaps. Again in 1994, Kushwaha *et al.* [35] reported a theoretical computation of band structures for 2-D nickel alloy cylinders in

aluminum host. In this study, the band gaps were proved to be a function of filling fraction and material type. However, the computation was restricted only to freely vibrating elastic materials. When the filling fraction was approximately 0.33, the largest band gap were reported in nickel alloy cylinders in aluminum matrix. Similarly, the largest band gap for aluminum cylinders in nickel alloy matrix was reported at the filling fraction of 0.7854 [35]. Later, several theoretical investigations on the wave propagation through elastic PCs were reported by researches [59].

Goffaux *et al.* [10] proposed a different approach for the formation of tunable phononic band gaps. Square-section rods that arranged in a square array in air theoretically analyzed in this effort. Also, widening properties of band gaps were explored by means of Plane Wave (PW) method. The PW method is inappropriate for solid-fluid incorporated PCs. However, the difficulties related to low and high filling fractions overcome in this experiment [10]. A Similar investigation is reported by F. Wu *et al.* [15]. For this study, specimens were constructed by arranging square mercury (Hg) rods in water. The relationship between the bandwidth and the rotation angle was discovered by rotating the square rods at an angle. In 1996, Sigalas *et al.* [36] experimentally investigated acoustic wave propagations in 2-D PCs constituted of steel cylinders in air. Full band gaps were observed while increasing the diameters of the steel cylinders. Sound attenuation in 2-D simple structures of phononic materials is introduced in this experiment. After this remarkable effort, many researchers motivated to explore attenuation properties of PCs later [36].

Good representations for sound attenuation and phononic band gaps were experimentally reported by Sanchez Perez *et al.* [21] in 1998. In this work, 2-D square and triangular arrays of rigid cylinders were arranged in air with different lattice parameters. Experimentally-observed band gaps were fairly similar to theoretically predicted values for the square array. However, the effective band gap for the triangular array was not observed in the theoretically predicted frequency range in this experiment [21]. In the same year (1998), a group of researchers [14] reported full band gaps in aluminum alloy plates having 2-D cylindrical holes. No wave propagation was observed within a certain frequency range even if the measurement direction was changed [14].

Analytical and numerical approaches are being used by many researchers to determine the specific requirements in the designing of PCs. Among them, plane wave expansion method (PWE) [56], transfer matrix method (TMM) [13], finite difference time domain method (FDTD),

multiple scattering theories (MST) [52], and variation method (VM) [8] are the most popular techniques. In addition to these methods, FFT can be used to analyze the waves that have propagated through PCs. In 1998, the transmission of longitudinal waves across the single layer of lead (Pb) spheres embedded in a polyester matrix was experimentally studied by Kinra *et al.* [51]. In this experiment, the ultrasonic through transmission test was followed by spectrum analyzing with FFT algorithm. However, all of those methods have unique advantages and disadvantages.

PWE method has a problem of convergence for dispersion relations if a liquid material is inserted into host solid material. Also, the materials with large contrast in elastic modulus and density are difficult to analyze using the PWE method [8, 10, 29]. In 2007, Wen *et al.* [17] studied the directional propagation behavior of flexural waves through two dimensional thin plate PCs made of steel cylinders in square periodicity in host Lucite. The PWE method was employed to determine the wave propagation characteristics. Garcia Pablos *et al.* [12] reported the existence band gaps in square arrays of cylindrical holes filled with Hg, air, and oil in finite slab of aluminum hosts. At the ΓX and ΓM symmetry points, the directional band gaps, which existed along (100) and (110) directions, were computed by FDTD method [12]. Tanaka *et al.* [55] studied numerical examples to resolve the dispersion relations of the acoustic waves in 2-D phononic structure using FDTD method. The dispersion relationships were numerically computed for 2-D PCs arranged in an aluminum matrix. Contrasted to previous experiments [12, 14], which claimed full band gaps in some regions, no full band gaps were observed for Hg cylinders in an aluminum matrix [55].

The previously described investigations [12, 14, 55] on 2-D phononic materials consisted of Hg filled cylinders in the aluminum matrix were critically evaluated by Torres *et al.* [32]. Amplitudes of the signal were verified that they decay along (110) direction more than (100) direction. The FDTD was again employed by a group of researchers to discover the band gap in square arrays of air-filled polymer tubes arranged in water media [41]. The same test was implemented for water-filled polymer tubes in air. For the former test, the results were obtained by selecting the lattice parameter for square arrays less than the wave length of the band gap. The authors concluded that the sonic band gaps are dependent of air filling fraction, transverse velocity of the tube material, thickness of the tube, and longitudinal speed of the sound [41].

In 2001, Vasseur *et al.* [18] observed band gaps in the structures made of 2-D triangular arrays of steel cylinders in an epoxy matrix. Experimental evidences were theoretically verified that band gaps are independent of the waves propagated in the plane normal to the steel cylinders. FDTD and PWE methods were employed in determining the acoustic transmission coefficient. Transmission power spectrum was evaluated using ultrasonic through transmission followed by FFT. Authors reported that 2-D triangular arrays of parallel cylinders in a given matrix are expected to show the largest acoustic band gap. This test suggested a more quantitative analysis to compare the theoretical and experimental results with other samples and with different thicknesses, etc. [19].

In the following year (2002), Vasseur *et al.* [20] again comprehensively researched on 2-D square arrays of filled and hollow circular copper cylinders surrounded by air. The PWE and FDTD were employed to compute transmission coefficients. The FDTD helped them distinguish the filled and hollow cylindrical scatterers. At the lower frequencies, similar results were reported for the theoretically and experimentally measured transmission coefficients. The authors concluded that if copper cylinders were filled with water, the transmission coefficients are dependent on the thickness of the copper tubes [20]. Zhang *et al.* [45] investigated the existence of broad acoustic band gaps experimentally and theoretically. For this study, the 2-D PCs were created by embedding rubber-coated square arrays of solid steel cylinders in an epoxy matrix. The transmitted power spectrum was produced using real time FFT and FDTD methods. Despite the lack of evidence, they concluded that the forbidden gap became wider due to soft elastic coating [45]. Attenuation of sound in the audible frequency range is a tradeoff between the dimension of the sonic crystals and the direction of the wave propagation. Unlike the usual sonic crystals, Hirsekorn *et al.* performed numerical simulations to compute sound attenuation of silicone-rubber-coated hollow steel cylinders arranged in an epoxy matrix [38].

L. W. Cai in 2003 [25] numerically analyzed multiple-scattering (MS) in single multilayered scatterers. This novel method proposed new means to analyze scattering in more complicated internal geometries. In the same year, this study [25] was extended further to realize the existence of resonance at low frequencies. The resonance frequency was known to be influenced on the properties of band gaps in multilayered cylindrical scatterers embedded in linearly elastic medium [26]. In 2008, a team of researchers consisting of J. H. Wen and co-workers tried to determine band gap phenomenon and the attenuation properties in 2-D PCs. The

band gaps were reported to be manipulated by the density and elastic modulus of scatterers. Wide and low frequency band gaps were observed in light hosting materials with heavy scatterers [18]. A novel approach to research on eccentrically layered scatterers was carried out by L. W. Cai [28]. The effect of the eccentricity on single and multiple scattering of an incident anti-plane shear wave (SH) were numerically analyzed and influences of eccentric orientation on the scattered wave field were studied in this study. A simple explanation of these findings is that if the outer diameter of the cylindrical scatterer is the same as the wave length (λ) of the matrix material, then there will be a substantial influence of eccentricity on the propagation pattern of the scattered wave. Numerical computations for phononic crystal structures with a fixed band gap were again carried out by L. W. Cai. The author concluded that the relative strength of the signals is influenced by the effect of eccentricity in the layered scatterers [27].

1.4 Thesis Goals

Numerous numbers of research on phononic materials showed that band gap properties are largely decided by the material properties and the geometry of the phononic crystal structure. Many investigations appear on 2-D PC systems, as they need relatively large lattice parameters and simple fabrication techniques. Researchers identified that PCs have novel properties and applications. PCs consist of different shapes and sizes of scatterers such as air-filled, liquid-filled, or coated. These PCs then require novel fabrication methods. Some studies showed that due to the anisotropy and complex structural parameters in the layered scatterers, the wave propagation becomes complex in PCs. As a result, the theoretical principles are difficult to implement in practice. Hence, the appropriate experimental techniques need to be developed to characterize the influence of eccentricity on the elastic or acoustic wave propagation patterns. Such experimental studies then allow understanding the effect of the internal features of the scatterers. However, a considerable experimental study has not been carried out so far to determine the existence of band gaps in such PCs.

In contrast to those numerous investigations reported in section 1.2 and 1.3, the primary goal of this research is to perform fabrication and experimental characterization of 2-D PCs having eccentrically layered scatterers. Low density polyethylene (LDPE), aluminum and Teflon are the chosen three host materials. Square and triangular array cylindrical cavities were drilled in three solid host materials in advance. Hence, 2-D PCs are arranged by inserting cylindrical

stainless steel rods at different orientations of eccentricities. Scatterer orientation angles are changed by inserting the paraffin-coated stainless steel rods into the cavities. Two sets of stainless steel rod diameters (2 *mm* and 2.5 *mm*) were used in the experiments. The main objective in this work is to characterize the influence of the eccentricity orientation angles on the transmitted amplitude spectra. The frequency dependent amplitude spectrums are anticipated to observe at the chosen frequency ranges. The amplitude spectrums are produced using the ultrasonic Through Transmission Test (TTT). Signal processing is carried out using Fast Fourier Transformation (FFT) function with the help of MATLAB.

1.5 Thesis Organization

This thesis presents a study on fabrication and experimental characterization of eccentrically layered scatterers in PCs. It is organized into four chapters. Chapter 1 introduced the background of PCs and the goals of the thesis. Chapter 2 establishes the experimental methodologies and limitations for experimental investigation of PCs. The fabrication procedures of PCs with eccentrically layered scatterers in different hosts are explained in Chapter 3. In addition, the importance of the intended experiment, the experimental setup, and the measures taken in the experiments present in Chapter 3. Chapter 4 of the thesis presents the results obtained from the experiments in the time and frequency domains. Conclusions are summed up at the end of the Chapter 4. On the basis of the results, the possible future research works are also discussed under the conclusions.

CHAPTER 2 - Methodology

2.1 Introduction

This chapter explains the concept of wave propagation and different mechanisms, which cause the formation of band gaps in phononic materials. The methodologies and the design criteria involved in the experimental study of such materials are also discussed in this chapter. Moreover, a discussion on important factors that govern the width, location, and shape of the band gaps in phononic materials are explained using simple theories of Bragg reflections. The fundamental concepts of elastic, acoustic, and ultrasonic wave propagation in materials are also highlighted. Finally, the concept of frequency response of the spectrum analysis techniques is presented.

2.2 Design of Phononic Band Gap Materials

According to the literature, Bragg scattering, and local resonators [8, 11, 13, 31, 32, 38, 53, 56] are the two mechanisms for the formation of phononic band gaps (PBGs). Bragg's theory says that the superposition of reflected waves takes place in materials having large acoustic mismatches. The local resonators are useful in the case of sonic applications, as they have strong attenuation at their resonant frequencies. The experimental results of the locally resonant sonic materials proved to have strong attenuation at lower wave lengths than those predicted by the Bragg's theory [38, 57].

2.2.1 Bragg-Scattered PBGs

Bragg-scattering occurs due to the interaction of periodically arranged lattice structures in materials. In periodically arranged solids, the individual atoms cannot move freely as they interconnected with chemical bonds. When the forces are applied, atoms move from their equilibrium positions. Then, the atoms exert forces on the neighboring atoms, which cause adjacent atoms to move through the material. Lattice distortions propagated through the solid materials are referred as phonons. At very high frequencies, phonons show strong interactions. Generally, the resultant wave forms become very complex as they involve a large number of parameters [40, 18]. Consider a 1-D crystal made out of several alternating layers of dissimilar substances. When a sound wave travels through such a crystal, at every interface, a portion of the

incident wave reflect back and a part of the original wave transmit through the crystal. As a result, these secondary portions of the incoming waves may interact with each other. Constructive interference occurs if the path difference between two interfering waves are equal to an integer multiple of their wave lengths. Otherwise, destructive interference wherein the propagation of waves through the material can be observed [40]. If there are a number of interfaces and if constructive interferences occur within the material, then reflection of all the energies of the original wave take place. Subsequently, the wave cannot propagate across the material. Hence, band gaps are created in the case of constructive interferences. The path difference between two interfering waves is determined by the lattice parameter (a) and the wave length (λ) of the material. The wave length of sound is inversely proportional to the frequency;

$$\lambda = \frac{C}{f} \tag{1}$$

where C is the sound velocity and f is the frequency. Interferences occur when,

$$a \approx \lambda . \tag{2}$$

According to Bragg's theory, the relationship of the center frequency of the band gap to the center distance between two adjacent scatterers (a), and the longitudinal sound velocity (v) of the host material can be written as,

$$f = n . \frac{v}{2a} \quad (n = 1, 2, \ldots). \tag{3}$$

Eqn. (1), (2), and (3) show that the center frequency of the band gap is inversely proportional to the lattice parameter [13, 20, 38, 40]. This gives an exciting idea that a band gap [49, 45] can be created at any frequency or at any wave length by changing the lattice parameter of a solid. Thus, the geometry and the dimensions of the materials are influenced on the formation of phononic band gaps within which propagation of waves are restricted.

2.2.2 Local Resonators

Sound attenuation bands in the audible frequency range can only be achieved using large structures. Under a certain frequency range, scatterers in PCs will act as resonators. These local resonators can bring the attenuation frequencies into the audible range. They react with elastic travelling waves that have large wave lengths. This behavior lead the restriction of wave propagation at certain frequencies [9, 18]. M. Hirsekorn *et al.* [38] analyzed PCs with local

resonators made of silicone rubber-coated steel cylinders in the matrix of epoxy. Attenuation obtained at very low frequency range from 0.3 kHz to 6 kHz. This yielded a strong attenuation at low frequencies than those predicted by Bragg-scattering. Recently, the Bragg reflection and local resonator methods were extensively studied by D. Yu *et al.* [13]. Both methods applied effectively to control the vibration of the fluid carrying pipe system arranged in regular lattice pattern.

2.2.3 Effect of Geometry and Material Parameters

Investigations on PCs having various scattering inclusions and host materials are being carried out by many researchers. Generally, Bragg-scattering relates to material properties such as density, Young's Modules, stiffness and structural parameters such as filling ratio, lattice parameter, and geometry [18]. The formation of PBGs in PCs is determined by the material properties and the geometry of the periodic lattice structures [14, 55]. It is assumed that no band gaps are formed in homogeneous elastic media. On the contrary, the band gaps appear in inhomogeneous structures when the density and the sound velocity are adjusted [10]. The larger the variations between material parameters, the easier the band gap formation. Therefore, understanding the influences of material properties and geometry on the formation of band gaps is essential. Simply, the wave propagation mechanisms in both solid and liquid materials are then easy to realize.

The mechanical waves are of two types: acoustic and elastic. Typically, elastic waves propagate in elastic solids. Acoustic waves are sort of oscillations travel through a liquid or a gas. Seismic waves are a type of elastic waves that occur as a result of an earthquake. When a sound wave propagates in a solid, they can have longitudinal (P or compression waves), transverse (S or shear waves), and surface (Rayleigh) components of displacements. A longitudinal wave is characterized by the particle motion in the same direction as the wave propagation. Transverse waves cause the particle motion perpendicular to the direction of wave propagation. Rayleigh waves move in an elliptical path as shown in Figure 2.1. In fluids, acoustic pressure waves are longitudinal.

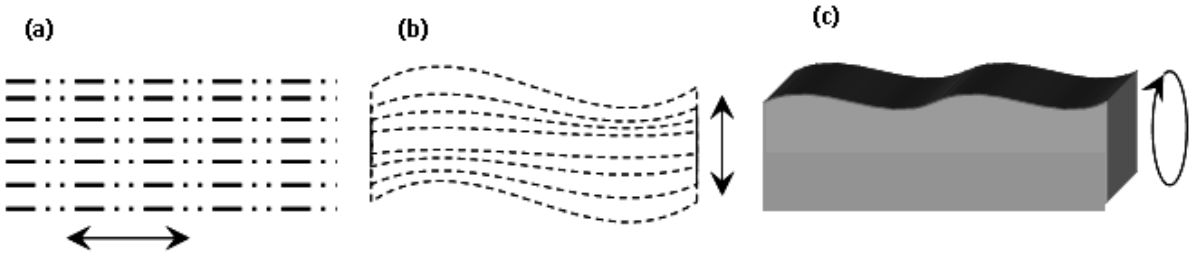

Figure 2-1: Types of mechanical waves (a) P, (b) S and (c) Rayleigh

Three conditions: mass continuity, equation of state, and force equation are essential to derive wave equation for acoustic waves. Elastic wave equation for a homogeneous medium can be written as [18, 40],

$$\mu\left(\frac{\partial^2 u}{\partial x^2}+\frac{\partial^2 u}{\partial y^2}\right)+(\lambda+\mu)\frac{\partial}{\partial x}\left(\frac{\partial u}{\partial x}+\frac{\partial v}{\partial y}\right)=\rho\frac{\partial^2 u}{\partial t^2} \tag{4}$$

$$\mu\left(\frac{\partial^2 v}{\partial x^2}+\frac{\partial^2 v}{\partial y^2}\right)+(\lambda+\mu)\frac{\partial}{\partial y}\left(\frac{\partial u}{\partial x}+\frac{\partial v}{\partial y}\right)=\rho\frac{\partial^2 v}{\partial t^2} \tag{5}$$

where u and v are displacement along x and y directions respectively, λ and μ are called Lame's constants, and ρ is the density of the material. They are given in equation (6). It must be noted that the material properties of E is the elastic modulus and that of υ is the Poison's ratio. They are given by,

$$\mu=G=\frac{E}{2(1+\upsilon)} \quad and \quad \lambda=\frac{\upsilon E}{(1+\upsilon)(1-2\upsilon)} \tag{6}$$

Generally, the classical wave equation [18, 20, 40] is given as follows:

$$\frac{\partial^2 u}{\partial x^2}=\frac{\rho}{E}\frac{\partial^2 u}{\partial t^2}. \tag{7}$$

The incident of a plane wave into the elastic solids can be expected to propagate in two wave speeds, which associate with displacement components and potentials. When the displacement component is as the same direction as the wave propagation, they are called longitudinal waves. The speed of the longitudinal wave C_P is given by [32, 53],

$$C_P=\sqrt{\frac{\lambda+\mu}{\rho}}. \tag{8}$$

On the contrary, if the displacement component is perpendicular to the direction of wave propagation, they are called shear waves. The speed of the shear C_S is given by,

$$C_S = \sqrt{\frac{\mu}{\rho}}. \tag{9}$$

Hence, the wave speed ratio *k* can be defined as follows,

$$k = \frac{C_P}{C_S} = \sqrt{\frac{\lambda + 2\mu}{\mu}} = \sqrt{\frac{2(1-\upsilon)}{1-2\upsilon}}. \tag{10}$$

The study of the elastic wave propagation in inhomogeneous media is challenging due to the combine influence of longitudinal and transverse wave forms [10]. At a given frequency, the speed of the longitudinal waves is greater than that of the shear waves. For a particular material, the speed of the wave is changed only when the medium where it propagates is altered. When the sound energy travels through a material, the propagation relates to the elastic properties and the wave properties. When waves encounter a boundary or an interface with another material, a portion of the energies reflects back and the other portion transmits through the material. Acoustic impedance is a material property, which defined as the density multiplied by the sound speed.

The amount of energy reflected (reflection coefficient) is related to the relative acoustic impedance of the two materials. When a sound wave incidences on an interface between two materials of different acoustic impedances, the direction of the wave propagation may change. Consider an incident of a P-wave at an interface. When the angle of the incident longitudinal wave is altered, a portion of the sound energy converts to shear wave (refer to Figure 2-2).

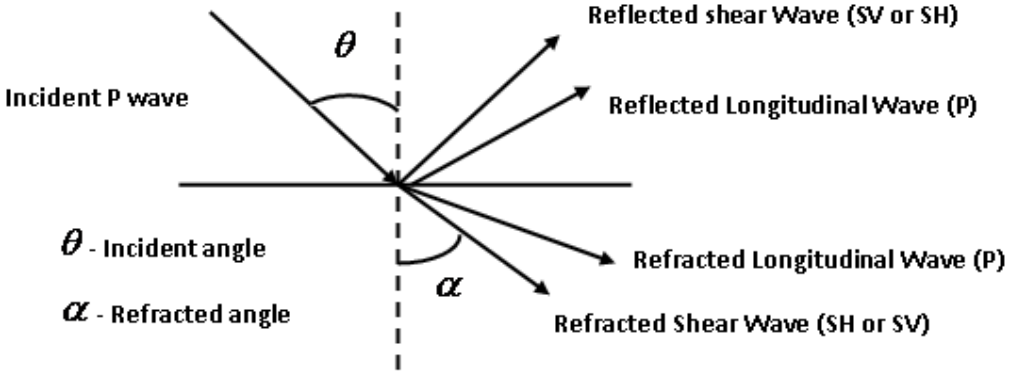

Figure 2-2: Different wave patterns observed at an interface

The various boundaries can be observed in materials with periodic structures. As a result, scattering of the original wave (due to reflection) occur at the interfaces. In a rigid scatterer, there is no displacement at the interface. In void scatterers, the shear stresses in the longitudinal

direction of the cylindrical scatterers are zero at the interface. Elastic scatterers can be obtained in elastic solids with refracted waves. Layered elastic scatterers are the subjects of this thesis. Depending on the type of materials and scatterers, the speed of the sound causes differences in the band gap configurations. The studies have also shown that the scattering process will be influenced by the changes in the geometrical parameters: the eccentric orientation angle and the inner radius of the scatterers [27].

The path differences change as the direction of propagation is varied at the interfaces. Depending on the frequency of their operation, it is necessary to maintain the lattice parameter of the structure in the order of wave length of the incident wave (see Equation 3). In 2001 and 2002, Vasseur *et al.* [22, 6] studied experimentally and theoretically on the sound attenuation in two types of sonic crystals. One structure was made by stainless steel cylinders in air, and the other was made by copper tubes in the air. It was found that the attenuation is same in both hollow and filled copper cylinders as the wave length λ is much greater than the diameters of each cylindrical scatterer [22, 6].

By integrating materials with large acoustic impendence differences, the width of the band gap can be increased while the reflectivity at the interfaces is drastically adjusted [18, 38]. If the wave length is too small compared to grain size, the energy losses occur due to reflections at boundaries. These losses increase linearly with the frequency. If the wave length is greater than grain size, then the energy losses occur due to the occurrence of surface waves [10]. The frequency of the band gap continues to reduce if the lattice parameter of the structure is decreasing. The PCs need large dimensions if the band gaps are needed to produce at very low frequencies. Therefore, the formation of band gaps with the Bragg scattering mechanism becomes difficult at low frequencies [18].

The width of the band gap relates to the ratio of the densities and velocities of different materials. If the ratio of the velocities is increased, the band gap becomes broad and so does the ratio of densities [55]. PCs are usually constructed by integrating solid or fluid materials. Sonic and hypersonic crystals are special types of PCs prepared by solid elastic materials in air [56]. Moreover, the band gap properties can be altered by varying the filling fraction and by embedding foreign materials with different elastic constants and mass densities [18, 31, 46, 35, 40]. Briefly, one can assume that the PCs are being composed of scatterers (liquid or solid) assembled in a regular periodic pattern. The PCs can be seen as 1-D, 2-D, and 3-D. If the

periodicity is only along one direction, it is called 1-D PC. 2-D PCs have periodicity in two directions and they are generally arranged by embedding solid or fluid cylindrical scatterers in various host materials. The 3-D PCs have periodicity along all three directions. The sspherical inclusions embedded in a matrix are an example for 3-D PCs.

On the other hand, PCs show macroscopic scale periodicity, which is very similar to the crystalline structure of solids. In crystallography, the crystalline solids are arranged at the Bravais lattice points. Many researches assumed that the wave propagation in inhomogeneous solid-solid structures limited to the XY-plane normal to the circular cylinders that are arranged parallel to *Z*-direction [20]. They are usually parallel circular cylinders along *Z*-axis that are arranged in the *XY*-plane in the host material. These cylindrical inclusions act as scatterers and their orientation in the 2-D structure analogues to lattice structure in the crystallography. They can be treated as the Bravais lattice points. Most of the 2-D PCs reported in the literature have a square or a triangular periodicity. If the lattice constant of the square arrays along the side of the crystal is *a*, then the lattice constant along its diagonal direction (triangular arrays) is $\sqrt{2}a$ (see Figure 2-3).

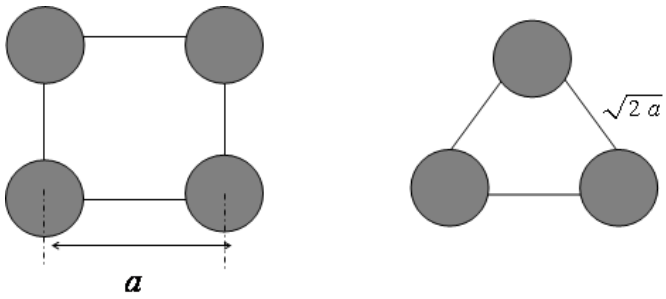

Figure 2-3: Square and triangular Bravais lattice points.

The band gaps are expected to observe in the square and triangular lattices at the frequencies proportional to $1/a$ and $0.707/a$ respectively. Band gaps are formed due to the reflections at the surface of dense scatterers. If the gaps are sufficiently wide enough, they are able to superimpose each other. This happens at various directions in the periodic structure. As a result, periodic structures will show reflections for any incoming waves at some frequency ranges in which all the band gaps overlap [19, 49]. This makes full or partial band gaps in PCs. Experiments in this thesis deal with 2-D structures having solid-solid inhomogeneous structures as shown in Figure 2-4.

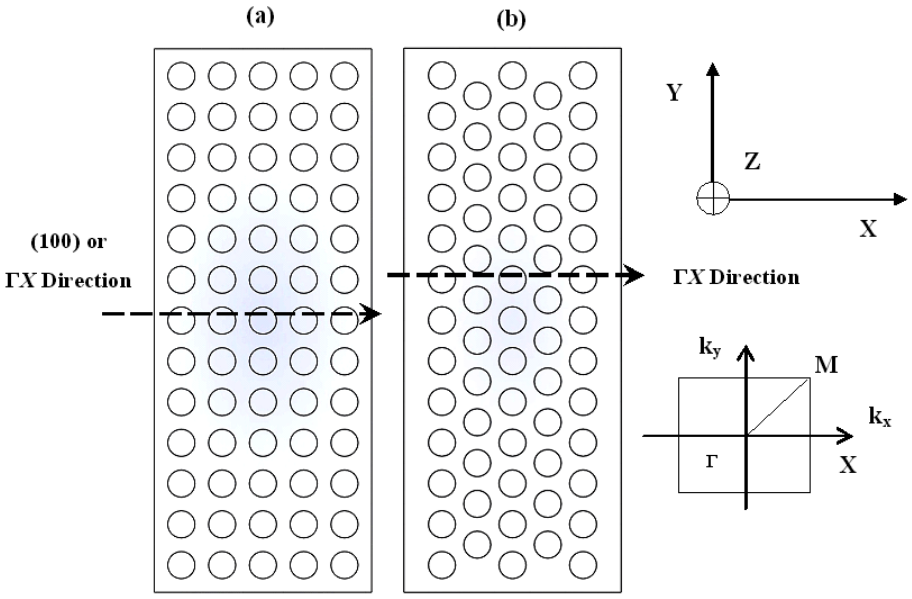

Figure 2-4: 2-D cross section of the scatterers embedded in hosts parallel to *Z*-direction in the *XY*-plane (*a*) 65 scatterers in square array (*b*) 63 scatters in triangular array. K_X and K_Y are 2D wave vectors in the XYZ coordinates system [19, 49, 50, 45, 18, 40].

2.3 Testing of Phononic Materials

Various techniques exist to experimentally investigate phonons in periodic structures. Brillouin Light Scattering (BLS) and ultrasonic Through Transmission Test (TTT) are popular methods for testing such structures. Since the lattice parameter and the wave length of the hypersonic crystals are in nano-scale, experimental observation of their properties is challenging. The BLS is a powerful non-destructive testing tool for detecting the properties of periodic composite structures that operate at high frequencies (GHz range). The BLS is also useful for detecting the dispersion relations of hypersonic PCs at high frequencies [48]. Phononic band gaps are undetectable if the band gap frequencies are well below the maximum detection limit of BLS.

On the contrary, in TTT, the ultrasonic waves are operable at high frequencies than the audible range. Furthermore, the practical use of ultrasonic frequencies for the assessment of materials is between 50 kHz and 10 MHz [55]. This method is a type of non-destructive test and it is often performed in examination of material properties. The ultrasonic transmission technique is capable of producing the transmitted spectra with either pulses or continuous waves [4, 19, 51]. Therefore, the ultrasonic TTT can be used to evaluate the attenuation and to assess the

frequency response of a transmitted wave passing through a material. Materials in which the lattice parameters are in the millimeter range, can be tested very effectively using ultrasonic waves. The intended dimensions of the PCs in this experiment are in millimeter scale, which is comparable with the frequency of the ultrasonic range. Therefore, in this experiment PCs can be tested by the ultrasonic TTT.

2.3.1 Ultrasonic TTT

An ultrasonic TTT system essentially includes a pulse generator, a transmitting transducer, a receiving transducer, and a data acquisition system in which a means for recording the signals enclosed. It involves sending an ultrasonic wave from an external surface into the material and receives the wave from its opposing surface of the material as shown in Figure 2-5.

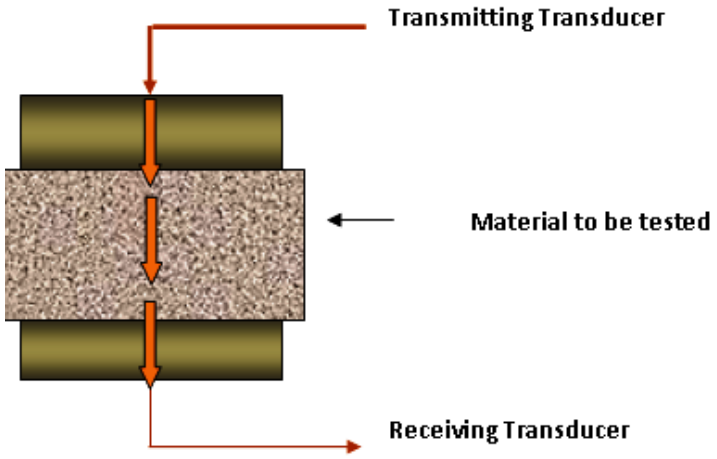

Figure 2-5: Schematic of Transmitting and Receiving Transducers

In the through transmission method, the primary quantity to be measured is the amplitude [10]. In such a test, the amplitude of the waves decreases as the ultrasonic waves pass through a given thickness of the material. The wave propagation involves with the disturbances in the medium. When the amplitudes of the received and transmitted signals are recorded, the attenuation can be obtained through signal analysis [5]. If A_1 and A_2 are the amplitudes of the transmitted and received signal respectively, the relative amplitudes of two ultrasound waves can be expressed as,

$$\text{Relative amplitude} = \frac{A_2}{A_1}. \tag{11}$$

When the relative amplitudes are expressed in terms of the logarithm of amplitude ratio, they are specified in units of decibels (*dB*). The relative pulse amplitude in decibels is related to the actual amplitude ratio by:

$$\text{Relative amplitude}\left(dB\right) = 20\,Log\frac{A_2}{A_1}. \tag{12}$$

The ultrasonic sound velocity: *C* can also be evaluated using [16],

$$C = \frac{\text{Distance between transducers}}{\text{Time it takes to travel that distance}}. \tag{13}$$

Ultrasonic waves propagate due to the transfer of mechanical disturbances across the material. Hence, the type of medium is influenced by the speed of the wave propagation.

2.3.2 Transducer Sound Fields

Many types of transducers use for ultrasonic testing such as as direct contact, angle beam, immersion, delay line, and dual element. These transducers are differentiated by the way they interact and generate ultrasonic waves into the specimens. A piezoelectric transducer can convert the electrical energy into the mechanical energy and also the mechanical energy into the electrical energy. As a result, a piezoelectric transducer can receive or transmit sound energy.

Among the various types of transducers, there are two main types of transducers : straight and angle beam. The straight beam contact transducers introduce sound energy perpendicular to the surface where it contacts. Due to the direct contact with the material, these transducers have been constructed in a wear resistant case. Direct contact transducers have advantages such as close acoustic impedance matching to most materials, testing of wide variety of materials, and preferring penetration through thick materials. The angle beam transducers utilize shear or longitudinal waves depending on the angle of contact.

Based on the way the particles oscillate, ultrasonic waves can propagate in solids in four principle modes: longitudinal, shear, surface, and plate waves. The longitudinal and shear waves are two principle propagations modes widely use in ultrasonic testing. The ultrasound that is generated by transducers propagates into a solid through the transfer of energy from one particle to another. At a given frequency and energy level, the distance that the sound wave propagates depends largely on the nature of the materials. In general, the materials that are hard and homogeneous will transmit sound waves more efficiently than those that are soft and

heterogeneous. The shape of the transmitted sound field is greatly affected by the transducer element diameter. Both reflection behavior and the shape of the sound fields are influenced by the transducer center frequency. At the megahertz frequency range, the sound energy does not travel efficiently through air or other gasses, but it travels freely through most liquids and common engineering materials. Two factors govern the distance that a sound wave travels in any given medium: **beam spreading** and **attenuation**.

2.3.2.1 Beam Spreading

The acoustic field of a transducer consists of all the frequencies within the bandwidth. The sound produced from an ultrasonic transducer originates from many points along the surface of the piezoelectric element. Figure 2-6 shows a typical transducer sound fields. Many waves interacting or interfering with each other in a sound field. This is called near field effect.

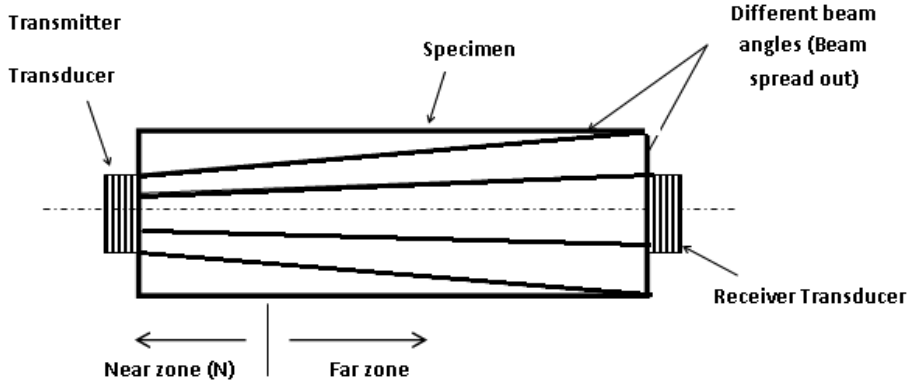

Figure 2-6: Schematic of a transducer wave fields

For a transducer of diameter D, and the wave length λ, the near field length N is given by:

$$N = \frac{D^2}{4\lambda} \tag{14}$$

If materials to be tested are positioned within the near field area, then accurate evaluation of flaws becomes exceptionally difficult. Despite such variations, the maximum sensitivity can be obtained in the near field region. Within the near field, the beam narrows and the overall beam size remains relatively constant. Therefore, the near field is important when testing very thin materials. APPENDIX A Table 2.2 shows how the near field length varied with the element diameter and the frequency of a transducer.

The area beyond the near zone in which the ultrasonic beam becomes more wide and uniform is called far field. The intensity that refers to the relative strength of a sound beam at a

certain point is low in the far field. The greatest concentration of the sound energies are at the center of the beam. The energy decreases as it moves away from the centre. Therefore, at the beginning of the far field, the beam strength is the greatest at the center of the beam. When the beam travels further, the edges get wider. Also, the strength of the beam becomes weak as it spreads outward. This situation is called beam spread. The conversion between the near field and the far field is sometime referred as the natural focus of a flat contact (or unfocused) transducer. For a flat faced transducer, the beam spread angle may be calculated approximately using the transducer diameter (D), wave length (λ) in the medium [48].

$$Spread\ angle, \theta = 2\sin^{-1}\left(0.5\frac{\lambda}{D}\right) \tag{15}$$

Because of the less concentrated sound fields in the beam spread, the lower amplitudes of the reflected waves can be observed. Due to the reflections from the other features outside of the inspection area, beam spread make trouble understanding signals [48]. The beam spread increases at the lower frequencies. It also increases with the smaller diameters of transducers. This can be clearly seen in the beam spread table in APPENDIX A.

2.3.2.2 Ultrasonic Attenuation

When the ultrasonic sound waves travel through a material, they begin to break due to the imperfections in the structure. Then, the organized phonons become random mechanical vibrations such as heat until the wave front is no longer detectable. Further weakening of the wave fronts is due to the phonons' interaction with each other. This is called scattering and absorption [43]. At this stage, the materials show band gaps at certain frequencies or at certain wave lengths. The scattering effect is varied when waves meet at different boundaries or at imperfections. The absorption is the conversion of sound energy into other forms of energy. Both scattering and absorption can increase as the frequency increases. The combined effect of scattering and absorption is called attenuation. Therefore, the attenuation always associates with the energy loss (amplitude) or gain. The attenuation coefficient is specific for a given material [5, 16],

$$A = A_0 \exp\left(-\alpha x\right) \tag{16}$$

where x is the distance travelled, α is the attenuation coefficient and A_0 is the amplitude when x=0. Considering x_1 and x_2 values,

$$\alpha = \frac{1}{(x_1 - x_2)} \ln\left(\frac{A_1}{A_2}\right) \tag{17}$$

2.3.2.3 Wave Length

The distance of sound has traveled during the period of one vibration is known as the wavelength. The sound wave length is inversely proportional to its frequency as given in equation (1). The wavelength of the ultrasound is determined by the characteristics of both the transducer (frequency) and the material through which the sound is passing (velocity). The longitudinal velocity is independent of sample geometry when the dimensions at right angles to the beam are large compared to the beam area and wavelength.

2.3.2.4 Frequency

The frequency of a transducer affects the penetration and flaw resolution. As the frequency increases, the distance that the sound wave travels will decrease through a material. However, the resolution of small discontinuities will improve. On the contrary, if the frequency decreases, the penetration of the sound wave will increase. In addition, high sound energy in the penetrated waves would result. The higher frequencies will be attenuated more rapidly than the lower frequencies in the medium. Hence, low test frequencies are usually employed in materials such as low density plastics and rubber where high attenuation coefficients are involved. When the frequency is too high, the sound waves will scatter at coarse grains. Therefore, a low frequency transducer is suitable for a material with large grains whereas fine grain structure needs a high frequency transducer. High frequency transducers usually have a constant diameter beam while the low frequency transducer has a diverged beam.

In summary, as the frequency goes up, the beam spreading decreases but the effects of attenuation and scattering are enhanced comparatively. This also means that the amount of energy provided to the transmitter transducer will be less than the energy travelled toward the receiver transducer. To optimize these variables, the appropriate transducer frequencies should be chosen depending on the application.

2.3.2.5 Element Size

In flat faced contact transducers, element size indicates the covering area or width of a material that can be inspected. Larger diameters of the transducer may decrease the inspection

time by increasing the coverage area while reducing the reflections at small discontinuities. In low frequency transducers, a very small element diameter will cause excessive beam divergence. Smaller element sizes will increase reflection amplitude from small discontinuities. The inspection may take a longer time as a smaller beam covers less area. A large diameter transducer has a small beam spread compared to the small diameter transducer. In high frequency transducers, these conflicting factors must be balanced based on the specific test requirements. For instance, if a large diameter transducer is used ,the beam divergence is low and a relatively constant diameter of the sound beam to cover large area can be obtained. It can be inferred that the long sound paths can be improved using a large diameter transducer with high frequency. Additionally, when the distance in which the sound path travelled is larger than the near field distance, the beam diameter will increase.

2.3.2.6 Bandwidth

Bandwidth is the range of frequencies to which a transducer can respond. A range of frequencies was decided to be used in the experiments. Bandwidth is determined using,

$$BW = \frac{f_u - f_l}{f_c}. \tag{18}$$

Where f_c is the center frequency, f_l is the lower frequency, f_u is the upper frequency, and BW is the band width of the transducer. By increasing the bandwidth of a transducer, penetration can be increased without sacrificing the resolution. When a transducer highly damped, it will respond above and below the central frequency. In converse, it responds poorly around central frequency if the transducer lightly damped. However lightly damped transducers increase penetration power through the material [2].

2.4 Data Processing Techniques

In an experimental setup of the ultrasonic TTT, a received signal is obtained in the receiver transducer. Usually, those signals are viewed in the oscilloscope in the time domain. In practice, a spectrum is always made over a finite time length (T_s). The time period may include the full length of a signal or it may compose of small region of a signal. When the time domain data converted into a frequency domain, it represents the available energy of the signal. There are many advantages of the frequency domain signals. It helps realizing the quality and usefulness of the signal. A plot of frequency against the amplitude is called a spectrum.

Conversion of time domain data into frequency domain is accomplished by means of techniques such as Fourier transformation (FT), Discrete Fourier transformation (DFT) and Fast Fourier transformation (FFT). They are capable of identifying various frequencies and characterize the magnitude of a wave. FFT is capable of producing frequency domain signals efficiently.

2.4.1 Fourier Transformation (FT)

Fourier transformation (FT) is a theoretical transformation of a continuous wave and the transformed signal will always reveal the frequency content of the signal.

$$f_{(t)} = a_0 + \sum_{n=1}^{N} a_n \sin(n\omega t) + \sum_{n=1}^{N} b_n \cos(n\omega t) \tag{19}$$

where, constant a_0 is the direct current offset in the *y*-axis. The coefficients a_n and b_n are the constituents of the spectral amplitudes. These constituents are the magnitude of the spectrum that are written as,

$$a_0 = \frac{1}{T}\int_0^T f(t)\,dt \tag{20}$$

$$a_n = \frac{2}{T}\int_0^T f(t)\sin(n\omega t)\,dt \tag{21}$$

$$b_n = \frac{2}{T}\int_0^T f(t)\cos(n\omega t)\,dt \tag{22}$$

Depending on the resolution of the chosen wave, these coefficients are varied. Resolution is the smallest frequency *f(t)* taken out from the frequency spectrum. If the resolution changes, the signal energy is different from one frequency to another by,

$$f_n(t) = n\, f(t) = n\frac{1}{T}\ . \tag{23}$$

where *n* is the number of points used in the summation. The fundamental frequency, ω can be written as,

$$\omega = 2\pi\, f_n = 2\pi n\frac{1}{T}. \tag{24}$$

Some received signals from signal generators are complicated. In Fourier transformation these complex received signals treated as a summation periodic wave of sine and cosine waves. The Fourier transformation can be represented as

$$f(t) = \sum_{n=-\infty}^{\infty} C_n e^{jn\omega t}, \tag{25}$$

where, coefficient C_n relates to the trigonometric coefficients and j is a complex number. These coefficients can be illustrated by

$$C_n = \frac{1}{2T}\int_{-T}^{T} f(t)e^{-jn\omega t}dt \tag{26}$$

$$C_n = A_n + jB_n \tag{27}$$

$$A_n = \frac{1}{T}\int_{0}^{T} f(t)e^{jn\omega t}dt = \frac{1}{2}(a_n - jb_n) \quad and \quad |A_n| = \frac{1}{\sqrt{2}}\sqrt{a_n^2 + b_n^2} \tag{28}$$

$$B_n = \frac{1}{T}\int_{0}^{T} f(t)e^{-jn\omega t}dt = \frac{1}{2}(a_n + jb_n) \quad and \quad |B_n| = \frac{1}{\sqrt{2}}\sqrt{a_n^2 + b_n^2}\ . \tag{29}$$

A_n and B_n are of exponential form, which represent positive and negative frequencies. Therefore, the magnitude of C_n is the half of the signal amplitude,

$$C_n = \sqrt{A_n^2 + B_n^2} \quad and \quad |C_n| = \frac{1}{2}\sqrt{a_n^2 + b_n^2} \tag{30}$$

Frequency domain data show the amplitude of the time domain signal. Frequency domain of each signal has a fundamental component.

Two sinusoids in their time and frequency domains are illustrated in Figure 2-7. The time domain signal shows how long the sound is (100 seconds) and how the amplitude varies over the time. However, it is useful to know how each frequency component of the sound contributes to the overall amplitude. Therefore, the frequency domain data are also plotted against each amplitude.

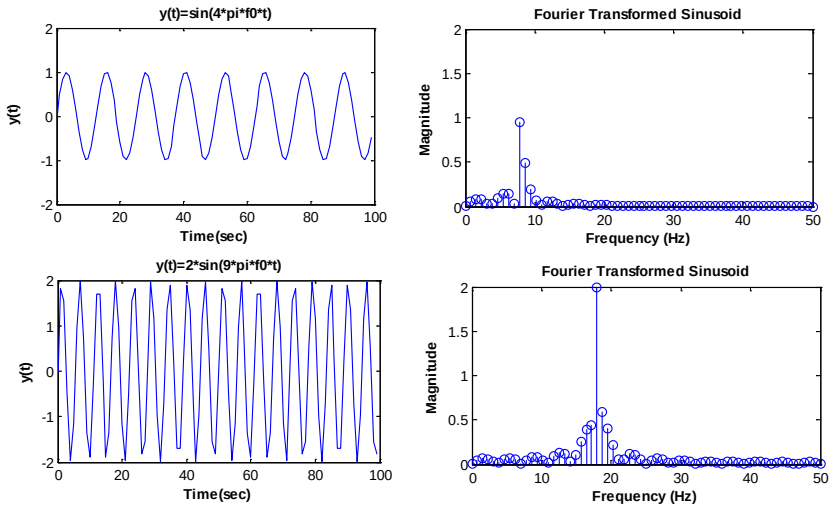

Figure 2-7: Two sinusoidal signals and their Fourier transformations

All in all, it is obvious that Fourier transformation is made from - ∞ to + ∞ to a periodic signal. Also, the FT is assumed to apply for periodic wave forms. In reality, signals may not be periodic at all or periodic signals may not exist. In the real world, a portion (sampling) of a wave is chosen so that the selected ends of the signal is connected with the periodicity. For a sampled signal, the Fourier transformation is not valid as it involves discrete samples (*N*). Therefore, the acquired discrete signal requires to be periodic before the Fourier transformation is implemented.

2.4.2 Discrete Fourier Transformation (DFT)

When evaluating a real signal in a computer or in a spectrum analyzer, it does not show the ideal results obtained from the Fourier transformation. In the spectrum analyzer, the digitizers sample the waves and then transform to discrete values. Therefore, some approximations are involved in realizing such waves by the digital signal processing. Discrete Fourier transformation (DFT) is such an approximation of the real world signal. The validity of such approximation is based on the type of wave form, sampling frequency (F_s) and the sample length (*N*) taken in the computation.

The first step in the signal processing in DFT is to convert the original signal into a number of sample points. This is called sampling the signal. Sampling frequency (sampling rate) measures how often a pulse or continuous wave is sampled. The quantity sampled is the amplitude of the original signal. The number of samples (*N*) is also needed before implementing signal processing techniques.

The theoretically expected sinusoidal wave and its sampled wave in the time domain are shown in Figure 2-8. For the discrete point of the sampled sine waves, N is 100 and F_s is 100. Theoretically, the signal is expected to be continuous, but in reality the sampled points will convert the signal into discrete points.

$$y_{(t)} = \sin(4\pi f_0 t) \tag{31}$$

According to the sampling theorem, the sampling frequency of the signal under investigation should be large enough in order to reproduce the original signal from the discrete sample points. Sample time (dt) is the time interval between samples. If the sampling rate is equal to 250 mega-samples per second (MSa/s), then the time between each sample is 1/Fs. Then the sampling time dt is 4 nano-seconds. According to the Nyquist theorem, the maximum frequency realized by any signal processing technique is represented by

$$\text{Highest frequency, } F_{Max} = \frac{F_s}{2} \tag{32}$$

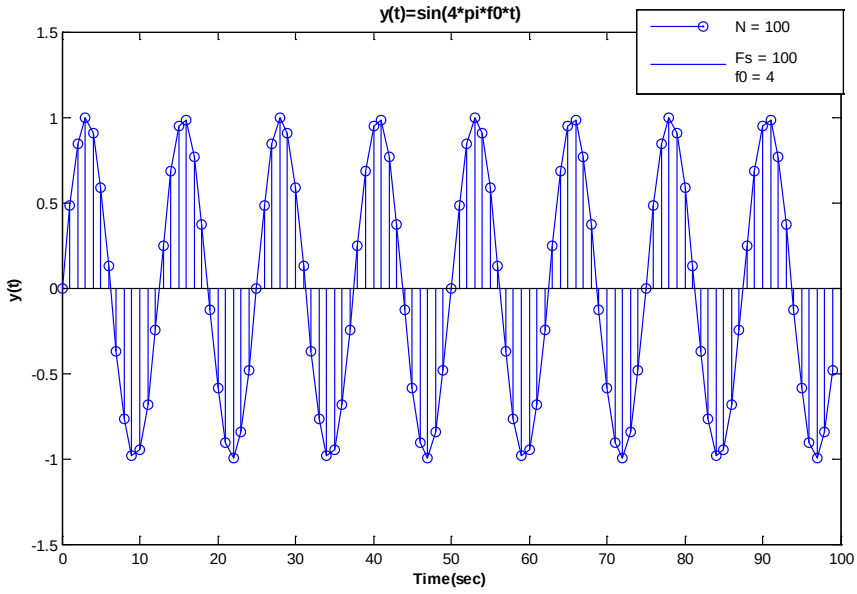

Figure 2-8: Discrete points of a sampled sine wave

When the sampling rate is low, it may fail to reproduce the original signal from the sampled values. Filtering of the original signal will prevent this kind of error in the signal. Normally, most of the signal generators and pulsar-receivers have low and high pass filters to set the target maximum frequency. The sampled signal is needed to separate into a fixed period

of time. The total length of time is called the total acquisition time. Assuming that there is N number of samples at the sampling time dt, then the total acquisition time is given by

$$\text{Total acquisition time} = N \times dt = \frac{N}{F_s} \tag{33}$$

If 20,036 data points are taken with the sample time 4 ns, then the length of sampled time is equal to 82 μs. Frequency resolution can be obtained using the total acquisition time as

$$\Delta f = \frac{1}{\text{Total acquisition time}} = \frac{f_s}{N} \tag{34}$$

If N is the number of samples in the sampled signal, then N is the last sample during the sample length. The sample number is defined as the sample k^{th} sample at any given time. Here, k is the frequency index for the discrete transformation. Sample index (n) is defined as the frequencies that are integer multiples of the fundamental frequency. The frequency of the first harmonic is given by $1/T$. Since $T= N/F_s$, the frequency of n^{th} harmonic waves can be determined by multiplying n with the frequency of the sample,

$$\text{Frequency of } n^{th} \text{ sample, } f_n = n \times \frac{F_s}{N} \tag{35}$$

Harmonic frequencies are defined by the magnitude and the phase of each discrete point in the wave. If the harmonic magnitudes plotted against the harmonic frequencies in the x and y axis of the Cartesian coordinates, the result is the frequency spectrum or frequency domain spectrum. Using the above definitions for the frequency index $k(t)$, the sample length N, and the sample index n, DFT of a signal $x(n)$, which sampled from continuous signal $x(t)$ is computed by,

$$X(k) = \sum_{n=0}^{N-1} x(n) e^{-j\frac{2\pi nk}{N}} \quad k = 0, 1, 2, \ldots, N-1 \tag{36}$$

The magnitude of the frequency domain data is given as

$$|X(k)| = \frac{A \times N}{2} \tag{37}$$

where A is the amplitude of the real signal. Consider a discrete signal $x(n)$ that has the sample length of N=5 and the sample index n=0:N-1.

$$x(n) = [1 \quad 1 \quad 1 \quad 1 \quad 1] \quad \textit{where} \quad n = 0, 1, 2, 3, 4 \tag{38}$$

When a real signal is sampled, it always includes real and imaginary parts. Therefore, the spectrum contains the negative and positive components of the frequencies after the

transformation is carried out. Numerical computations for the DFT can be performed using MATLAB.

2.4.3 Fast Fourier Transformation (FFT)

FFT [19, 45, 51] is a fast way of computing DFT to develop the frequency spectrum. FFT function takes fewer computations compared to DFT. Output of the FFT is complex in which the real and imaginary parts of a signal is obtainable. Compared with the DFT equation (refer to equation 36), the goal of the FFT function is to reduce the number of multiplications and additions. When the number of samples is large, the computation becomes more complex. Hence, DFT and FFT are the same concept and FFT is a way of computing the same function efficiently. Computer FFT algorithm in the signal processing only deal with the sampled signals. The FFT function can be computed using MATLAB software.

2.4.3.1 FFT Algorithm to Plot the Sinusoidal and Discrete Waves

Before explaining the properties of the FFT algorithm further, a plot of a sinusoidal wave and it's discrete points in the time and frequency domains are helpful to examine:

$$f_{(t)} = Sin(2\pi\ f_0\, t) \tag{39}$$

Where *fo* and *t* values are given in the FFT algorithm in APPENDIX B. Figure 2-9 shows the spectrum produced for the sinusoidal signal. The sampling rate is 100 samples per second and the numbers of samples shown in three frequency domain plots are 128, 256, and 1024. According to Nyquist theorem, the maximum frequency in the FFT algorithm is $F_s/2$, which is 50 Hz. The frequencies after the 50 Hz correspond to negative frequency of the signal. When the numbers of sample points are increasing, the resolution of the signal increases.

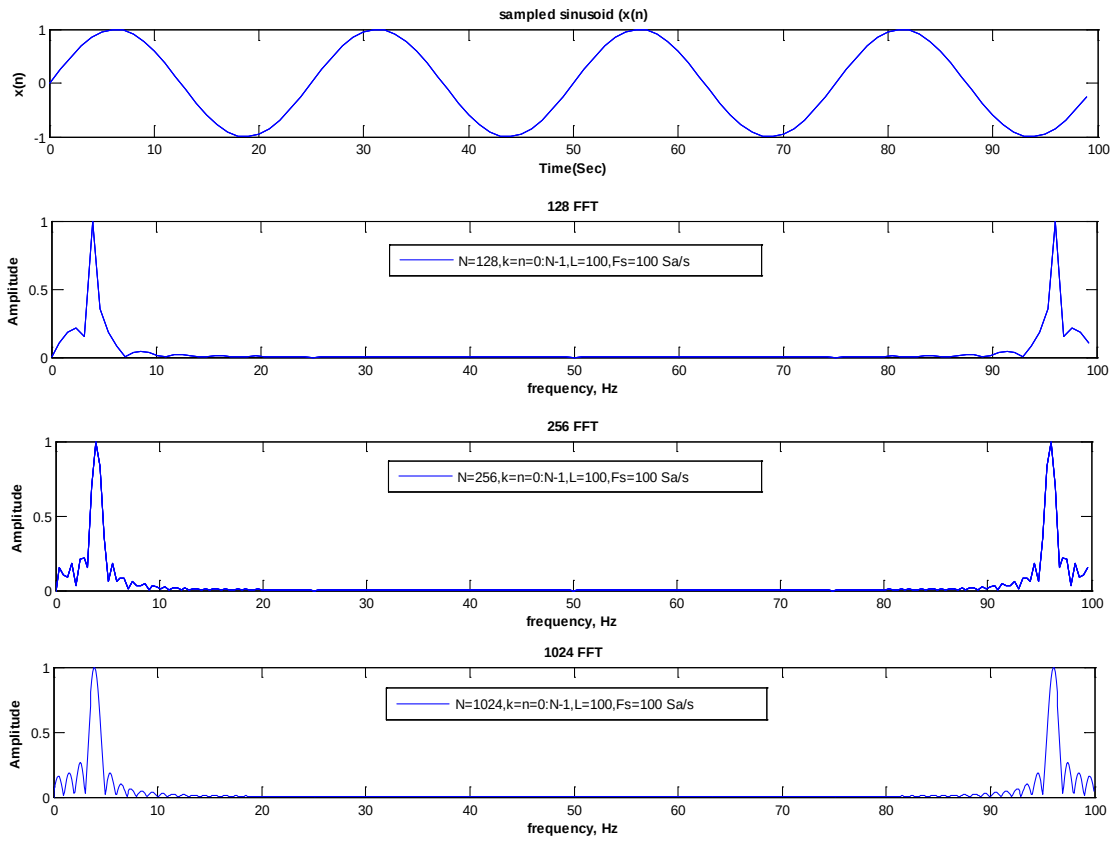

Figure 2-9: Fast Fourier transformation (FFT) of a sinusoid and its time domain signal

Figure 2-10 shows the FFT of the discrete signal *x(n)*, which is given in the discrete points as

$$x(n) = [1\ 1\ 1\ 1\ 1] \quad n = 0,1,2,3,4 \tag{40}$$

Where n=0The FFT algorithm can be developed (see APPENDIX A) to compute the frequency domain spectrum of the discrete signal. The sampling rate is 10 samples/sec. As depicted in Figure 2-10, the frequency domain is symmetric about the Nyquist frequency of $F_s/2$, which is 5 Hz. These frequencies are greater than the Nyquist frequency corresponds to the negative frequencies. Also, when the sampling length is increasing, the resolution of the spectrum increases. If the value of the sample length increase from N=16 to N=512, the resolution enhanced while the amplitude spectrum unchanged. When N=16, the spectrum does not cover the integer number of cycles in the original signal. Therefore, some irregularities present in the spectrum.

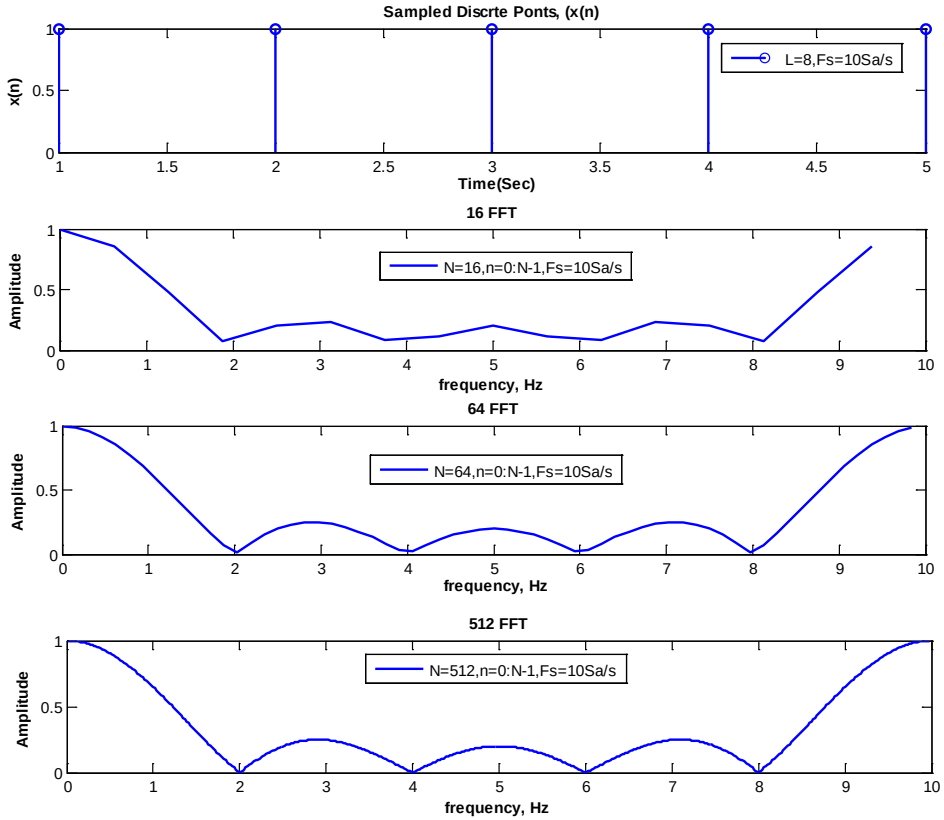

Figure 2-10 Fourier transformation (FFT) of a discrete signal

2.4.3.2 FFT Window

Similar to the DFT, FFT needs sufficient number of sample points to reproduce the original signals. If no appropriate numbers of periodic points are chosen, then there will be a discontinuity at the edges of the time window. This is called spectral leakage. In order to obtain a better approximation for the signal, various window functions are used. These window functions allow the edges of the chosen waves approach to zero. There are mainly three window types of implementing FFT in MATLAB: rectangular, hanning, and flattop.

2.4.3.3 Complex Amplitude

The quantities measured in the FFT function are the amplitude and the phase for each frequency. Those quantities have real and imaginary components that derive from Euler's equation. The complex amplitude generates exponential Fourier series and hence the magnitude of the spectrum is half of the value of trigonometric series. Therefore, magnitude needs to compensate by multiplying by 2,

$$x_{(n)} = 1/2\ Sin(2\pi\ f_0\, t) \tag{41}$$

FFT function computes complex amplitudes by scaling the overall length of the input signal *x(n)*. Therefore, the amplitudes need to divide by the length of input time domain data. Then, the syntax for the amplitude of the spectrum is represented in MATLAB FFT algorithm as follows:

```
2*abs(fft(xn))/length(xn);
```

2.4.3.4 One-Sided Spectra

If the maximum frequency of the original signal is higher than *N*/2, the frequency spectrum cannot reproduce from the original signal. Figure 2-11 shows that the FFT of the sinusoid plotted only for 50 samples even though it has the sampling length of 100 points (*L*). This is because, in the signal analysis, wave forms can only generate *N*/2 data points. The rest of the data are negative frequencies generated by the real signal. The frequency domain shows both negative and positive frequencies. Only one-sided spectra can be generated by cutting off negative frequencies (see APPENDIX B for MATLAB algorithm).

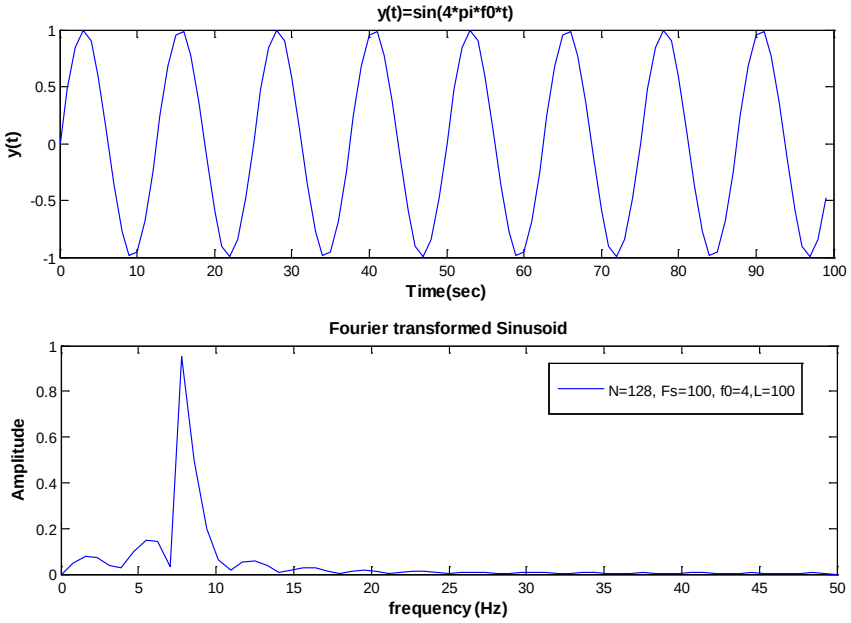

Figure 2-11: One-sided Fourier spectrum of a sinusoid

2.4.3.5 Zero Padding

Discrete points of the wave forms can only generate *N*/2 data points using the FFT algorithm. When there is no power of two in the sampling length *N*, the FFT will automatically take the power of two of the *N*. The general rule for the number of points to be taken in the spectrum analysis is to take the power of two. The following syntax can be used to get the power of two.

```
NFFT = 2^nextpow2 (L);      % Next power of 2 from length of the signal x(n)
```

If *N*=10, then DFT compute through FFT algorithm. The power of two of samples can be obtained in two ways. First, two sample points can discard, then *N*=8. Then, 8-point FFT can obtain. Second, six zeros can insert at the end of the discrete points so that *N*=16. Then it generates 16-point FFT. In the latter case, the FFT function allows zero padding by means of adding zeros into the signal at the end. The zero padding gives better resolution but it does not give much information. Figure 2-12 shows the FFT of a sinusoid and the zero padded spectrum.

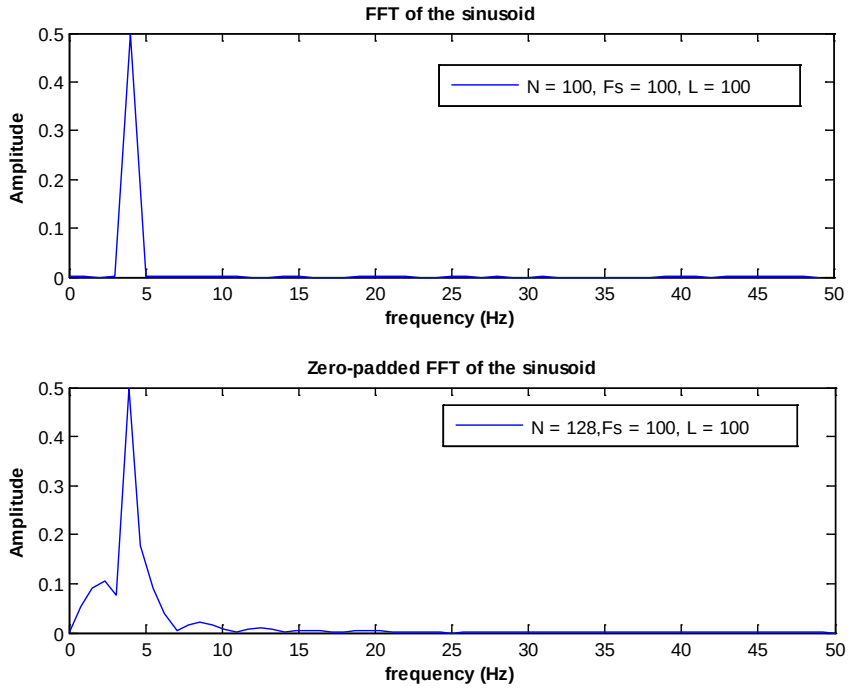

Figure 2-12: Zero-padded sinusoid for the next power of two

CHAPTER 3 - Experiments

3.1 Introduction

This chapter consists of three main sections. Section 3.2 puts forward the design and fabrication techniques of layered scatterers in aluminum, LDPE, and Teflon hosts. The experimental procedures carried out in the process of ultrasonic transmission technique and the measures taken in the experiment are described in section 3.3. Specifications, performances, and functions of each apparatus utilized in the experiment are also included in this section. Data processing techniques are discussed in the last section of this chapter.

3.2 Design and Fabrication of Test Samples

Poly-Tetra-Fluoro-Ethylene (PTFE), which is popularly known as Teflon, low density polyethylene (LDPE), and aluminum 6061-T6 were chosen as the host materials for constructing phononic materials. Nine rectangular shape test pieces having arbitrarily chosen length of 2.5 *inches*, height of 2 *inches*, and thickness of 1 *inch* were produced in each host. As shown in Figure 3-1, periodic square and triangular arrays of cylindrical cavities were fabricated by drilling holes on those test pieces. Diameters of the drilled holes were chosen arbitrarily as 3.175 *mm*. When periodic cylindrical cavities are drilled in advance, the band gaps are fixed as the lattice parameter is constant. The lattice parameter a was maintained in each unit cell as 1.5×a inches (0.1875 *inch*). The equilateral triangular and square array samples consisted of 63 and 65 holes respectively along the length of 2.5 *inches*. Both arrays composed of 5 holes in the thickness side (1 *inch*). The drawings for the custom designed test pieces are given in APPENDIX C.

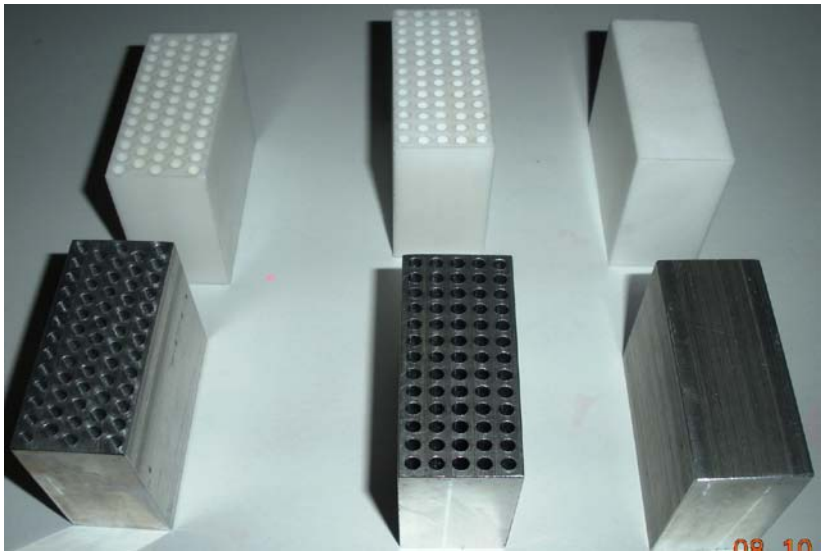

Figure 3-1: Teflon and aluminum triangular, square, and rectangular block test pieces

The circular cylindrical stainless steel (SS) rods were chosen as the hard scatterers to be embedded into the cylindrical cavities in three different hosts. Eccentric orientation of each scatterer was created by keeping the test pieces at an angle to the horizontal and then by filling the surrounding space next to the SS rods with paraffin wax at various angles. Different orientation angles ranging from 0 degree to 90 degrees at the increment of 22.5 degrees was accomplished by wooden-supports as illustrated in Figure 3-2.

Figure 3-2 Arrangement for eccentricities 22.5 *degrees* and 67.5 *degrees* in aluminum test pieces

The inner diameter of the layered scatterers were changed by means of two sets of diameters of stainless steel rods: 2 *mm* and 2.5 *mm*. The molten wax was prepared by secondary heating of a solid wax-container. First, a container of solid wax was held in a large water-filled basin as shown in Figure 3-3. Subsequently, the water basin was kept on a rectangular hot plate and then heated until the solid wax is melted. The entire structure prepared with the wooden

supports was then immersed in the molten paraffin wax. Angles of 0 degree and 90 degrees were obtained by simply holding them inside the flat molten-wax container.

Figure 3-3: Immersing the structure in molten paraffin wax bath

Melting temperature of LDPE is around 95 – 105 °C. Therefore, temperature of the molten wax maintained well below 100 °C to prevent subsequent melting of LDPE samples. Test pieces were allowed to solidify under the room temperature for more than 12 *hours*. Finally the test pieces were cleaned for the next stage of ultrasonic testing.

3.3 Experimental Setup

The propagation of ultrasonic waves is influenced by material properties through which it propagates. The ultrasonic TTT was set up by placing one transducer on one surface of a test material while other transducer on the opposite surface of the same test material. Figure 3-4 shows the experimental setup used for the ultrasonic TTT. The experimental setup consisted of (1) a pulsar-receiver, (2) a transmitter transducer, (3) a test specimen, (4) a receiver transducer, (5) an oscilloscope, and (6) a data processing computer.

In the through transmission test, mainly the longitudinal waves were introduced into a solid block using two pair of matched piezoelectric contact transducers. Those waves were captured by a receiver from its opposing surface. In such a configuration, transmitter-transducer transmits the sound waves and waves are captured by a receiver-transducer as shown in Figure 3-4. The transducers were excited using two pulsar-receivers. One pulsar-receiver was a computer controlled Panametrics 5900PR pulsar-receiver, and the other was a manually controlled

Olympus 5072PR pulsar-receiver. High voltage pulses produced by the pulsar-receiver unit were converted to ultrasonic waves using the transducers.

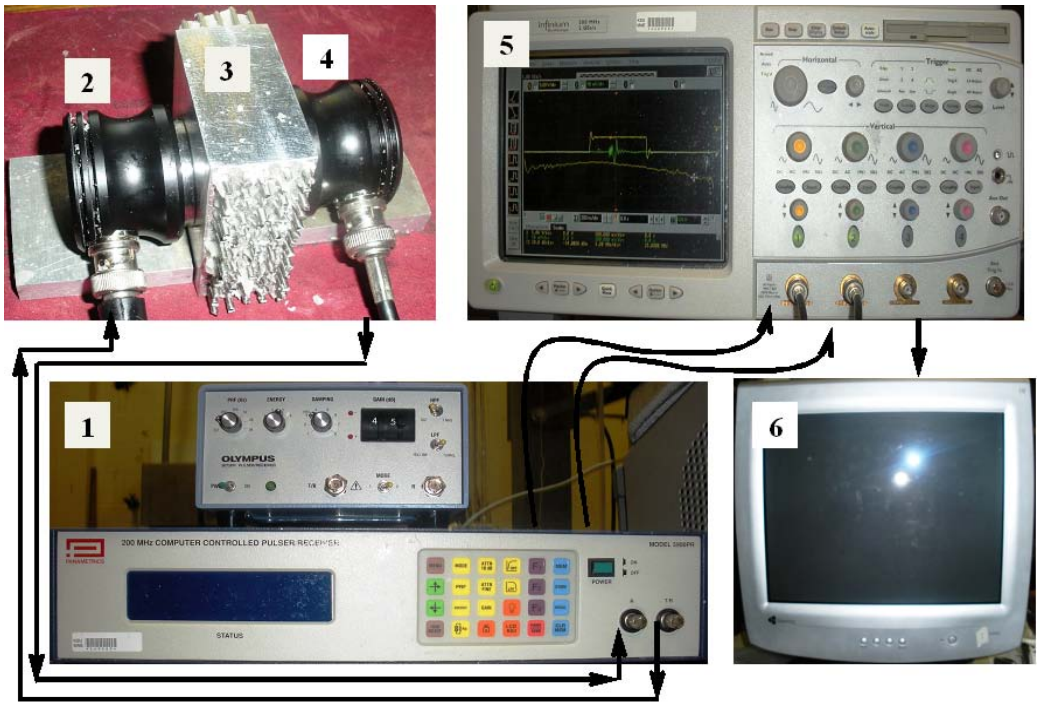

Figure 3-4: Block diagram of the experimental setup

High attenuating LDPE and Teflon samples were tested using the low center frequency (0.5 MHz) transducers. The high center frequency (2.25 MHz) transducers were employed to test low attenuating aluminum samples. The chosen piezoelectric contact transducers confirm near field lengths of 9.63 *inches* and 2.14 *inches* for 2.25 MHz and 0.5 MHz transducers respectively (see APPENDIX A for the near field table). Since the thickness of the test pieces are 1 *inch*, the specimens obviously were placed in the near field region of the transducers. If the materials to be tested are positioned within the near field region, a maximum sensitivity and complex wave fronts can anticipate.

The input pulse, which was emitted by the transmitter transducer was perpendicular to the thickness 1 *inch* of the PC. The transmitter transducer was connected between the pulsar of the pulsar-receiver unit and the test piece. The receiver transducer connected in between the opposing surface (2×2.5 *inche*s surface) of the test specimen and the receiver of the pulsar-receiver unit. Voltage level of the received signal was enhanced in the pulsar-receiver unit and then displayed in a oscilloscope. The collected time domain data in the oscilloscope were further processed in the frequency domain using FFT-algorithm with the help of MATLAB software in

the personnel computer. Specifications, performances, limitations, and functions of various components used in the experiment, are explained in detail in sections 3.3.1, 3.3.2, and 3.3.3.

3.3.1 Pulsar-Receiver Unit

The pulsar-receiver is an electronic device used to generate high voltage electrical pulse. Generally transmitting transducers are driven by the energy generated in a pulsar-receiver . Electrical responses arriving from receiving transducer are also amplified in the pulsar-receiver. Two pulsar-receivers: computer controlled Panametrics 5900PR, and manually controlled Olympus 5072PR are shown in Figure 3-5.

Figure 3-5 Pulsar-receivers for exciting piezoelectric transducers

A high voltage pulsar and a high gain receiver are needed to test high attenuating materials such as plastics. Therefore, high energy input is needed for exciting the transducers to test LDPE and Teflon samples. Manually controlled Olympus 5072PR pulsar-receiver is able to operate in pulse-echo and TTT. Low pass filters that are either full band width 35 MHz or 10 MHz to improve signal to noise ratios are embedded in this pulsar-receiver when working at low frequencies. The pulse repetition frequency control (PRF) was available from 100 Hz to 5000 Hz in this pulsar-receiver. This allowed the user to control the frequency at which the pulses are applied to the transducers. Aluminum samples were tested using The Panametrics 5900PR pulsar-receiver. The setting for each pulsar-receiver is shown in Table 3-1. These settings were kept constant throughout all the tests to make the consistency of the time domain spectra.

Table 3-1: Pulsar-receiver settings for each test

Parameter	Olympus 5072PR Pulsar-Receiver	Panametrics 5900PR Pulsar-Receiver
Pulse Repetition Rate (PRR) [Hz]	100	200
Energy [µJ]	52	32
Damping [Ω]	50	50
Attenuator [dB]	-	20
Gain [dB]	45	26
LPF [MHz]	10	20
HPF [kHz]	Out (complete bandwidth)	1
RF output phase	0°	0°

3.3.2 Contact Transducers

When the ultrasonic waves are introduced into the test pieces, the waves are propagated through the material by means of sound waves. When the sound waves meet disturbances, a portion of the wave is reflected back and transmitted through the test pieces. The transmitted portion of such signal was collected using the receiving transducer. Good damping properties are needed in the receiving transducers to increase the resolution of the received signals. The transducer performances are mainly dependent on the cabling, the transducer configuration, the frequency, and the element diameter.

The transducer selection was carried out based on the criteria that the wave length of ultrasonic wave is equal to the diameter of a cylindrical cavities of the periodic array. Since the sound velocity is constant for a given specimen, the wave length is dependent on the frequency of the transducer. In conformity with the ultrasonic sound velocities of the aluminum, Teflon, and LDPE, the required transducer center frequencies were approximately calculated using,

$$D = \lambda = \frac{V}{f}. \tag{42}$$

where V is the sound velocity and f is the frequency of the material. The maximum frequency was determined based on the criteria that the wave length is half of the diameter of the cylindrical holes (D/2). Table 3-2 shows the calculated transducer frequencies.

Table 3-2: Required transducer frequencies for aluminum, Teflon and LDPE

Material	Central Frequency, MHz (λ=D)	Maximum Frequency, MHz (λ=D/2)

Aluminum 6061- T6	1.984	3.968
Teflon	0.432	0.864
LDPE	0.620	1.240

Standard contact Olympus Videoscan transducers were chosen to get broadband performances (See APPENDIX B for transducer specifications). They are right angle BNC-connector style contact transducers with center frequencies 2.25 MHz (part number V104) and 0.5 MHz (part number V101). Both of them have the element diameter of 1 inch. The Videoscan transducers are un-tuned transducers, which provide heavily damped broadband performances [2]. Transducer specification details are given in APPENDIX A. Even though the test pieces are made of aluminum, Teflon, and LDPE, two sets of straight beam direct contact transducers with a wide band width were purchased to be able to test materials with various properties in the future. Two RG 58A/U cables with the length of 4 *feet* were also purchased to connect the transducers with other components in the experimental setup. Figure 3-6 shows the part number V104 contact transducers and cables.

Figure 3-6: Standard contact transducers and RG 58A/U BNC cables

The maximum efficiency of the sound transmission into the material was maintained by a application of couplant between the transducer and the test pieces. A couplant was used in between the test pieces and the transducers. In this experiment, two functions were anticipated using liquid petroleum-jelly as a couplant. First, it was expected to facilitate the medium wherein ultrasonic energy from the transducer could travel into the test specimen. Second, it was intended to remove the entrapped air in between the transducer and the test specimen boundaries and to reduce the impedance mismatch between air and test pieces.

3.3.3 Data Acquisition in the Oscilloscope

The data acquisition was carried out using HP infinium oscilloscope. Received RF analog output signals are digitized in the oscilloscope. This oscilloscope has a maximum frequency input of 500 MHz and the sampling rate of 2 *Giga-samples per second* (GSa/s). The resolution of the acquired signal is determined by the sampling rate. The higher the sampling rate, the better the resolution. Spectral analysis features such as built-in FFT algorithm, vertical scale, horizontal scale, the sampling rates, and the memory depth can be controlled in the HP infinium oscilloscope. Moreover, the user can display the wave form and allow to save the data into a file and recall them back. Therefore, each wave form was recorded at the oscilloscope in the time domain and then they were stored for further data processing. Through a series of trial and error, 1 *giga-sample per second* (GSa/s) was selected as the suitable sampling rate for the aluminum samples. Sampling rates for LDPE and Teflon samples were chosen as 250 *mega-samples per second* (MSa/s).

3.4 Data Processing Procedure

This section and upcoming details describe the signals produced in the time domain and the frequency domain. Generally, a time domain data shows how long the sound is travelled (time in seconds) and how did the amplitude vary in a particular time window. It can also be very useful to know how each frequency component of the sound contributes to the overall amplitude. This can be carried out by transforming the time domain into the frequency domain. Although there was a built-in FFT function in the oscilloscope the data were processed and presented using the MATLAB FFT algorithm in the personal computer. The time domain data were multiplied by a rectangular window function before they transformed. According to the sampling theorem, the sampling rate should be selected so that it is twice as greater than the maximum expected frequency of the tested samples. Therefore, with the series of tests, it was found that the sampling rate of 1 GSa/s is suitable for the PCs made in the aluminum host. Also, the sampling rate of 250 MSa/s showed much information for the real time signal produced in the oscilloscope for the PCs made in LDPE and Teflon hosts.

3.4.1 Transducers

As the first step of the data processing, transducer spectra were generated with the help of FFT function using MATLAB software. The suitable time lengths (T_s) and the sampling rates

(F_s) for the different PCs were decided after analyzing the transducer spectra. Both transducers with center frequencies 0.5 MHz and 2.25 MHz were employed for the formation of time domain spectra for all the PCs made in host aluminum. PCs made in host Teflon and LDPE were tested using 0.5 MHz transducer alone. Each PC was expected test within the chosen bandwidths.

Expected bandwidth for 0.5 MHz transducers to test aluminum samples was 0.15 MHz-0.9 MHz. The time domain data collected at two different sampling rates: 1 GSa/s and 500 MSa/s for both 2.25 MHz and 0.5 MHz transducers. Figure 3-7 is the amplitude signal obtained at the 0.5 MHz transducer in both time and frequency domains. Compared to the sampling rate of 500 MSa/s, the spectrum can be seen as a uniform spectrum for the sampling rate of 1 GSa/s. As shown in Figure 3-7 (*b*), the bandwidth for the 0.5 MHz transducer was chosen in the frequency range of 0.15 MHz -0.9 MHz.

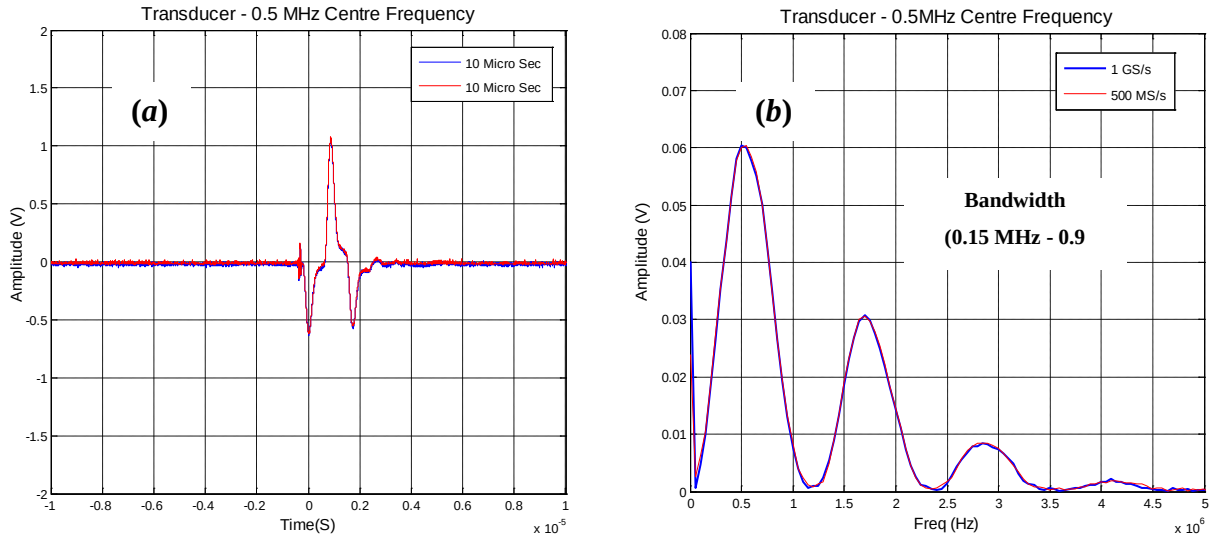

Figure 3-7: Different sampling rates for 0.5 MHz transducers (*a*) time and (*b*) frequency domain

When Fs was 1 GSa/s, the frequency domain sample length (*L*) was 20,036 and the number of samples (*N*) was 500 mega-samples. Hence, the sample index (*n*) was 20,035. When the sampling rate was 500 MSa/s, the frequency domain sample length (*L*) was 10,018 and the number of samples (*N*) was 250 *mega-samples*. Hence, the sample index (*n*) was 10,017.

The following text explains the procedures used to identify the bandwidth of the 2.25 MHz transducer to test aluminum samples. The chosen frequency range is from minimum 0.9 MHz to maximum 3.2 MHz having the bandwidth of 2.3 MHz. This is shown in Figure 3-8 (*a*) and (*b*). When the sampling rate was 1 GSa/s, the frequency domain sample length (*L*) was 20,036, the number of samples (*N*) was 500 *mega-samples*, and the sample index (*n*) was 20,035.

Further, when F_s was 500 MSa/s, the frequency domain sample length (L) was 10,018 and the number of samples (N) was 250 *mega-samples*. Hence, the sample index (n) was 10,017. In this case, a uniform spectrum was obtained at the sampling rate of 1 GSa/s. Therefore, the sampling rate for both 0.5 MHz and 2.25 MHz transducers were chosen at 1 GSa/s to test aluminum samples.

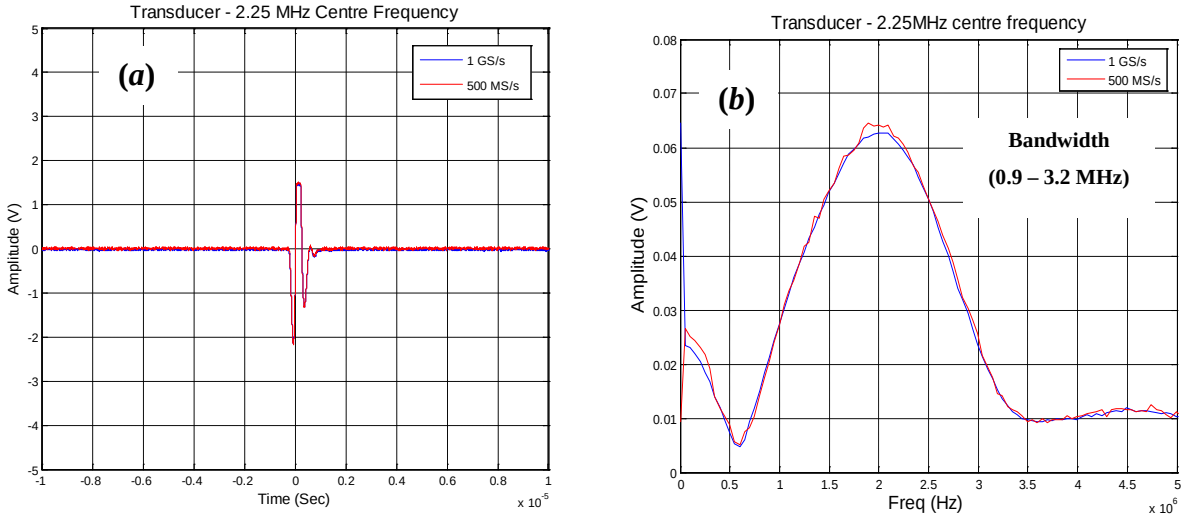

Figure 3-8: Different sampling rates for 2.25 MHz transducer (*a*) time and (*b*) frequency domains

Similarly, the target test frequency range for both LDPE and Teflon samples were chosen from 0.15 MHz to 0.9 MHz using the 0.5 MHz transducer. This can be seen in Figure 3-9. The time domain data were produced at the sampling rate of 250 MSa/s to collect maximum number of discrete points. When Fs was 250 MSa/s, the frequency domain sample length (L) was 20,036 and the number of samples (N) was 125 *mega-samples*. Hence, the sample index (n) was 10,017. Further, when Fs was 100 MSa/s, then the frequency domain sample length (L) was 10,018. The number of samples (N) was 50 *mega-samples* and the frequency index (k) was 10,017 for the frequency domain spectrum as depicted in Figure 3-9.

By keeping sampling rates constant, different positions or time lengths from the time domain data were chosen. Different energy contents of the FFT spectra of the signals at different sampling lengths are shown in Figure 3-10.

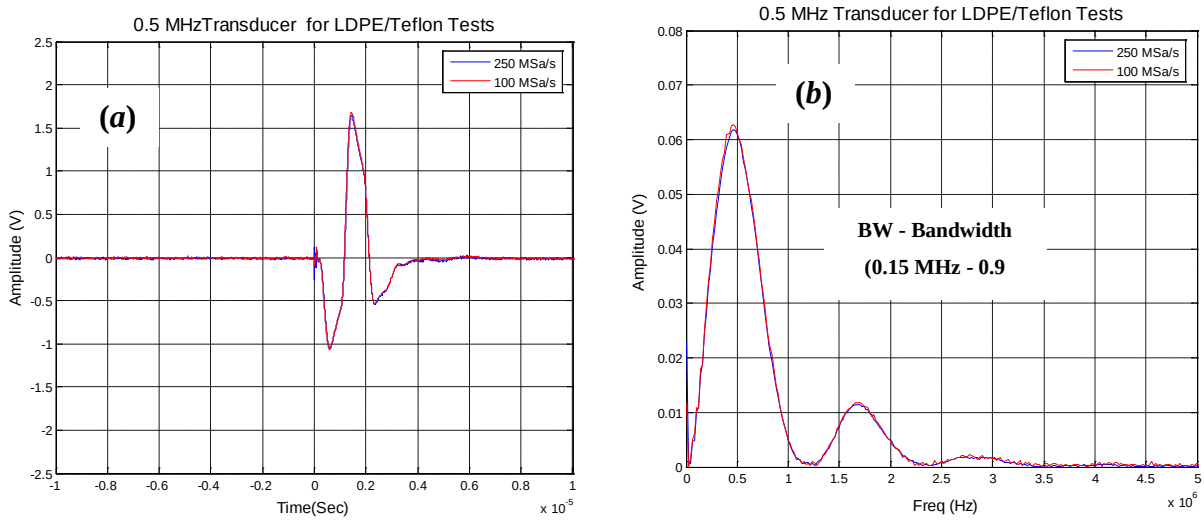

Figure 3-9: Different sampling rates for 0.5 MHz transducer (*a*) time and (*b*) frequency domain

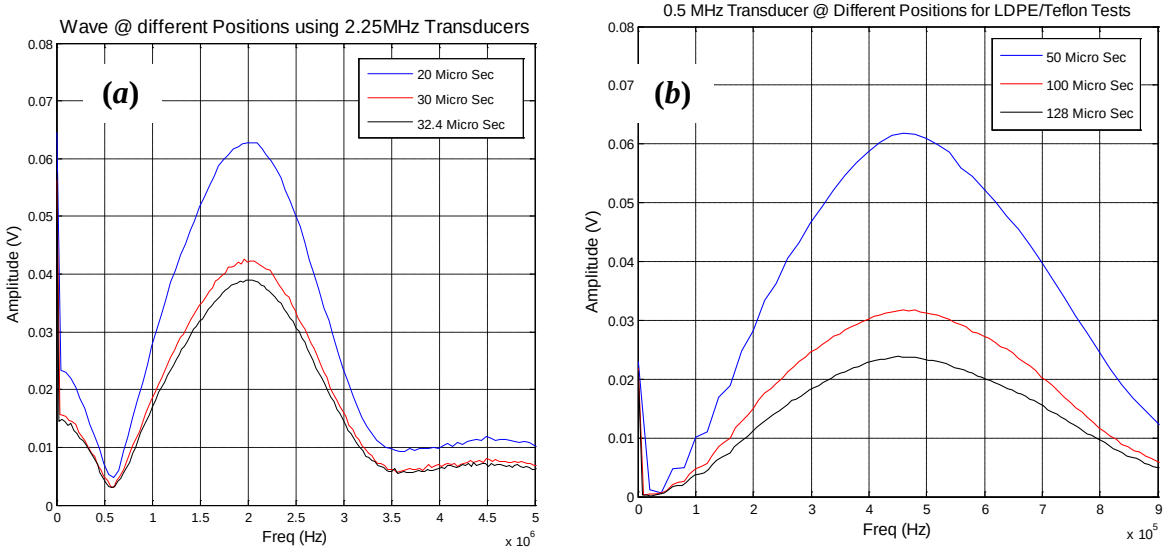

Figure 3-10: Signal obtained at different time lengths for the transducers (*a*) 2.25 MHz (*b*) 0.5 MHz

3.4.2. Solid Blocks

Prior to test the PCs made in each host, the wave forms were obtained for solid block and square or triangular array samples as the second step. The ultrasonic TTT was carried out for all the solid blocks and for the square and triangular array samples with no inserts. The data processing was carried out to generate the frequency domain spectra.

3.4.2.1 Aluminum

Figure 3-11 (*a*) and (*b*) show different sampling rates of the spectra in the time and frequency domains for the aluminum solid blocks. It was collected (*N*) 20,036 and 10,018 data points at the sampling rates of 1 GSa/s and 500 MSa/s respectively. The test was carried out within the sampling length of 20 μs. Although the sampling rates are different, two spectra were fully aligned with each other. It can be noted that the sampling rate 500 MSa/s is not a very sharp curve due to the lack of data points.

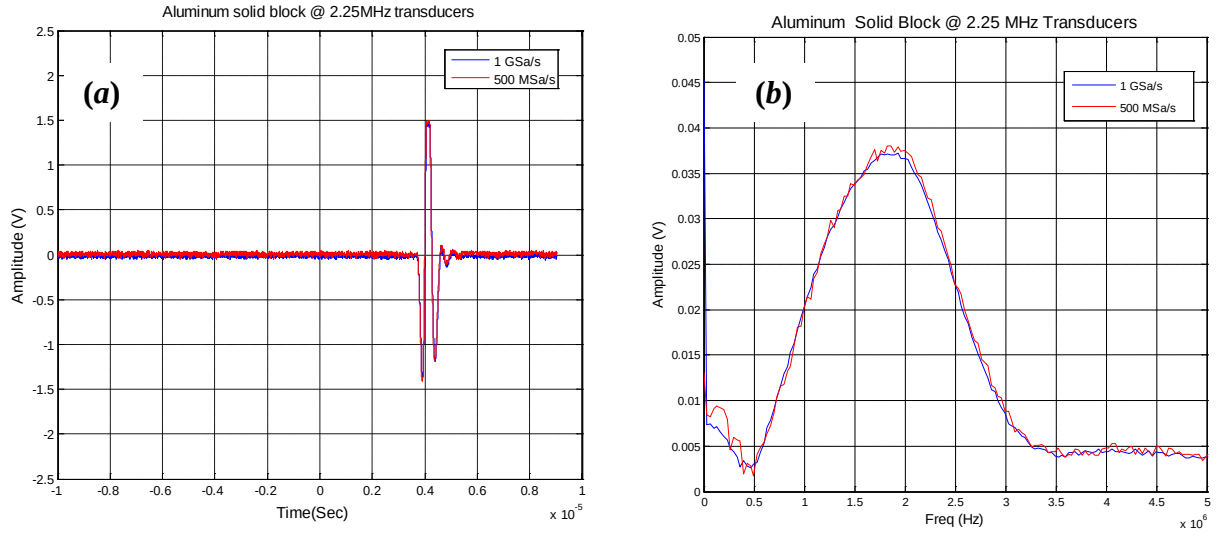

Figure 3-11: The signal obtained from aluminum solid block (*a*) time domain (*b*) frequency domain

Figure 3-12 shows the spectra obtained at different time lengths at the sampling rates of 1 GSa/s. Figure 3-12 (*a*) and Figure 3-12 (*b*) show the time and frequency domain spectra respectively. The dissimilar amplitudes can be observed at different time intervals as a result of the different energy content in each signal. Also, it can be noted that as the record length is increased, the band width of the spectrum is narrowed.

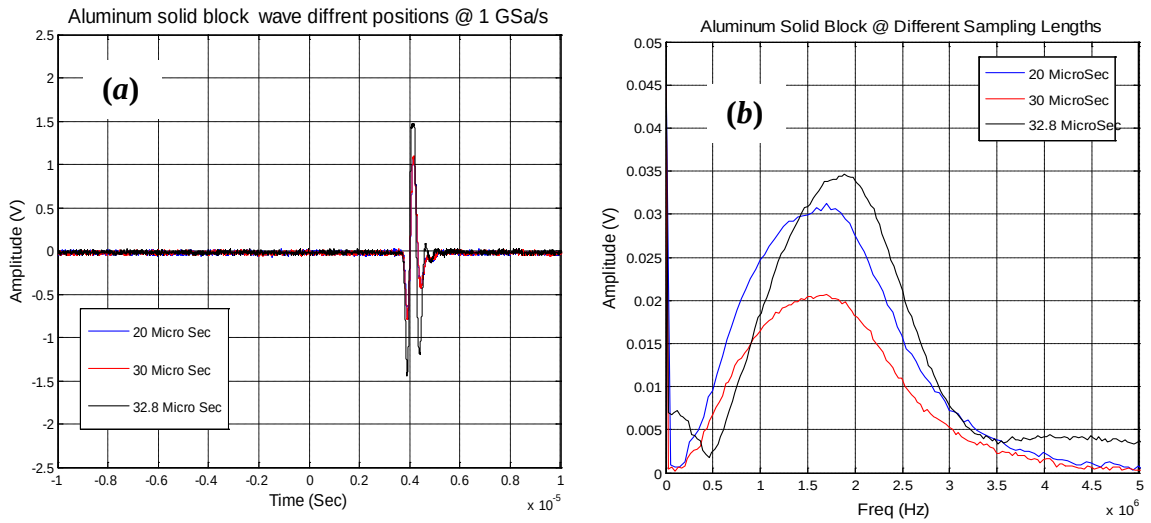

Figure 3-12: Different time lengths in the signal in (*a*) time and (*b*) frequency domains

3.4.2.2 Teflon

The following text explains the spectra obtained from the Teflon solid blocks. The time domain data produced at the sampling rate of 250 MSa/s within the time period of 126 μs. This can be seen in Figure 3-13 (*a*). The figure shows the sampling length (N) of 32,768 and the frequency index (k) of 32,767. Although the original frequency range was ±125 MHz, Figure 3-13 (*b*) shows the spectrum in the chosen frequency range from 0 to 0.9 MHz.

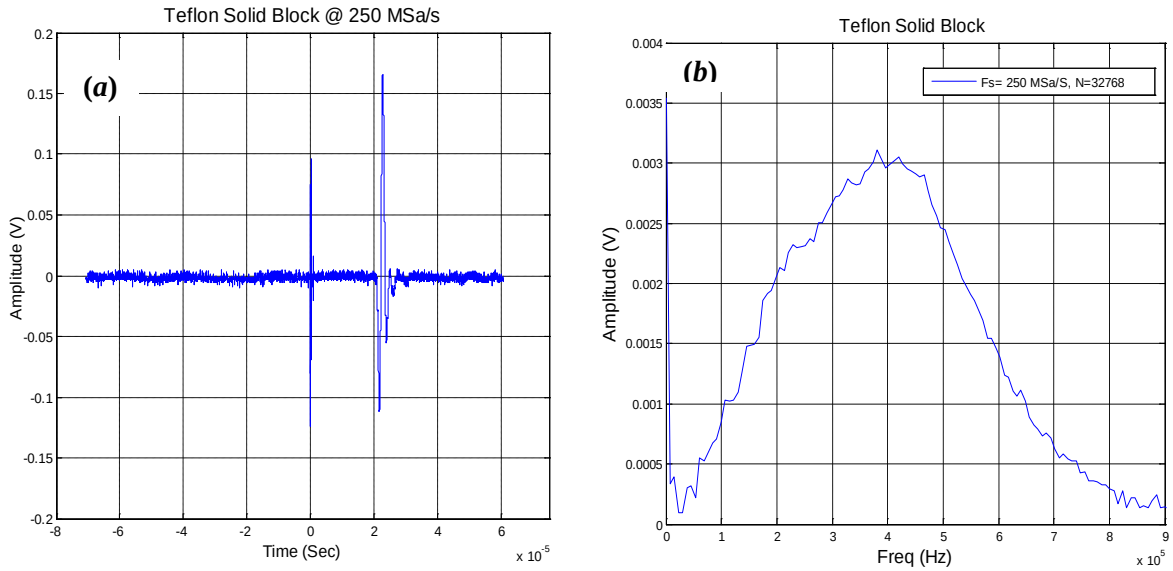

Figure 3-13: The signal obtained from Teflon solid block (*a*) time domain (*b*) frequency domain

3.4.2.3 LDPE

LDPE solid blocks were tested using the ultrasonic TTT. The amplitude spectra produced at the sampling rate of 250 *MSa/s* within the time period of 126 μs. Figure 3-14 shows the spectrum in the time and frequency domains. Spectra have reported the sampling length 32,768 (*N*) and frequency index (*k*) of 32,767. Although the actual frequency range is ±125 MHz, the spectrum is shown in the chosen frequency range from 0 to 0.9 MHz.

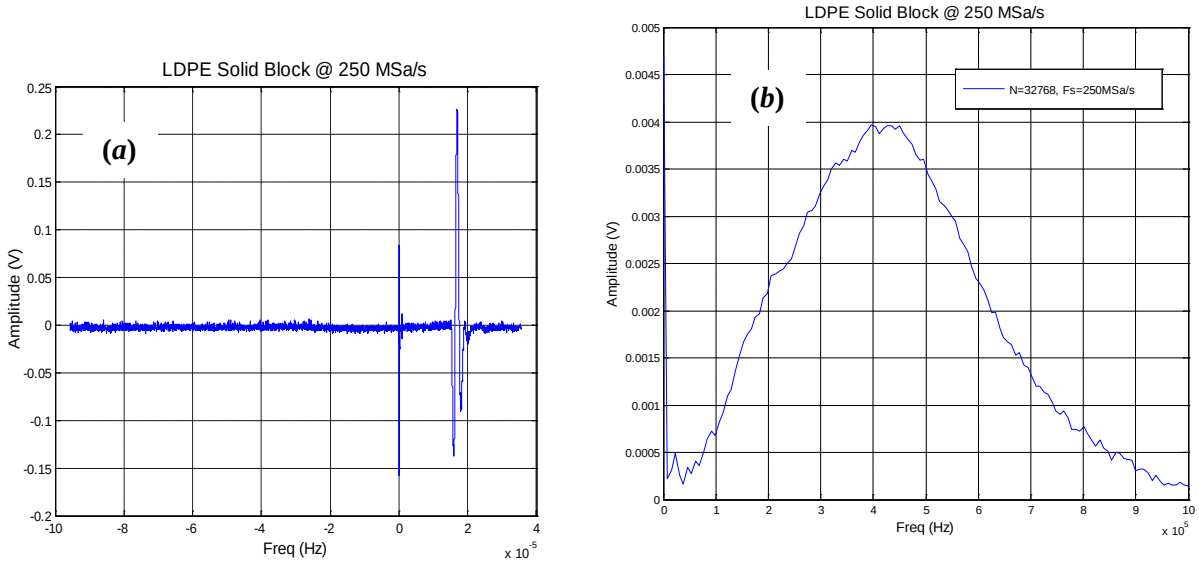

Figure 3-14: The signal obtained from LDPE solid block in (*a*) time and (*b*) frequency domain

3.4.3 PCs with Layered Scatterers

PCs, in which eccentrically layered scatterers are embedded, were tested using 2.25 MHz and 0.5 MHz transducers. Three identical ultrasonic TTT were repeated for each eccentricity orientation angle ranging from 0 *degree* to 90 *degrees* at the increment of 22.5 *degrees*. A similar procedure was carried out for the PCs having 2 *mm* and 2.5 *mm* diameter SS rods. Then, the average of the each identical orientation angle was computed in the frequency domain. The amplitudes of the signals can be changed due to the variations in the film thickness of the couplant. The forces applied to hold the transducers in contact with the specimen can also be varied from one test to another. As a remedy, the averages of the each orientation angle were computed using least square error method. Finally, all the average curves were normalized with respect to spectra produced by the transducers alone. Results are presented in Chapter 4.

CHAPTER 4 - Results and Discussion

4.1 Introduction

A brief discussion on the experimental methodology and the selection of materials in constructing PCs is given in section 4.2. Section 4.3 deals with characterization of time domain and frequency domain spectra produced by the test pieces with no inserts. Frequency dependent transmitted spectra produced by the PCs with layered scatterers are presented in section 4.4. Possible sources of errors and comparison of different phononic materials in the experiments are discussed in section 4.5. Finally, conclusions are summarized in section 4.6.

4.2 Overview of Materials and Experiments

2-D PCs are assumed to be arranged in XY-plane of the host material as shown in Figure 4.1. The dimensions of both square and triangular array test specimens are 2.5×2×1 *inches*. Z-direction was selected as the height of 2 *inches* which is parallel to the circular cylinders. The square and triangular array samples comprised of 65 and 63 circular cylindrical holes respectively. Also, both square and triangular array samples consisted of 5 circular cylindrical holes in the X-direction.

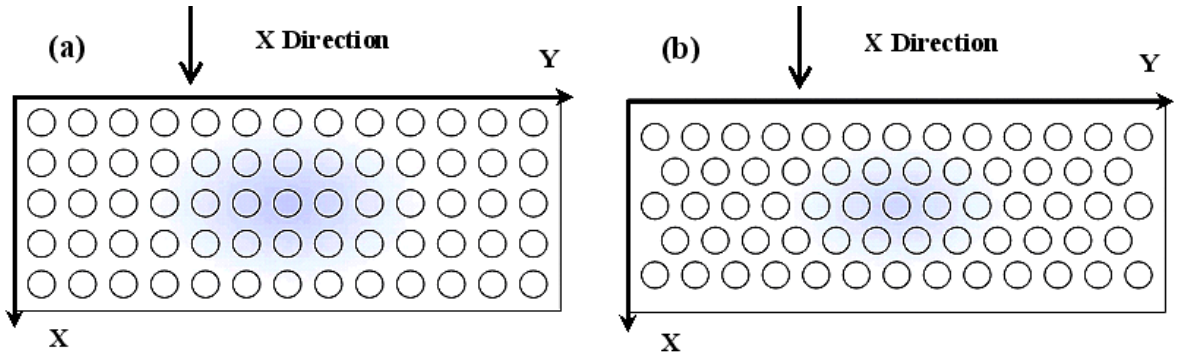

Figure 4-1: Directions of ultrasonic wave propagation in (a) square and (b) triangular arrays

The parallel circular cylinders in each matrix are expected to act as scatterers. In the triangular array, the eccentrically layered scatterers are located at the corners of the equilateral triangles. The scatterers are located at the four corners of a square in the square array. The diameter of the cylindrical holes was 0.125 *inch*. The diameter of the cylindrical void (D) selected to be comparable with the wave length ($\lambda=D$). Also, the lattice parameter was chosen as $1.5\times D$ for each array. Then, the lattice parameter (a) of each array was computed as 0.1875 *inch*. The layered scatterers created inside the cylindrical voids in each matrix. The main feature of the

layered scatterer was that it consisted of two materials. One material was the circular stainless steel (SS) rods with diameters 2 *mm* and 2.5 *mm* and the other was the paraffin wax coating. Each test specimen was subjected to ultrasonic TTT followed by signal processing.

In the ultrasonic TTT, a short pulse produced by the transmitter-transducer was sent to the test specimen along the X-direction. Transmitted signals were captured by the receiver-transducer and they were sent back to the oscilloscope through a pulsar-receiver. A good representation of the typical signal energy and strength could be made using a raw time domain signal, which is displayed in the oscilloscope. The time domain data were obtained by three identical tests carried out for different eccentricity orientation angles ranging from 0 degrees to 90 degrees at the increment of 22.5 *degrees*. These data were converted to the frequency domain using FFT function in MATLAB software. Amplitude spectra for aluminum samples were produced using 0.5 MHz and 2.25 MHz transducers in the frequency range from 0.15 MHz to 3.2 MHz. Similarly, amplitude spectra for PCs made in LDPE and Teflon hosts were tested using 0.5 MHz transducers in the frequency range from 0.15 MHz to 0.9 MHz. The average curves for different eccentric orientation angles were prepared by the least square error method. All the average curves were normalized by dividing the same wave propagated between transducers.

4.3 Transmitted Spectra Produced by PCs with No -Inserts

This section explores time and frequency domain spectra obtained in 2-D PCs with no inserts. The square and triangular arrays in three different host materials are examined in sections 4.3.1, 4.3.2, and 4.3.3.

4.3.1 Aluminum Host

Figure 4-2 (*a*) and (*b*) are the time domain signals obtained using ultrasonic TTT. These signals are shown within the chosen frequency range from 0.9 MHz to 3.2 MHz for the PCs having square and triangular arrays in the aluminum host. Signal analyses were carried out using 32,768 samples (*N*) within the sampling length of 32.8 μs.

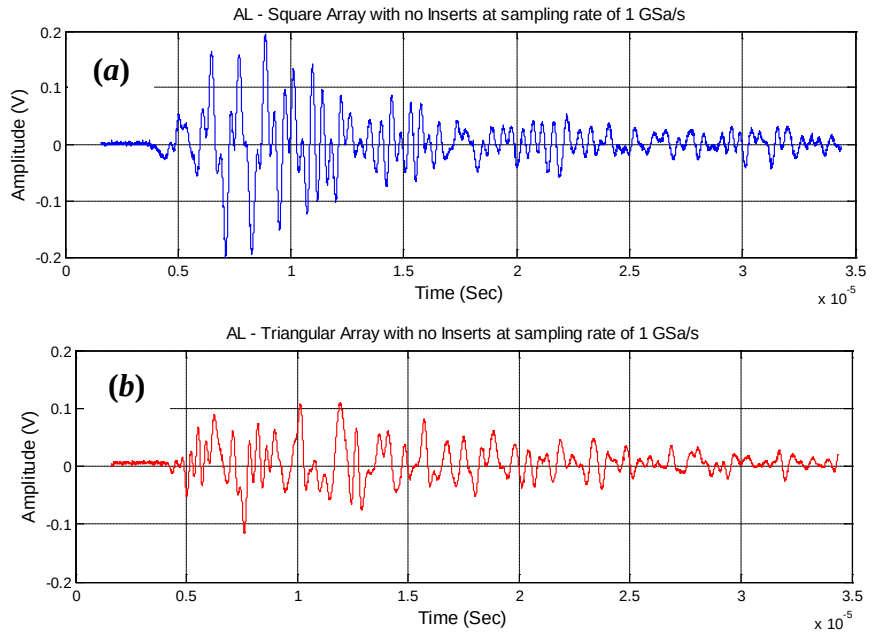

Figure 4-2: Time domain signals obtained in the aluminum host.

It can be seen that the signals transmitted through the aluminum square and triangular array test pieces are strongly attenuated. The normalization of these signals was performed by dividing each spectrum by the transducer spectrum. Figure 4-3 presents the normalized frequency domain spectrum obtained within the bandwidth of 2.3 MHz.

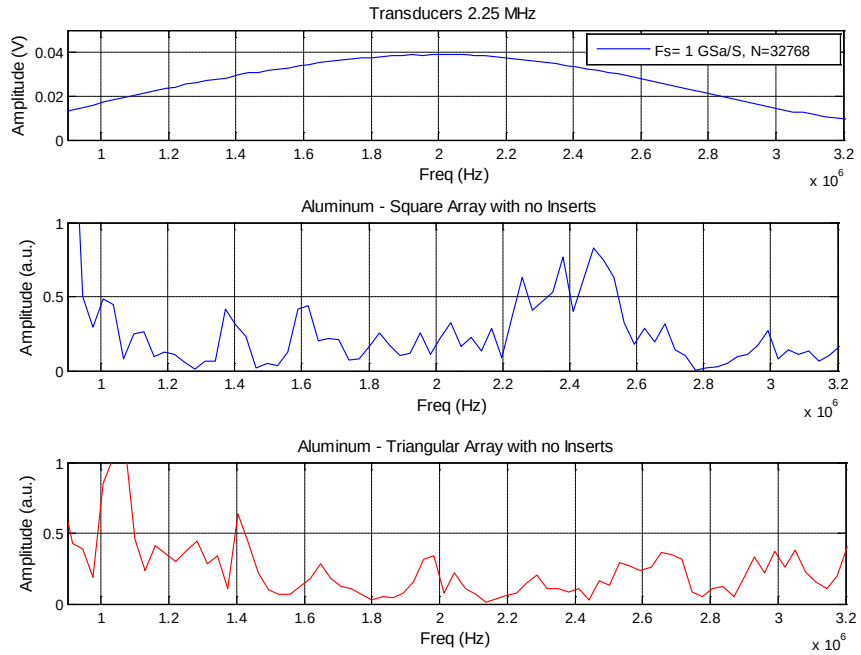

Figure 4-3: Transducer spectrum and normalized amplitude spectra in the aluminum host.

The total frequency index, k is 32,767 and the sampling frequency is 1 GSa/s. Two significant amplitude drops in the square array samples can be observed in the frequency ranges from 0.5 MHz to 1.35 MHz and then from 2.6 MHz to 3.2 MHz. Similarly, in the triangular array samples, the amplitude spectra are closer to zero at the frequencies centered around 1.8 MHz and 2.1 MHz.

4.3.2 Teflon Host

Figure 4-4 shows the time domain signals produced by the PCs in the Teflon host with no inserts. The time domain data collected at the sampling length of 200 μs and at the sampling rate of 100 MSa/s. A strong attenuation of amplitudes can be observed in both square and triangular array samples.

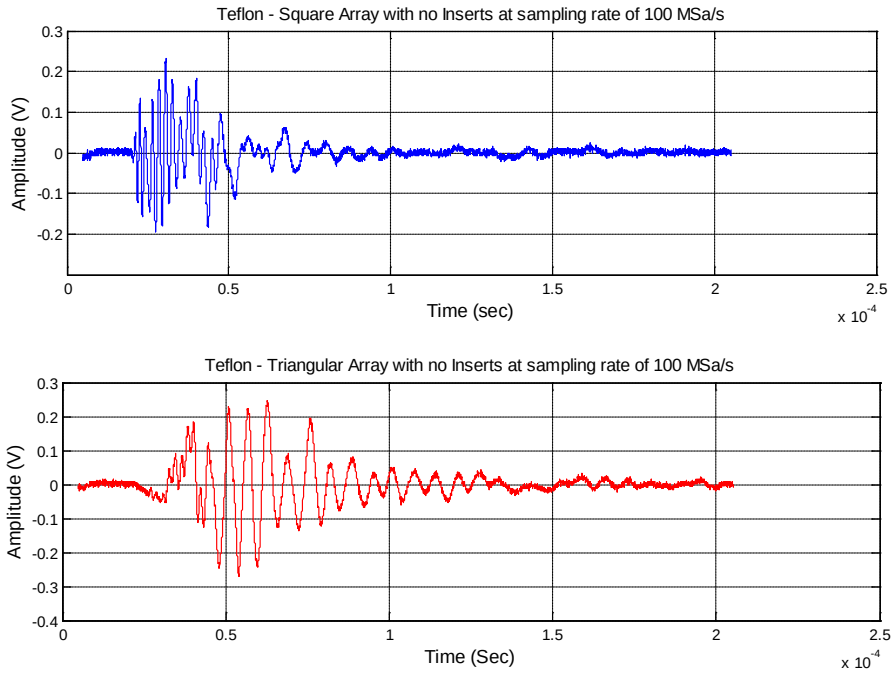

Figure 4-4: Time domain signals obtained in the Teflon host.

The time domain data shown in Figure 4-4 were transformed into frequency domain using FFT algorithm. The normalized frequency domain spectra are shown in Figure 4-5 in the chosen frequency range from 0 MHz to 0.9 MHz.

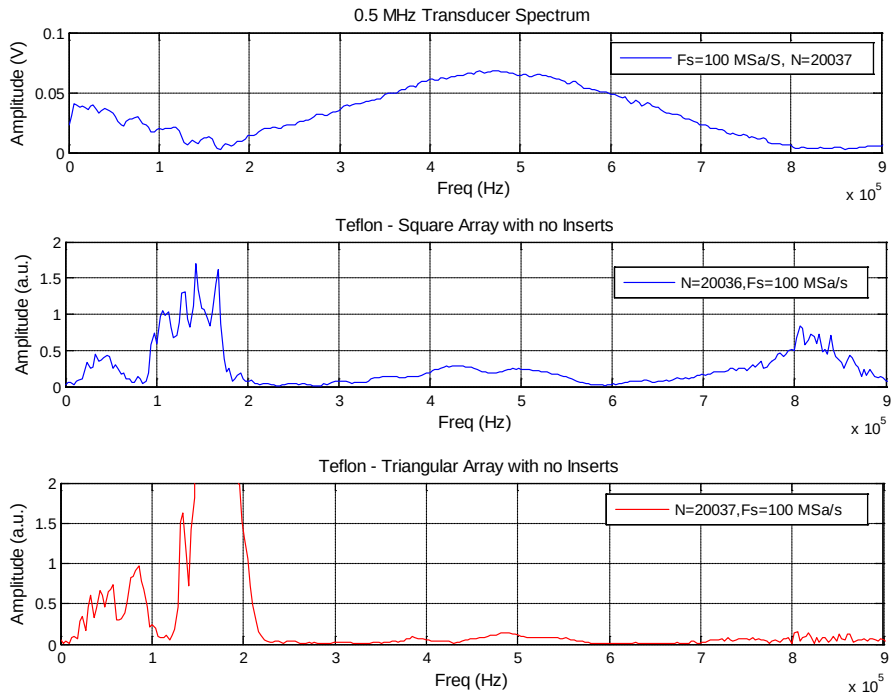

Figure 4-5: Transducer spectrum and normalized amplitude spectra in the Teflon host.

Compared with the square array, the triangular array PCs have a high peak amplitude in the frequency range from 0.1 MHz to 0.2 MHz. This peak again drops significantly around 0.2 MHz. Amplitudes of both samples attenuated in the frequency range from 0.2 MHz to 0.9 MHz.

4.3.3 LDPE Host

The ultrasonic TTT was employed to identify the spectra of square and triangular array samples in the LDPE host. The time domain signals obtained from ultrasonic test are shown in Figure 4-6. The total sampling length and sampling rate are 200 μs and 250 MSa/s respectively. A strong attenuation can be observed for both arrays. Average of the three identical time domain signals was transformed into the frequency domain. The amplitude spectra were observed in the chosen frequency range from 0 MHz to 0.9 MHz. Strong peaks centered at 0.05 MHz for both arrays can be observed as illustrated in Figure 4-7. Compared to the square array, the triangular array sample has a high peak amplitude in the frequency range from 0 MHz to 0.1 MHz. Relative to the peak amplitudes, amplitude of the spectra are decreasing approximately starting at 0.1 MHz and at 0.15 MHz for the square and the triangular array samples respectively. The two samples are attenuated at the frequency range from 0.1 MHz to 0.9 MHz.

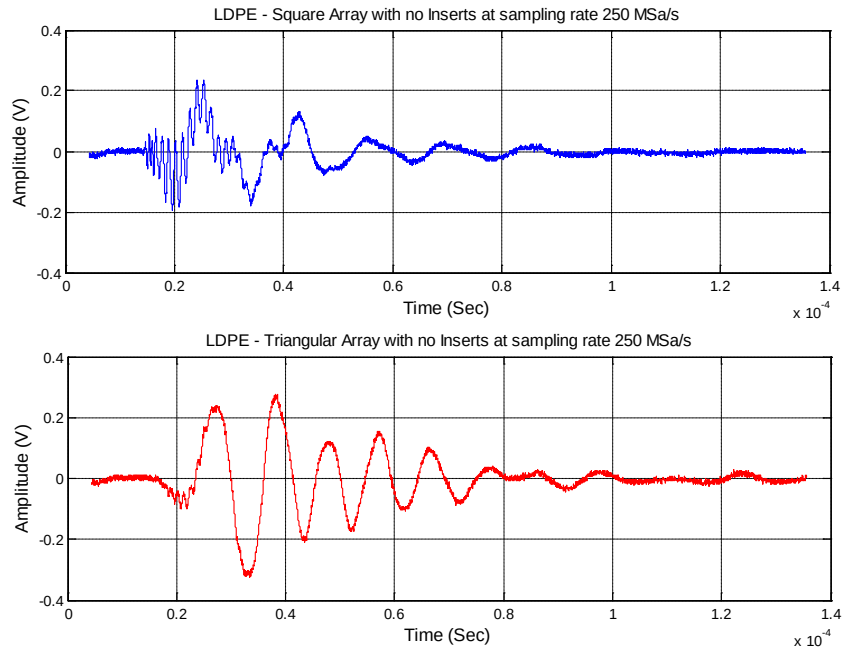

Figure 4-6: Time domain signals obtained in the LDPE host.

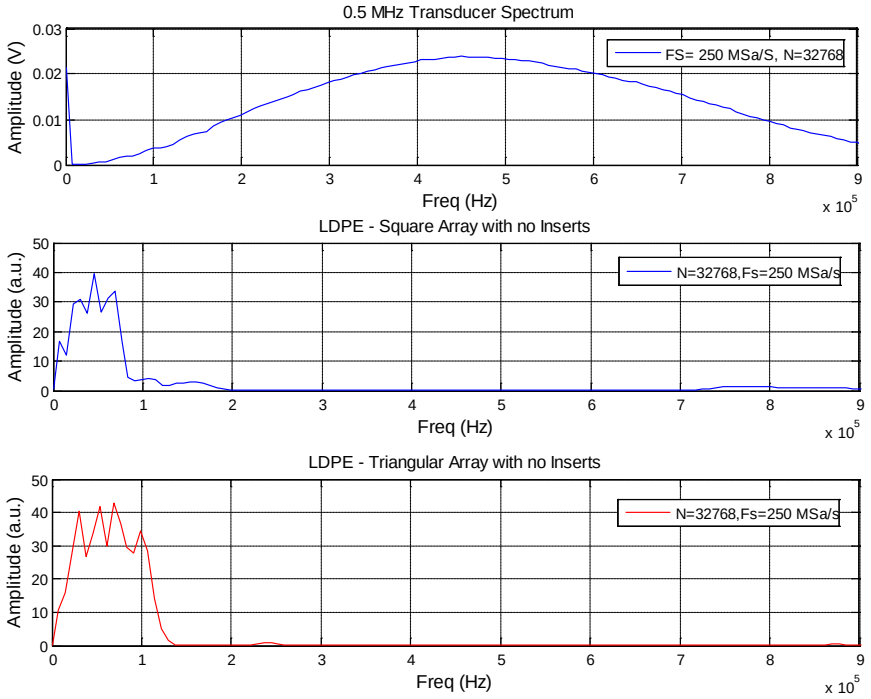

Figure 4-7: Transducer spectrum and normalized amplitude spectra in the LDPE host.

The amplitude spectra can roughly be compared with each phononic material with no inserts. The PCs constructed by arranging hollow circular cylinders in LDPE and Teflon host materials easily attenuate in the ultrasonic testing. The large frequency gaps can readily be observed in LDPE or Teflon hosts compared with the similar PCs made in the aluminum host.

4.4 PCs with Eccentrically Layered Scatterers

The important objective in this experiment was to characterize the influences of eccentricity orientation angles on the transmitted amplitude spectra. This section explains both time domain and frequency domain spectra produced for PCs having eccentrically layered scatterers.

4.4.1 Symmetry of the Test pieces

The PCs having eccentric orientations were tested by sending the ultrasonic wave on one of the sides of the test pieces along X-direction. The direction of the incident ultrasonic wave was reversed by flipping the samples and then tested along the same direction. Figure 4-8 shows typical wave propagation through the test piece. By symmetry of the test pieces, the output signals produced from both sides should be equal. If the samples have prepared without any entrapped air or irregularities in the wax filling, the waves obtained from each side coincide with each other. The spectra obtained from such a test are explained in the remainder of this section.

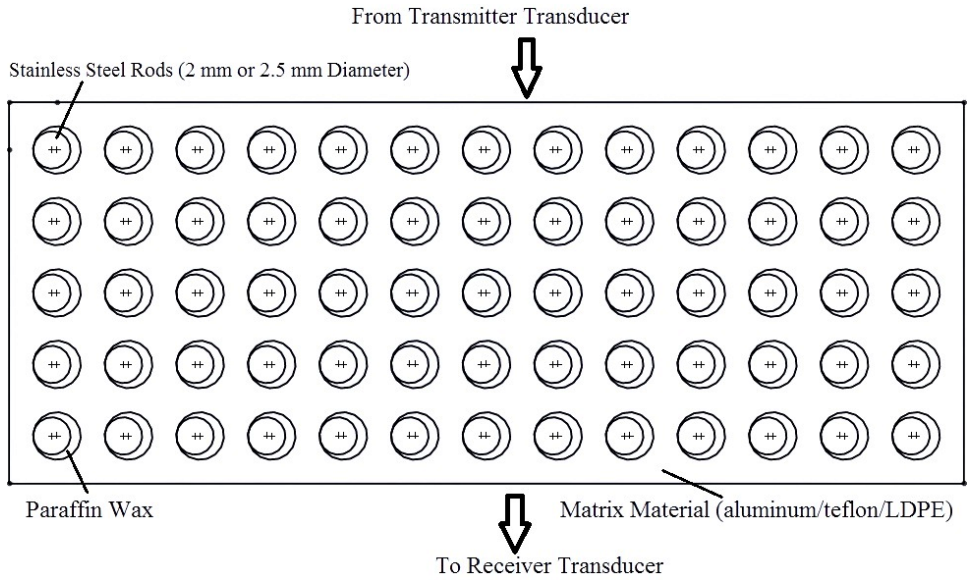

Figure 4-8: Schematic of a square array sample input side (1st side) and output side (2nd side).

4.4.1.1 PCs in the Aluminum Host

The time domain data for PCs in the aluminum host were obtained using 2.25 MHz transducers at the sampling rate of 1 GSa/s. Figure 4-9 shows a comparison of spectra obtained

from triangular and square array scatterers made in the aluminum host. The eccentric orientation angles were chosen arbitrarily as 45 degrees. The Figure 4-9 also includes the different plots for 2 mm and 2.5 mm diameter SS (SS) rods. Both plots have similar number of samples (N=32,768). The frequency domain spectrum is shown in the frequency range from 0.9 MHz to 3.2 MHz.

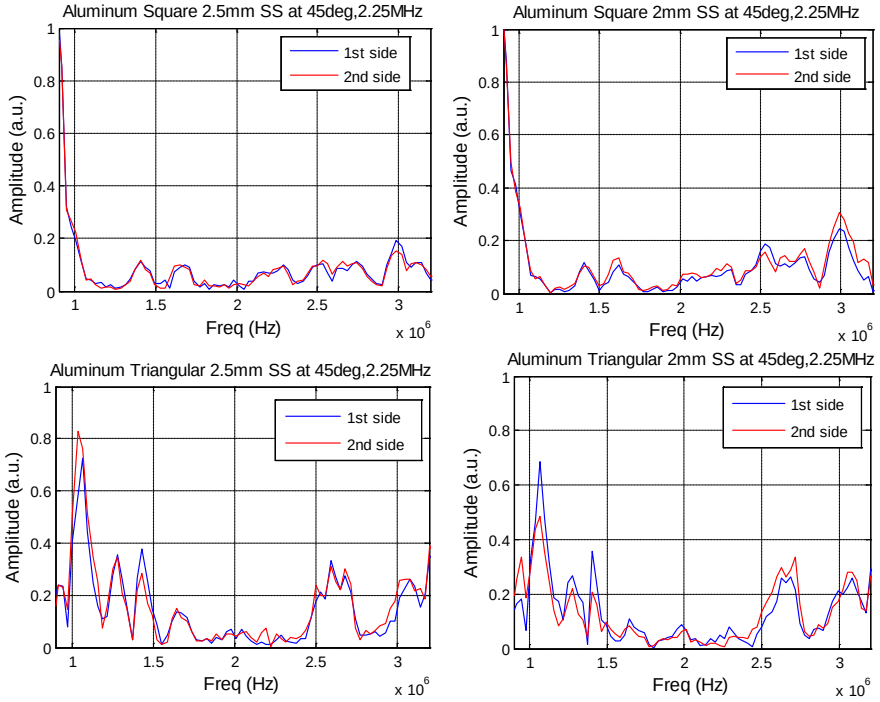

Figure 4-9: Comparison of PCs in the aluminum host along the X-direction.

The output waves of either side of the square arrays coincide each other despite small deviations (see top two graphs of Figure 4-9). Both 2 *mm* and 2.5 *mm* inserts show almost the same pattern in their amplitude spectra. When the frequency is around 1.2 MHz and 1.9 MHz, low amplitudes can be observed for the wave propagation through square array PCs. For the triangular array, a minimum amplitude can be seen approximately from 1.8 MHz to 2.4 MHz (see the bottom two plots of Figure 4-9). Even though the peak heights are different for the triangular arrays, the amplitude spectra show a same pattern along the frequency axis. It can be assumed that the PCs in the aluminum host are perfectly arranged so that the transmitted waves observed from either side along X-direction are comparable.

4.4.1.2 PCs in the Teflon Host

This section describes the ultrasonic wave propagation through the X-direction of the phononic like material composed of eccentricity-layered scatterers in the Teflon host. For the arbitrary chosen eccentric orientation angle of 67.5 *degrees*, the spectra for the square and triangular arrays are shown in the Figure 4-10. Almost all the spectra are similar for each array in spite of the different inserts of 2 *mm* and 2.5 *mm* diameter SS rods. From the spectrum, it can be inferred that the wave propagation is similar even if the direction of the incident ultrasonic wave is reversed.

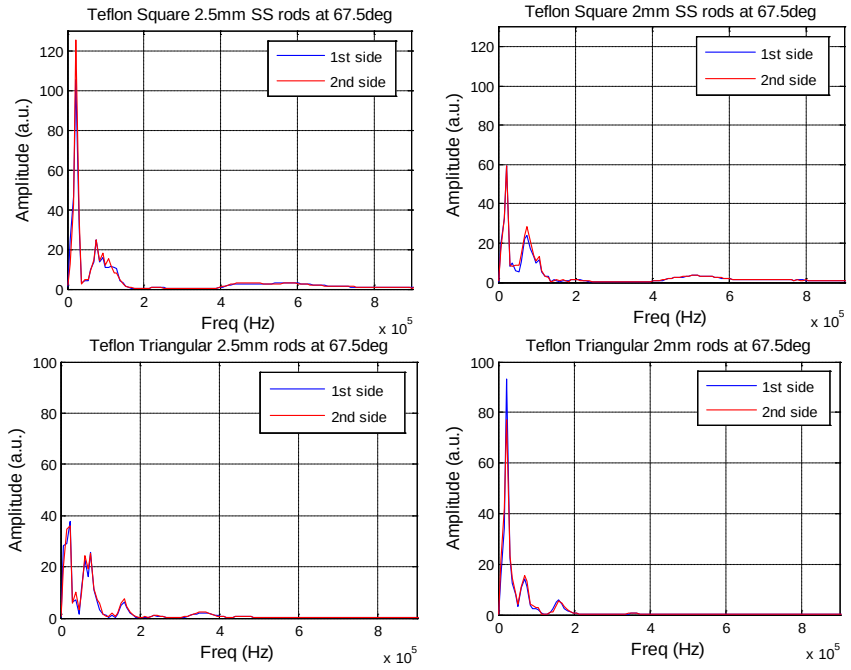

Figure 4-10: Comparison of PCs in the Teflon host along the X-direction.

4.4.1.3 PCs in the LDPE Host

Similar to the test pieces in the Teflon host, test pieces in the LDPE host were also tested using ultrasonic waves. Then the same wave pattern was obtained by interchanging input and output sides. Figure 4-11 shows the time domain data obtained at the sampling frequency of 250 MSa/s.

Spectra produced by the test pieces in the LDPE host coincide each other. The normalized spectra with respect to the transducer spectra are also similar. This implies that the PCs arranged in the LDPE host prepared well for the experiment.

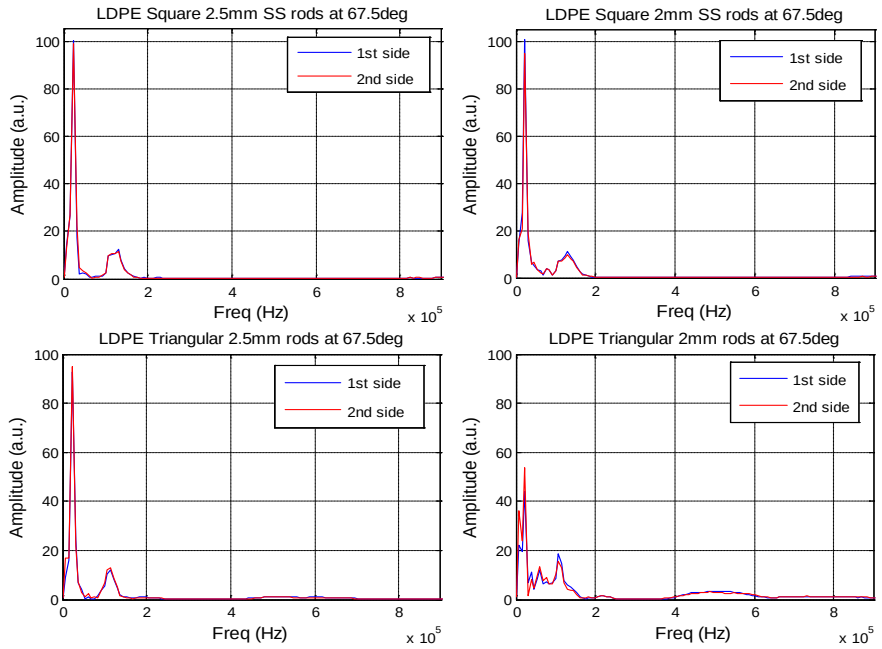

Figure 4-11: Comparison of PCs in the LDPE host along the X-direction.

4.4.2 Comparison of Normalized Spectra

Five identical test samples, with the eccentric orientation angles ranging from 0 degrees to 90 degrees at the increment of 22.5 *degrees*, were tested using ultrasonic TTT. A similar procedure was carried out for the insertion of 2 *mm* and 2.5 *mm* diameter SS rods.

4.4.2.1 PCs in the Aluminum Host

Spectra for each square array scatterers in different eccentric orientation angles are shown in Figure 4-12 and 4-13. The time domain data for Figure 4-12 was obtained using 0.5 MHz transducers at the frequency range from 0.15 to 0.90 MHz. The time domain data for Figure 4-13 was obtained using 2.25 MHz transducers at the frequency range from 0.9 MHz to 3.2 MHz. The frequency domain data for both plots have the sampling rate of 1 GSa/s in the time length of 32.4 μs.

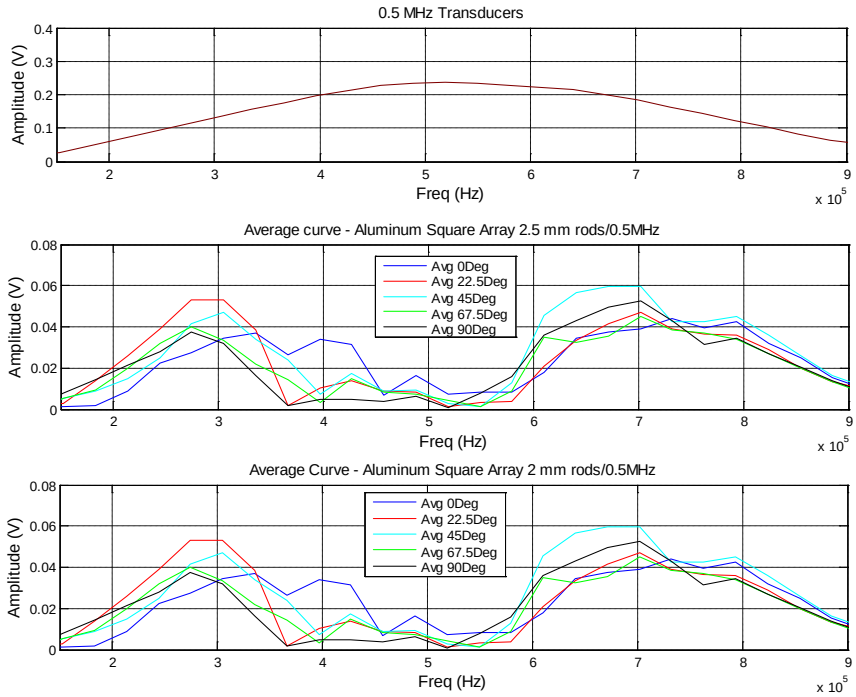

Figure 4-12: Transducer spectrum and amplitude spectra for PCs in the aluminum host.

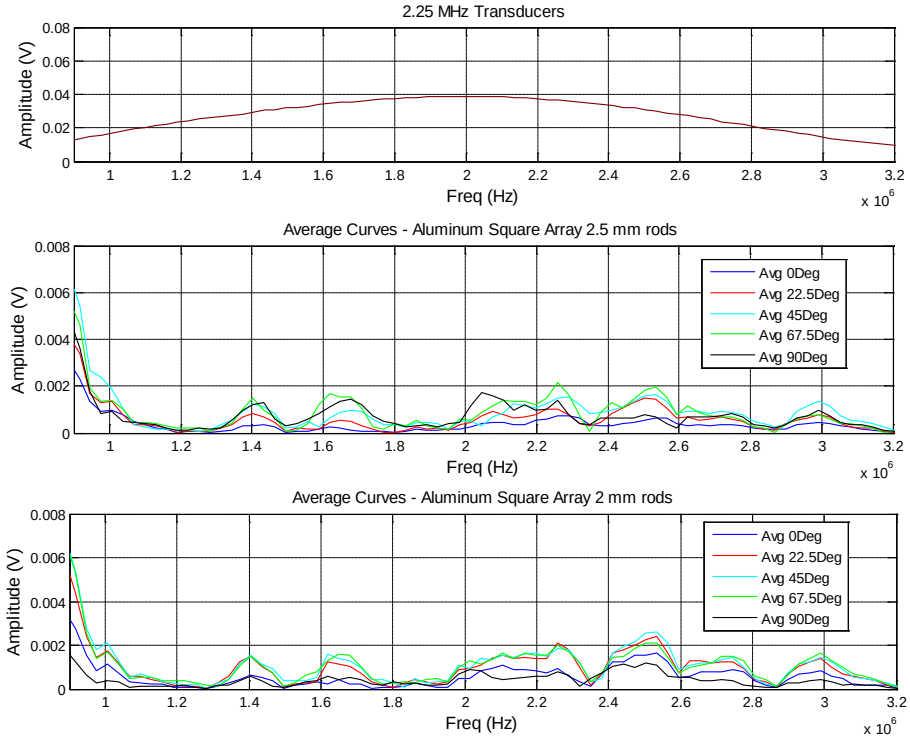

Figure 4-13: Transducer spectrum and amplitude spectra for PCs in the aluminum host.

The spectra shown in Figure 4-12 and 4-13 normalized with respect to the transducer spectra. Figure 4-14 shows the normalized spectra for the square array scatterers in the aluminum

host. The top two plots of the Figure 4-14 shows the spectra in the frequency ranges from 0.15 to 0.9 MHz and from 0.9 to 3.2 MHz with the insertion of wax-coated 2.5 *mm* diameter SS rods. The bottom two plots show the same spectra for the insertion of wax-coated 2 *mm* diameter SS rods. The most noticeable attenuation of amplitudes occurs in the frequency range between 0.9 MHz and 3.2 MHz. In the frequency range from 0.15 to 0.9 MHz, there is an overall trend of high peak amplitudes. Also, due to the different eccentric orientation angles, the amplitudes are significantly varied at the center frequencies of 0.5 MHz and 2.25 MHz. Both 2 *mm* and 2.5*mm* inserts do not show much difference in their amplitude spectra.

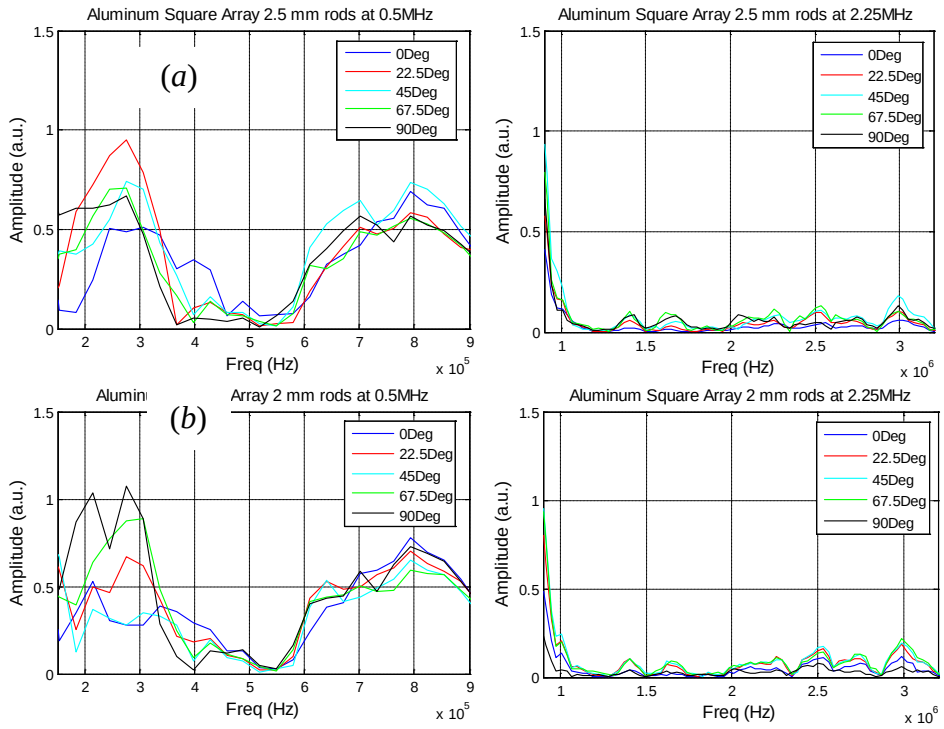

Figure 4-14 : Amplitude spectra for PCs in the aluminum host.

The amplitude spectra for the PCs having triangular array scatterers are shown in Figure 4-15 and Figure 4-16. Both plots have the sampling rate of 1 *GSa/s* within the time length of 32.4 *μs*. The time domain data for producing Figure 4-15 was obtained using the 0.5 MHz transducers in the frequency ranges of from 0.15 to 0.9 MHz. The time domain data for Figure 4-16 was obtained using the 2.25 MHz transducers in the frequency range from 0.9 MHz to 3.2 MHz.

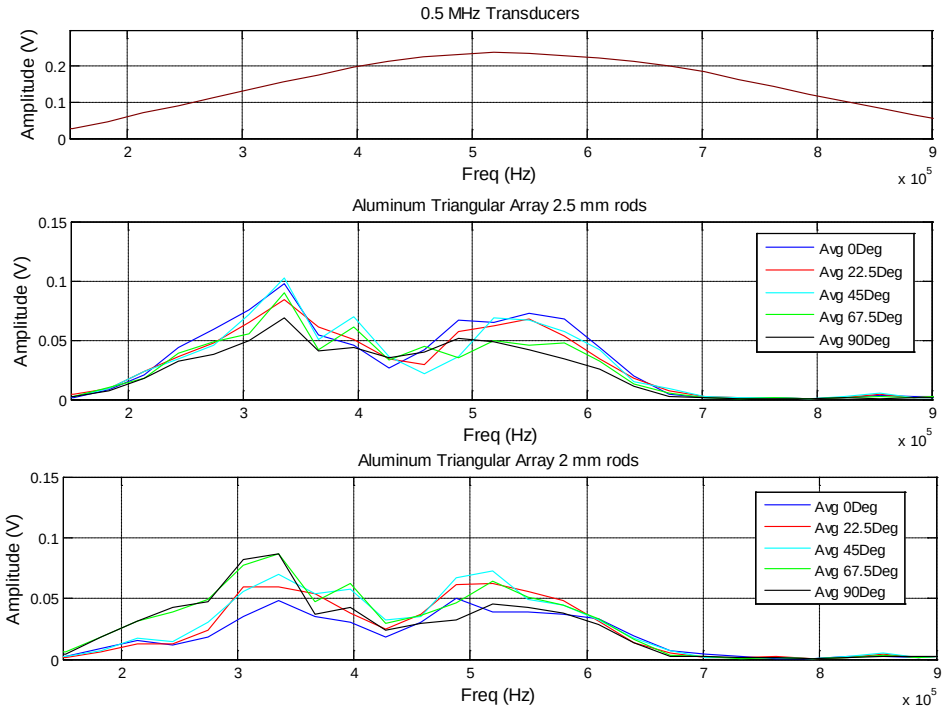

Figure 4-15: Transducer spectrum and amplitude spectra for PCs in the aluminum host.

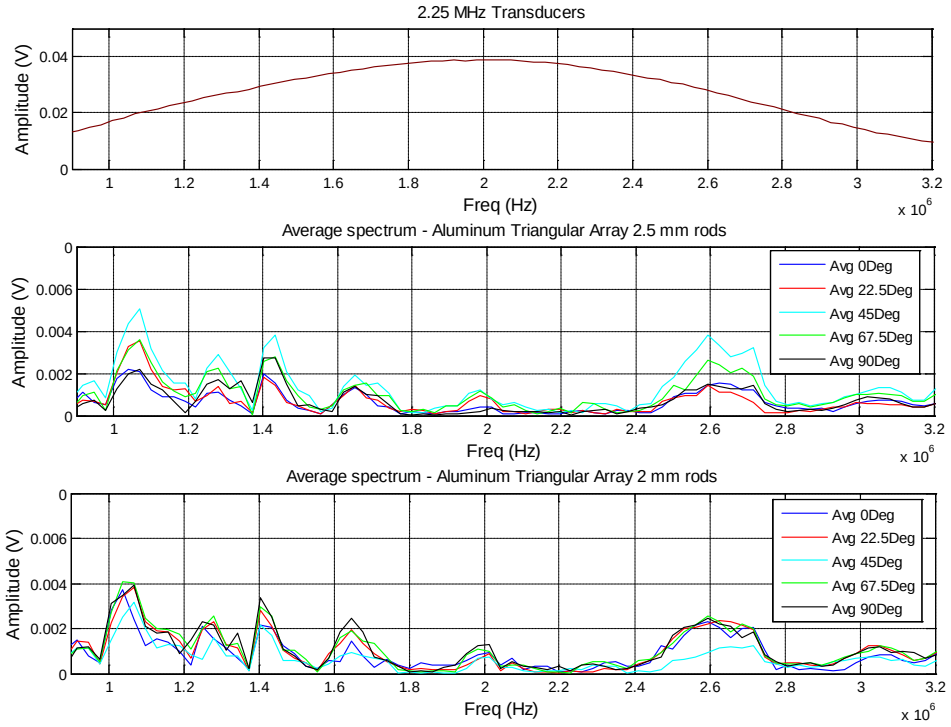

Figure 4-16: Transducer spectrum and amplitude spectra for PCs in the aluminum host.

The normalized amplitude spectra for the triangular array layered scatterers in the aluminum host are shown in Figure 4-17. The top two plots in Figure 4-17 show the spectra in the frequency range from 0.15 to 0.9 MHz and from 0.9 to 3.2 MHz for the insertion of 2.5 *mm*

diameter SS rods. The bottom two plots of Figure 4-17 show the same spectrum for the insertion of wax-coated 2 *mm* diameter SS rods. Attenuation of amplitudes can be seen in the frequency range between 0.9 MHz and 3.2 MHz. Also, in the frequency range from 0.15 to 0.7 MHz, there is an overall trend of high peak amplitudes.

Comparing both spectra for the square and triangular periodicity, a similar behavior can be observed in the frequency domains. Compared to the square array, the triangular array sample does not show a significant loss of amplitudes at the frequency range centered around 0.5 MHz. Instead, it shows a drop in the amplitude at the frequency 0.7 MHz. Also, the overall amplitude of the triangular symmetry is much less than that of the square arrays. The PCs with 2.5 *mm* diameter paraffin-coated SS rods attenuated more than 2 *mm* inserts. This behavior is common for both square and triangular arrays in the aluminum host.

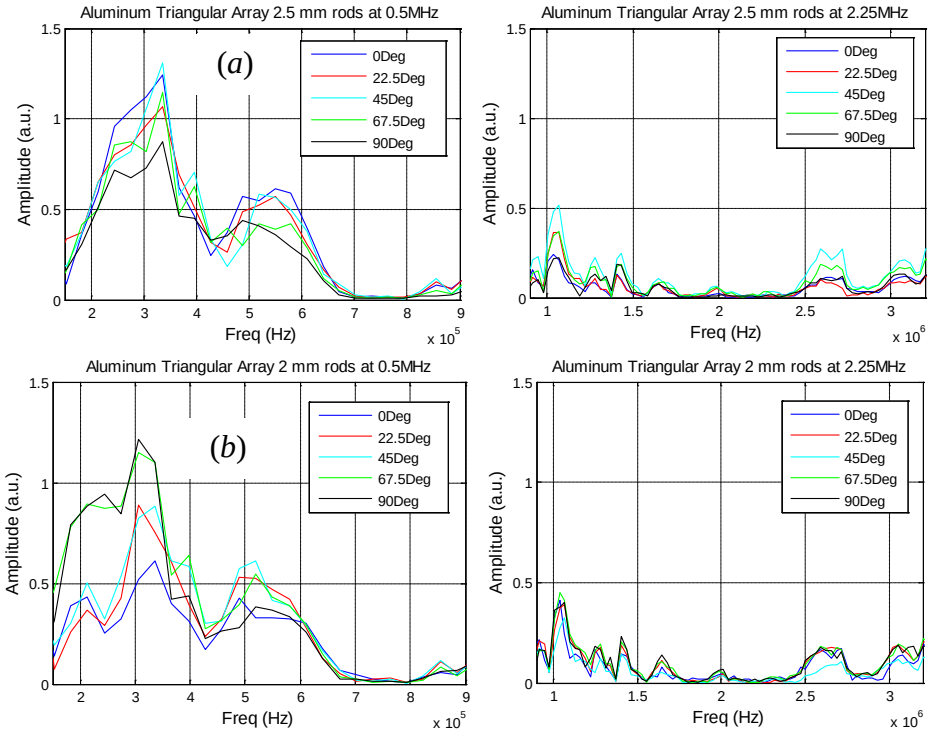

Figure 4-17 : Transducer spectrum and amplitude spectra for PCs in the aluminum host.

On the other hand, the phononic Bragg predicted band gaps can be computed using eqn. (3). Table 4-1 presents the Bragg-scattered band gap frequencies in the aluminum host in the range from 0.15 MHz to 3.2 MHz.

Table 4-1: Expected center frequencies of the band gaps for the aluminum host according to the Bragg theory

Material	Band gap number, *n*	Centre frequency of the gap [MHz]
Aluminum [Lattice parameter, 3.175 *mm* and P-wave velocity 6299 ms^{-1}]	1	0.99
	2	1.98
	3	2.98
	4	3.97

4.4.2.2 PCs in the Teflon Host

At least three identical PCs in the Teflon host at five different eccentric orientation angles were tested using ultrasonic TTT. The time domain data obtained at the sampling frequency of 250 MSa/s within the time length of 124 μs. The average curves for each square array orientation angle in the Teflon host are shown in Figure 4-18. The upper plot of Figure 4-18 shows the spectrum for the transducers with the center frequency of 0.5 MHz. When the eccentricity orientation angles were changed, the amplitudes of the spectra are altered. This can be observed for both 2 *mm* and 2.5 *mm* diameter SS rods in the Teflon host. Compared with the insertion of 2 *mm* SS rods, 2.5 *mm* SS rods make a greater variation in the amplitude spectrum especially at the frequency centered around 0.5 MHz.

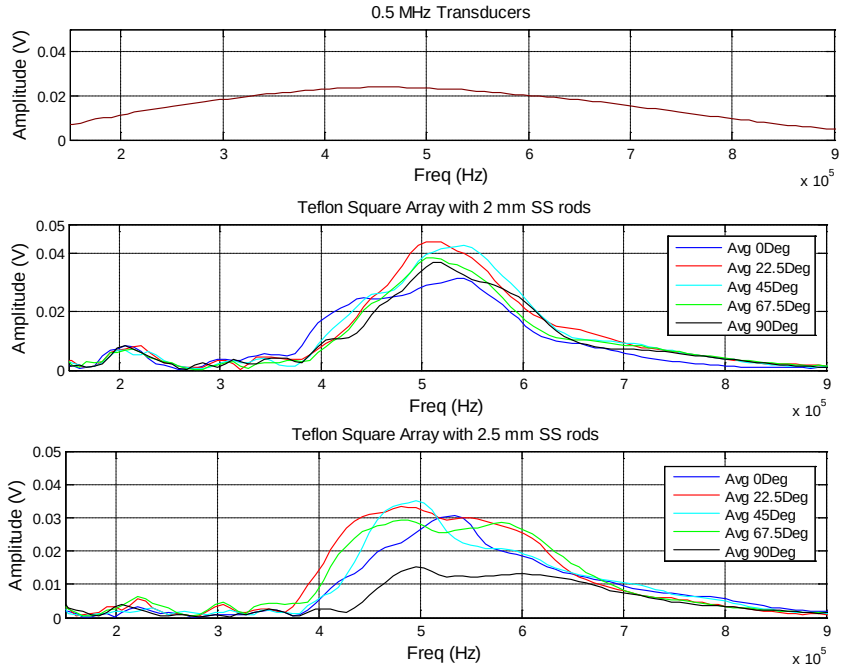

Figure 4-18: Transducer spectrum and amplitude spectra for PCs in the Teflon host.

Figure 4-19 shows the normalized spectra for the PCs made in the Teflon host in square array.

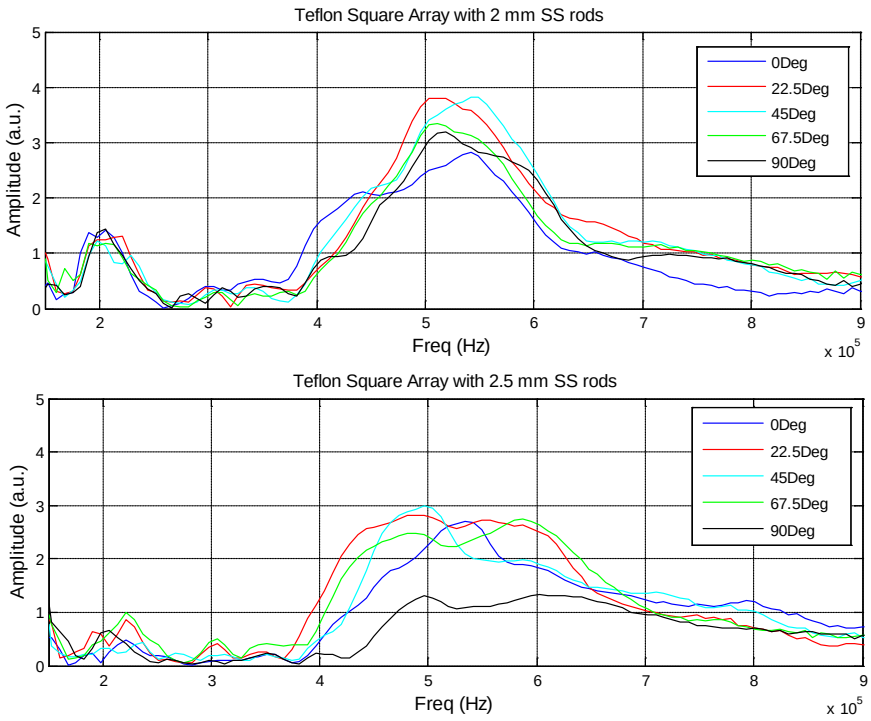

Figure 4-19: Normalized amplitude spectra for the PCs in square array in the Teflon host.

As depicted by the Figure 4-19, relative strength of the amplitudes are significantly altered when the frequency is centered around 0.5 MHz due to the presence of various eccentric orientation of the layered scatterers. If the spectrum is enlarged a little further, the influence of the eccentricity orientation angle on the band gaps can be observed clearly. However, the noise of the sound will make the signal amplitude imperfect if the spectrum is enlarged further. Also, the different eccentricity orientation angles show certain rise and falls only at certain frequencies for almost every PC made in the Teflon host.

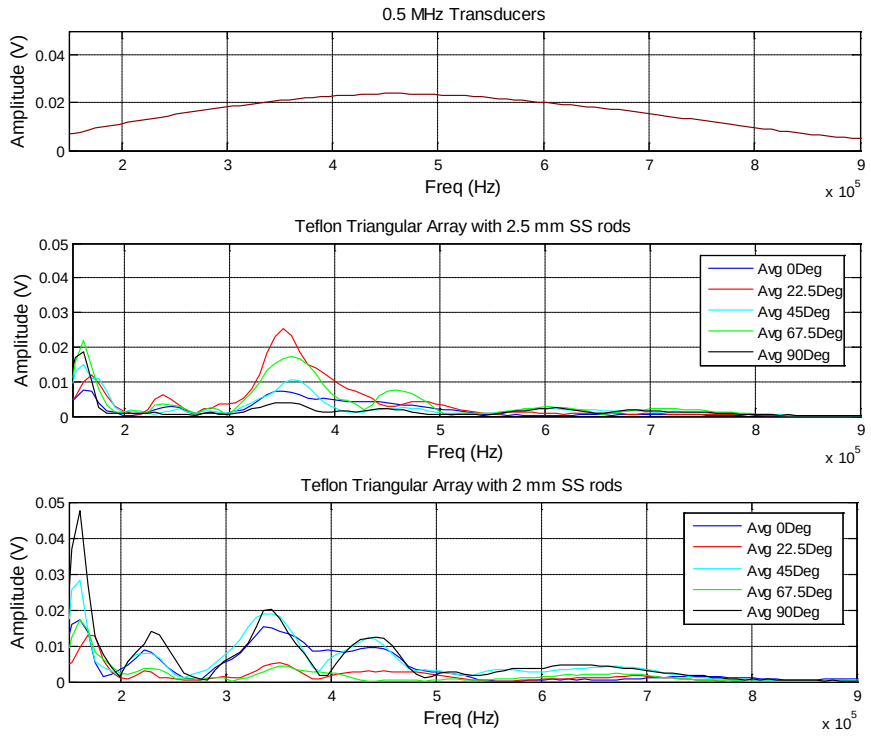

Figure 4-20: Transducer spectrum and amplitude spectra for PCs in the Teflon host.

Figure 4-20 shows the average of the each orientation angle produced by the triangular array PCs in the Teflon host. The upper plot shows the spectrum for the transducers with the center frequency of 0.5 MHz. The lower two plots show the average spectra for the PCs with the insertion of 2.5 *mm* SS rods and 2 *mm* SS rods. The time domain signals for both plots were obtained at the sampling rate of 250 MSa/s within the time length of 124 μs. Figure 4-21 shows the normalized spectra of triangular array PCs in the Teflon host. Similar to the square array, the triangular array spectrum shows a significant change of the relative strength of the amplitudes when the frequency is around 0.5 MHz.

Compared with the amplitude spectra in the square array PCs, the triangular array PCs have a wide frequency range in which the amplitudes of the spectra tend to zero. This kind of attenuation can be observed especially in the frequency range between 0.5 MHz and 0.9 MHz. Compared with the square array, the overall amplitude-drop in the triangular array is relatively high. Although the scatterer diameters are changed from 2 *mm* to 2.5 *mm*, PCs in both triangular and square arrays do not show any significant change.

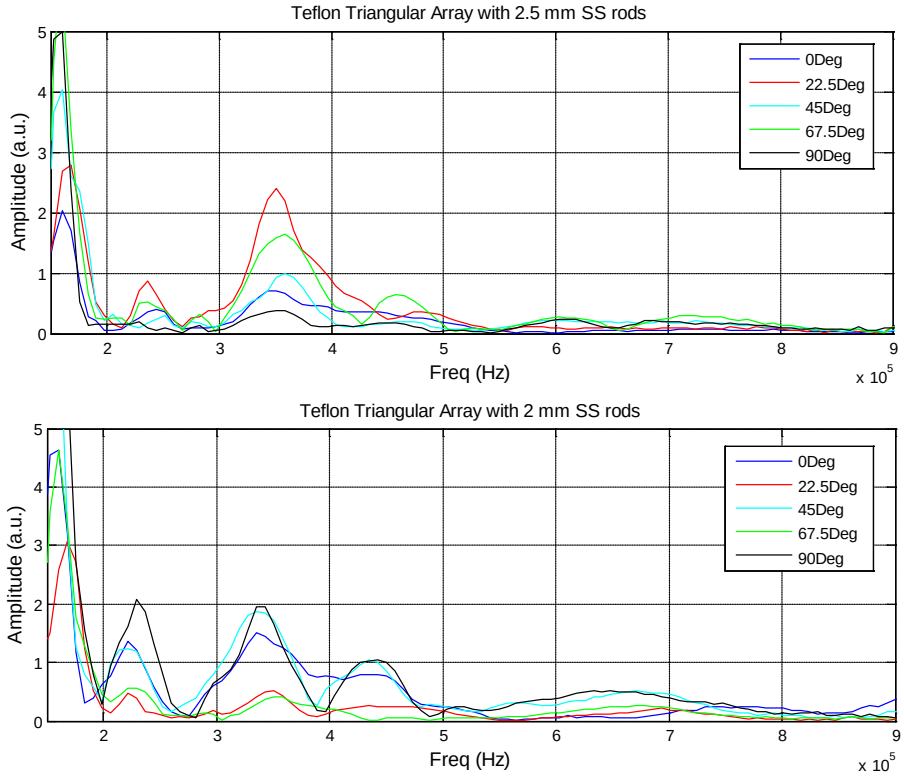

Figure 4-21: Normalized amplitude spectra for PCs in triangular array in the Teflon host.

If Bragg-scattered band gaps are expected in the Teflon host, there should be at least three gaps within the chosen frequency range from 0.15 MHz to 0.9 MHz (see Table 4-2).

Table 4-2: Expected center frequencies of Bragg-predicted band gaps for the Teflon host

Material	Band gap number, n	Centre frequency of the gap [MHz]
Teflon [Lattice parameter, 3.175 *mm*, P-wave velocity 1380 ms^{-1}]	1	0.22
	2	0.43
	3	0.65
	4	0.87

4.4.2.3 PCs in the LDPE Host

The time domain data for the PCs made in the LDPE host were obtained at the sampling frequency of 250 MSa/s within the time length of 124 μs. Spectra produced for PCs having 2 *mm* and 2.5 mm diameter SS rods in the square arrays are shown in Figure 4-22. It can be inferred that the square array 2 *mm* and 2.5 *mm* SS rods have significantly changed the amplitudes of the signals.

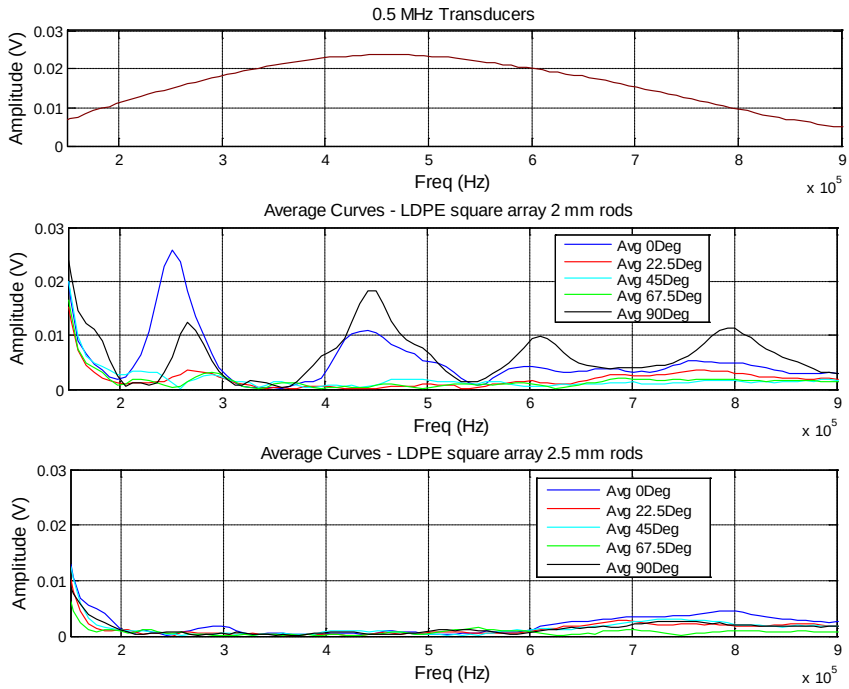

Figure 4-22: Transducer spectrum and amplitude spectra for PCs in the LDPE host

Figure 4-23 shows the normalized spectra at the chosen frequency range from 0.15 to 0.9 MHz for the PCs having two sets of diameters of SS rods.

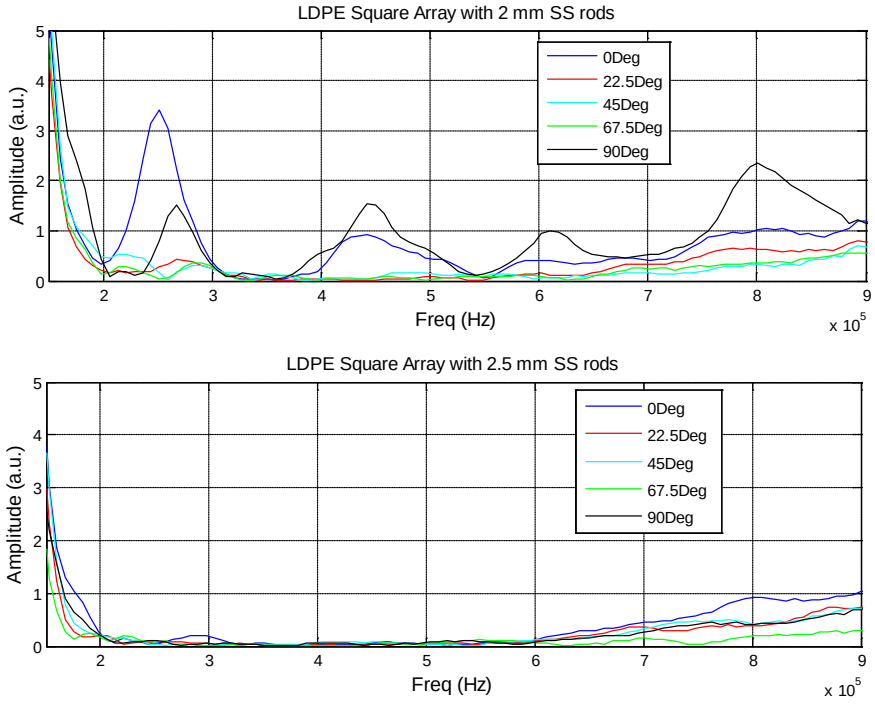

Figure 4-23: Normalized amplitude spectra for the PCs in square array in the LDPE host.

Compared with the PCs with 2 *mm* diameter SS rods, PCs with 2.5 *mm* SS rods are highly attenuated at the frequency range from 0.15 MHz to 0.9 MHz. The relative strengths of signal amplitudes are also significantly influenced by the eccentric orientations of the layered scatterers. This can be clearly seen at the frequency range centered at 0.5 MHz. Also the width of the attenuation frequency gap is wider for the presence of 2.5 *mm* SS rods than 2 *mm* SS rods.

Similar to the square arrays, the amplitude spectra were obtained for the triangular array test pieces having 2 *mm* and 2.5 *mm* diameter paraffin-coated SS rods. Figure 4-24 shows spectra produced for each eccentric orientation angles. The time domain data obtained at the sampling rate of 250 *MSa/s* within the time length of 124 μs. It can be observed in Figure 4-24 that the presence of eccentric orientation has altered the relative strengths of signal amplitudes when the frequency is centered around 0.5 MHz.

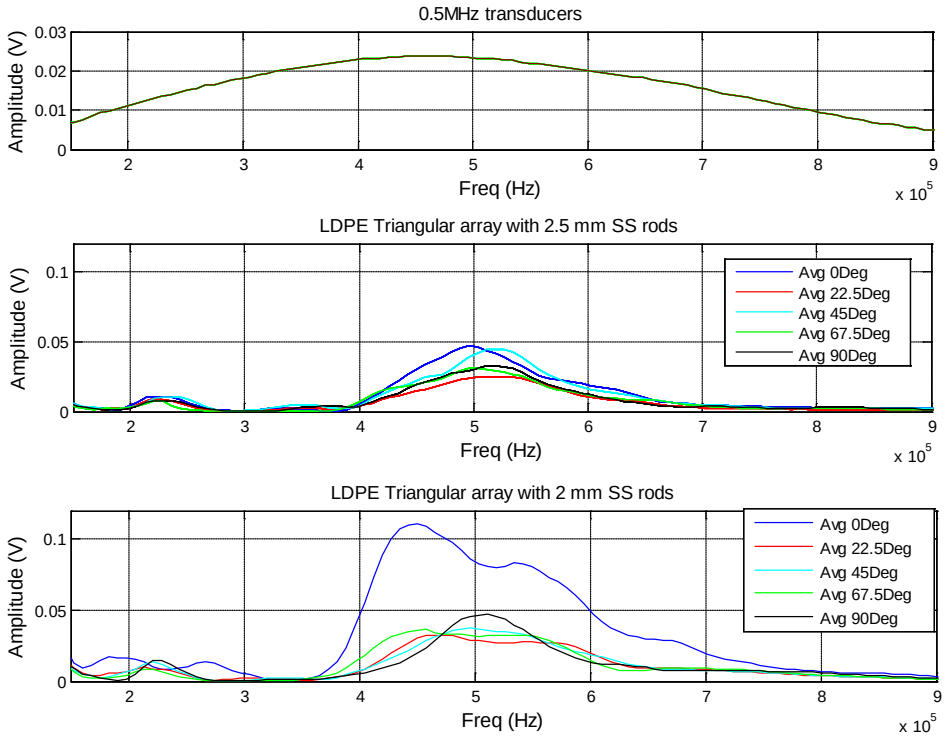

Figure 4-24 : Transducer spectrum and amplitude spectra for PCs in the LDPE host.

The normalized spectra for the PCs in the LDPE host are illustrated in Figure 4-25. The upper and lower plots show the spectra obtained with the insertion of 2.5 *mm* and 2 *mm* SS rods respectively.

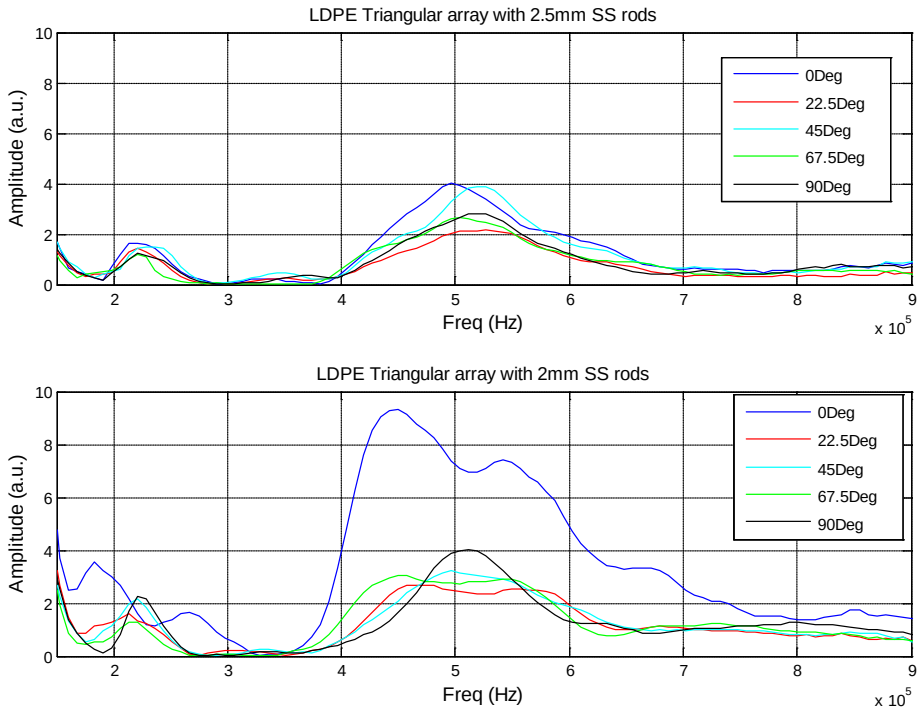

Figure 4-25 : Normalized amplitude spectra for the PCs in triangular array in the LDPE host

Observing the results presented in Figure 4-25, the normalized spectra show the attenuation of amplitudes at the frequency range between 0.15 MHz and 0.9 MHz. Compared with the PCs having square array scatterers, PCs having triangular array scatterers significantly altered the relative strengths of amplitudes. It can also be noted that the amplitude spectrum is changed due to the presence of different eccentric orientation of the scatterers.

PCs in the LDPE host having triangular and square arrays show a significant change in their amplitude spectra. This implies that the geometry has significantly influenced on the transmitted spectra. If the Bragg-scattered phononic band gaps are expected in an ideal LDPE host, at least one significant gap should exist in the frequency range between 0.15 MHz and 0.9 MHz. The Bragg-predicted band gaps for the ideal LDPE host are given in Table 4-3.

Table 4-3: Expected center frequencies of the Bragg predicted band gaps for the LDPE host

Material	**Band gap number, *n***	**Centre frequency of the gap [*MHz*]**
LDPE [Lattice parameter, 3.175 *mm*, P-wave velocity 1970 ms^{-1}]	1	0.31
	2	0.62
	3	0.93

4.5 Discussion

In this experiment, inhomogeneous structures were constructed by incorporating materials having different elastic modulus and densities. Different materials, which were used to construct PCs in this experiment have large contrast in their acoustic properties. The acoustic properties of materials used in the experiment are presented in Table 4-4.

Table 4-4: Acoustic properties of materials [17, 18, 38].

Parameter	Stainless Steel	Aluminum 6061-T6	Teflon	LDPE	Paraffin wax	Air
Density [kg/m^3]	7780	2799	2200	940	900	1.23
P–wave velocity [m/s]	5985	6299.2	1380	1970	3199	340
S–wave velocity [m/s]	3199	3110				0
Lames Constants (λ,μ) and Young's Modulus E [GPa]	λ = 119.4 - 210.6	E=72				λ =1.42x10^{-4}
	μ = 79.6 - 81.4	λ=41, μ =25				

The location and the width of the band gaps were largely established by the large difference in the elastic constant, the mass density, and the geometry of the structure. The reasons can be explained as follows:

By changing the Lame's constants (λ and μ) periodically, the speed of sound through the material is varied. The PCs with layered scatterers in LDPE or Teflon hosts have large contrast in their velocity and density ratios compared with the similar PCs constructed in aluminum hosts. Due to the presence of large acoustic mismatches, formation of boundaries within the PCs can be anticipated. When the ultrasonic wave propagates through such boundaries, the scattering is possible. Consequently, certain frequency band gaps in which materials impede the propagation of waves are desirable.

On the other hand, the triangular and square array samples show peak amplitudes at different locations. Periodically arranged paraffin-coated steel rods can act as scatterers. When the eccentric orientation angles of the layered scatterers are changed, the amplitudes of the spectra also varied significantly. However, the trends of such changes are unpredictable from the amplitude spectra. The only thing that could be predicted is that the relative strengths of the amplitudes altered or shifted at certain frequency ranges due to the eccentric orientation of the scatterers. By means of the eccentricity in the paraffin-coated SS rods, the angle between an incident wave and the inner diameter of the SS rods (scatterers) can be changed. These scatterers

can readily attenuate the ultrasound at certain frequencies. The inner diameter of the SS rods was chosen to be comparable to the wave length ultrasonic signal. Therefore, by varying the inner radius of the SS rods, only the mass of the scatterers is varied. The frequency dependent amplitude spectrums could be observed due to the presence of various eccentric orientation angles. The 2.5 *mm* diameter paraffin-coated SS rods made the PCs more attenuated than that of 2 *mm* inserts. This behavior is observed in both square and triangular lattice structures. In this experiment, fixed band gaps were created using three different phononic like materials. Therefore, lattice parameter does not change the frequency responses of the amplitude spectra. Within the chosen frequency ranges, the change of the relative strengths of the signals could be observed significantly. Therefore, the scattering process can be assumed to be influenced by the changes in the geometrical parameters such as the eccentric orientation angle and the inner radius of the scatterers.

Compared with the square array PCs, triangular array PCs are more attenuated. This behavior is common for the PCs made in the aluminum, Teflon, and LDPE hosts. This can be explained as follows: The diameter of the cylindrical holes (*D*) was 0.125 *inch* and the lattice parameter (*a*) of each array was computed as 0.1875 *inch*. Concerning 2-D square and triangular arrays, the areas of an equilateral triangle A_T and a square A_s can be computed as

$$A_T = \frac{1}{2} \times a \times \cos 30 \times \frac{a}{2} = 7.612 \times 10^{-3} inch^2 \tag{43}$$

$$A_S = a \times a = 0.035 inch^2 \tag{44}$$

As the triangular array samples have relatively small areas, the PCs in triangular array are closely packed compared with the PCs having square array scatterers. In this experiment, there are two filling ratios for the 2-D PCs in square and triangular arrays. Filling ratios for the square lattice [40, 55] and triangular lattice [19] were computed using eqn. (45) and (46). Compared with the square array, the triangular array samples possess a high filling ratio. Therefore, the triangular array samples are more inhomogeneous. As a result, they are more attenuating than that of square array samples.

$$Filling\ Ratio\left(Square\ Lattice\right) = \frac{\pi D^2}{4a} \approx 0.1 \tag{45}$$

$$Filling\ Ratio\left(Triangular\ Lattice\right) = \frac{\pi D^2}{2a^2\sqrt{2}} \approx 0.5 \tag{46}$$

Table 4-5: Experimentally observed 1st largest frequency band gaps in different PCs

Matrix materials for PC	Experimentally observed approximate 1st Band gap [KHz]				Bragg predicted 1st band gap [KHz]
	Square array scatterers		Triangular array scatterers		
	2 *mm* steel rods	2.5 *mm* steel rods	2 *mm* steel rods	2.5 *mm* steel rods	
Aluminum	400	400	700	700	990
Teflon	150	50	100	50	220
LDPE	150	50	150	50	310

The attenuation of the amplitudes was observed at low frequencies than those predicted by Bragg theories. Assuming Bragg-scattered frequency band gaps are existed in each host, the first significant amplitudes, which are closer to the frequency axis, can be tabulated as in Table 4-5. It can be observed that hard scatterers in low density host materials make the PCs more attenuated at lower frequencies.

The study of the elastic wave propagation in the inhomogeneous media is challenging due to the combined influence of the longitudinal and transverse wave forms. However, in this experiment, a great deal of information about the elastic response of the samples between transmitter and receiver transducers could be obtained using ultrasonic TTT. Whenever the transmitter and the receiver transducer positions are not aligned with each other, there can be a loss of signal energy that flew in the direction of the receiver transducer. Hence, inherent errors due to the misalignments can be expected in ultrasonic TTT. Near field measurements of the transmitted waves were carried out in the ultrasonic test. Hence, relatively low thickness of the specimen could maintain in the ultrasonic testing. Obviously, this experiment introduces the fabrication of phononic materials with relatively small geometry and dimensions.

4.6 Conclusion

2-D phononic materials having eccentrically layered scatterers in aluminum, Teflon, and LDPE hosts were constructed using simple fabrication methods. Great deal of information about those materials could be obtained using ultrasonic through transmission test. The ability of making frequency gaps due to the ultrasound attenuation was experimentally demonstrated using FFT algorithm in MATLAB. The effect of the geometry and the influence of material properties on the phononic band gaps were observed in each test piece. It is challenging to perform a

comparison of each phononic material since they have large contrast in the acoustic properties. Roughly, it is inferred that the largest gaps are observed for high density scatterers in low density host materials. Rest of the conclusion is summarized as follows:

1. The changes in the frequency dependent amplitudes could be observed due to the presence of various eccentric orientation angles. When the wave length of the waves is comparable with the outer diameter of the scatterers, the amplitude spectra are highly sensitive to the eccentric orientation angles at the chosen frequencies, which are the centre frequencies of transducers.
2. Due to the presence of periodic structures and the large acoustic mismatches in the PCs, the attenuation of amplitudes was observed at certain frequency ranges. Compared with the same PCs having square array scatterers, the relative strengths of the signals produced by triangular array scatterers are small.
3. When the internal scatterer diameters are increased, the attenuation of the amplitudes is also increased for the PCs made in each host. The frequency gaps are observed for high density scatterers in low density host materials at low frequencies than those predicted by Bragg's law. Resonant frequencies observed in the frequencies are much below the center frequencies (0.5 MHz and 2.25 MHz) of the transducers.
4. PCs are able to control sounds and vibrations within the chosen frequency ranges. The frequency dependent attenuation leads us to find some applications such as sound filters and vibration controllers at the chosen frequency ranges.
5. Numerical results are not yet developed for the layered scatterers in the chosen frequency ranges. Therefore, the unique results obtained in the experiment can be used as the initial data in the future numerical computations.

References

[1]. A. Khelif, A. Choujaa, S. Benchabane, B. Djafari-Rouhani, V. Laude, Guiding and bending of acoustic waves in highly confined phononic crystal waveguides, Appl. Phys. Lett., Vol. 84, No. 22, pp 4400 - 4402 (2004)

[2]. A. Khelif, B. Djafari-Rouhani, J. O. Vasseur, P. A. Deymier, Ph. Lambin, L. Dobrzynski, Transmittivity through straight and stublike waveguides in a two-dimensional phononic crystal, Physical Review B, Vol 65, pp 174308-1 – 174308-5 (2002)

[3]. A. Khelif, P. A. Deymier, B. Djafari-Rouhani, J. O. Vasseur, L. Dobrzynski, Two Dimensional Phononic Crystal with Tunable Narrow Pass Band: Application to a Waveguide with Selective Frequency, J. Appl. Phys., Vol. 94, No. 3, pp 1308 - 1311(2003)
[4]. A. Khelif, A. Choujaa, B. Djafari-Rouhani, M. Wilm, S. Ballandras, V. Laude, Trapping and guiding of acoustic waves by defect modes in a full-band-gap ultrasonic crystal, Physical Review B Vol. 68, pp 214301 (2003)
[5]. A. Q. Chen, S. Freear, D. M. J. Cowell, Measurement of Liquid Content using Ultrasound Attenuation, 5th World Congress on Industrial Process Tomography, Bergen, Norway, pp 820 – 826()
[6]. A. Sukhovich, L. Jing, J. H. Page, Negative Refraction and Focusing of Ultrasound in Two-Dimensional Phononic Crystals, Physical Review Letters B, Vol 77, pp 014301-1 – 014301-9 (2008)
[7]. B. C. Gupta, Z. Ye, Theoretical Analysis of the Focusing of Acoustic Waves by Two Dimensional Sonic Crystals, Physical Review E, Vol 67, pp 036603-1 – 036603-6 (2003)
[8]. C. Goffaux, J. S. Dehesa, Two-dimensional Phononic Crystals Studied using a Variational Method: Application to Lattices of Locally Resonant Materials, Physical Review B, Vol 67, pp 144301-1 - 144301-10 (2003)
[9]. C. Goffaux, J. S. Dehesa, P. Lambin, Comparison of the Sound Attenuation Efficiency of Locally Resonant Materials and Elastic Band-Gap Structures, Physical Review B, Vol 70, pp 184302 (2004)
[10]. C. Goffaux, J. P. Vigneron, Theoretical Study of a Tunable Phononic Band Gap System, Physical Review B, Vol 64, pp 075118-1 - 075118-5 (2001)
[11]. C. Y. Huang, J.H. Sun, T.T. Wu, A Two-Port ZnO/Silicon Lamb Wave Resonator using Phononic Crystals, Appl. Phys. Lett., Vol 97, 031913-1 - 031913-3 (2010)
[12]. D. García-Pablos, M. M. Sigalas, F. R. Montero de Espinosa, M. Torres, M. Kafesaki, N. García, Theory and Experiments on Elastic Band Gaps, Physical Review Letters, Vol 84, No 19, pp 4349-4352 (2000)
[13]. D. Yu, J. Wen, H. Zhao, Y. Liu, X. Wen, Vibration Reduction by Using the Idea of Phononic Crystals in a Pipe-Conveying Fluid, Journal of Sound and Vibration, Vol 318, pp 193–205 (2008)
[14]. F. R. Montero de Espinosa, E. Jiménez, M. Torres, Ultrasonic Band Gap in a Periodic Two-Dimensional Composite, Physical Review Letters, Vol 80, No 6, pp 1208 – 1211(1998)
[15]. F. Wu, Z. Liu,Y. Liu, Acoustic Band Gaps Created by Rotating Square rods in a Two Dimensional Lattice, Physical Review E, Vol 66, pp 046628-1 - 046628-5 (2002)
[16]. G. Wrobel, L. Wierzbicki, S. Pawlak, A Method for Ultrasonic Quality Evaluation of Glass/Polyester Composites, Archives of Materials Science and Engineering, Vol 28, No 12, pp 729 - 734(2007)
[17]. J. H. Wen, G. Wang, D. L. Yu, H. G. Zhao, Y. Z. Liu, X. S. Wen, Directional Propagation Characteristics of Flexuaral Waves in Two Dimensional Thin Plate Phononic Crystals, Chin. Phys. Lett., Vol 24, No 5, pp1305 –1308 (2007)
[18]. J. H. Wen, G. Wang, D. L. Yu, H. G. Zhao, Y. Z. Liu, X. S. Wen, Study on the Vibration Band Gap and Vibration Attenuation Property of Phononic Crystals, Sci. China Ser. E-Tech. Sci., Vol 51, No 1, pp 85 –99 (2008)
[19]. J. O. Vasseur, P.A. Deymier, B. Chenni, B. Djafari-Rouhani, L. Dobrzynski, D. Prevost, Experimental and Theoretical Evidence for the Existence of Absolute Acoustic Band

Gaps in Two-Dimensional Solid Phononic Crystals, Physical Review Letters, Vol 86, No 14, pp 3012 - 3015 (2001)
[20]. J. O. Vasseur, P. A. Deymier, A. Khelif, P.H. Lambin, B. Djafari-Rouhani, A. Akjouj, L. Dobrzynski, N. Fettouhi, J. Zemmouri, Phononic Crystal with Low Filling Fraction and Absolute Acoustic Band Gap in the Audible Frequency Range: A theoretical and Experimental study, Physical Review Letters, Vol 65, pp 056608-1 - 056608-6 (2002)
[21]. J. V. Sánchez-Pérez, D. Caballero, R. Mártinez-Sala, C. Rubio, J. Sánchez-Dehesa, F. Meseguer, Sound Attenuation by a Two-Dimensional Array of Rigid Cylinders, Physical Review Letters, Vol 80, No 24, pp 5325-5328 (1998)
[22]. J. Wang, X. Xu, X. Liu, G. Xu, A Tunable acoustic filter made by periodical structured materials, Appl. Phys. Lett., Vol 94, pp 181908 (2009)
[23]. J. W. Ju, Li-S. Weng, Y.Liu, Ultrasonic Frequency-Dependent Amplitude Attenuation Characteristics Technique for Nondestructive Evaluation of Concrete, ACI Materials Journal, pp 177 - 185(2006)
[24]. L. Svilainis, V. Puodziunas, Ultrasonic NDE System: the Hardware Concept, SSN 1392-2114 ULTRAGARSAS, Vol 29, No 1, pp 34 – 40 (1998)
[25]. L. W. Cai, J. Acoust. Soc. Am., Multiple Scattering in Single Scatterers, Vol 115, No 3, pp 986 – 995 (2004)
[26]. L. W. Cai, J. Acoust. Soc. Am., Scattering of Anti-Plane Shear Waves by Layered Circular Elastic Cylinder, Vol 115, No 2, pp 515 – 522 (2004)
[27]. L. W. Cai, Tunable Phononic Band Gap Crystal using Eccentric Multilayered Scatterers, 2004 ASME International Mechanical Engineering Congress and Explotion, Anaheim, CA, November 13-20 (2004)
[28]. L. W. Cai, Scattering by Elastic Anti-Plane Shear wave by Multilayered Eccentric Scatterer, Quarterly J. Mech. & Appl. (2005)
[29]. L. Y. Wu, L. W. Chen, R. C. C. Wang, Dispersion Characteristics of Negative Refraction Sonic Crystals, Physica B, Vol 403, pp 3599 – 3603 (2008)
[30]. K. L. Jim, C. W. Leung, S. T. Lau, S. H. Choy, H. L. W. Chan, Thermal Tuning of Phononic Band Structure in Ferroelectric Ceramic/Epoxy Phononic Crystal, Appl. Phys. Lett., Vol 94, pp193501-1 –193501-3 (2009)
[31]. M. H. Lu, L. Feng,Y.F. Chen, Phononic crystals and acoustic meta-materials, Materials Today, Vol 12, pp 34-42 (2009)
[32]. M. Torres, F. R. Montero de Espinosa, D. Garcıa-Pablos, N. Garcıa, Sonic Band Gaps in Finite Elastic Media- Surface States and Localization Phenomena in Linear and Point Defects, Physical Review Letters, Vol 82, No 15, pp 3054 – 3057(1999)
[33]. M. S. Kushwaha, P. Halevi, L. Dobrzynski, B. D. Rouhani, Acoustic Band Structure of Periodic Elastic Composites, Physical Review Letters, Vol 71, No 13, pp 2022 – 2025 (1993)
[34]. M. S. Kushwaha, P. Halevi, Band Gap Engineering in Periodic Elastic Composites, Appl. Phys. Lett., Vol 64, No 9 (1994)
[35]. M. S. Kushwaha, P. Halevi, G. Martinez, Theory of Acoustic Band Structure of Periodic Elastic Composites, Physical Review B, Vol 49, No 4, pp 2313 – 2332 (1994)
[36]. M. M. Sigalas, N. Economou, Europhys.Lett, Attenuation of Multiple-Scattered Sound, Vol 36, No 4, pp 241-246 (1996)
[37]. M. S. Kushwaha, Appl. Phys. Lett, Stop-bands for Periodic Metallic Rods: Sculptures that can Filter the Noise, Vol 70, No 24 pp 3218 - 3220 (1997)

[38]. M. Hirsekorn, P. P. Delsanto, N. K. Batra, P. Matic, Ultrasonics, Modelling and simulation of acostic wave propagation in locally resonant sonic materials, Vol 42, pp 231 - 235 (2004)
[39]. M. Ke, Z. Liu, C. Qiu, W. Wang, J. Shi, Physical Review B, Vol 72, pp 064306-1 - 064306-5 (2005)
[40]. M. Sigalas, M. S. Kushwaha, E. N. Economou, M. Kafesak, I. E. Psarobas, W. Steurer, Classical vibrational modes in phononic lattices: theory and experiment, Z. Kristallogr, Vol 220, pp 765–809 (2005)
[41]. P. H. Lambin, A. Khelif, Stopping of Acoustic Waves by Sonic Polymer-Fluid Composites, Physical Review E, Vol 63, pp 066605-1 - 066605-6 (2001)
[42]. R. M. Sala, J. Sancho, J. V. Sanchez, V. Gomez, J. Llinares, F. Meseguer, Sound Attenuation by Sculpture, Nature, Vol 378, No 16 pp 241 (1995)
[43]. R. Kazys, R. Raisuits, A. Vladisauskas, Ultragarsas, Vol 2, No. 51, pp 1392-2114 (2004).
[44]. S. C. S. Lin, B. R Tittmann, J. H. Sun, T. T. Wu, T. J. Huang, Acoustic Beam Width Compressor using Gradient-Index Phononic Crystal, J. Phys. D: Appl. Phys., Vol 42 pp 185502 (5) (2009)
[45]. S. Zhang, J. Cheng, Existence of Broad Acoustic Band Gaps in Three-Component Composite, Physical Review B, Vol 68, pp 245101-1 - 245101-6 (2003)
[46] T. Gorishnyy, M. Maldovan, C. Ullal, E. Thomas , Sound ideas, Physics World Feature: Phononic crystals, pp 2-7 (2005)
[47]. T. Gorishnyy, C. K. Ullal, M. Maldovan, G. Fytas, E. L. Thomas, Hypersonic Phononic Crystals, PRL, Vol 94, 115501-1 - 115501-4 (2005)
[48]. T. Gorishnyy, J. H. Jang, C. Y. Koh, E. L. Thomas, Direct Observation of a Hypersonic Band Gap in Two-Dimensional Single Crystalline Phononic Structures, Appl. Phys. Lett., Vol 91, pp 121915(2007)
[49]. T. Miyashita, Sonic Crystals and Sonic Wave-Guides, Meas. Sci. Techno., Vol 16, pp R47 – R63 (2005)
[50]. T. T. Wu, L. C. Wu, Z. G. Huan, Frequency Band-Gap Measurement of Two-Dimensional Air/Silicon Phononic Crystals using Layered Slanted Finger Interdigital Transducers, J. Appl. Phys., Vol 97, pp 094916-1 - 094916-7 (2005)
[51]. V. K. Kinra, N. A, Day, K. Maslov, The Transmission of a Longitudinal Wave Through a Layer of Spherical Inclusions with a Random or Periodic Arrangement, J. Mech. Phys. Solids, Vol 46, No 01, pp 153-165 (1998)
[52]. V. R. Garcia, E. F. Garcia, L. M. G. Raffi, J. V. S. Perez, Acoustic Barriers Based on Sonic Crystals, ASME, Vol 1, pp 477- 484 (2007)
[53]. W. Gang, S. L. Hui, L. Y. Zong, W. J. Hong, Accurate evealuation of lowest band gaps in ternary locally resonant phononic crystals, Chin. Phys. Soc., Vol 15, No 8, pp 2-7 (2006)
[54]. Y. Pennec, B. D. Rouhani, J. O. Vasseur, A. Khelif , P. A. Deymier, Tunable Filtering and demultiplexing in Phononic Crystals with Hollow Cylinders, Physical Review E, Vol 69, pp 046608-1 - 046608-8 (2004)
[55]. Y. Tanaka, Y. Tomoyasu, S. Tamura, Band Structure of Acoustic Waves in Phononic lattices: Two-Dimensional Composites with Large Acoustic Mismatch, PRB, Vol 62, No 11, pp 7387-7392 (2000)
[56]. Y. Y. Chen, Z. Ye, Acoustic Attenuation by Two-Dimensional Arrays of Rigid Cylinders, Physical Review Letters, Vol 87, No 18, pp 184301-1 - 184301-4 (2001)

[57]. Z. G. Huang, T. T. Wu, Analysis of Wave Propagation in Two-dimensional Phononic Crystals with Hollow Cylinders, World Academy of Science, Engineering and Technology, Vol 53, pp 279 – 283 (2009)
[58]. Z. Hou, J. Liu, W. Kuang, Y. Liu, S. Wu, Sonic Crystal with open Resonant Cavities, Physical Review E, Vol 71, No 13, pp 026608-1 - 026608-7, 2025 (2007)
[59]. Z. Liu, X. Zhang, Y. Mao, Y. Y. Zhu, Z, Yang, C. T. Chan, P. Sheng, Science, Vol 289, pp 1734 – 1736 (2000)

Appendix A - Transducer Properties

Near Field Table

Table A-1: Near field length for transducer element diameters and centre frequencies

ELEMENT DIAMETER (INCHES)	FREQUENCY (MHz)										
	0.4	0.5	1.0	1.5	2.25	3.5	5.0	10.0	15.0	20.0	25.0
.125	.027	.033	.067	.100	.150	.234	.334	.669	1.00	1.34	1.67
.250	.107	.134	.268	.401	.602	.936	1.34	2.68	4.01	5.35	6.69
.375	.241	.301	.602	.903	1.35	2.11	3.01	6.02	9.03	12.0	15.0
.500	.428	.535	1.07	1.61	2.41	3.75	5.35	10.7	16.1	21.4	26.8
.625	.669	.836	1.67	2.51	3.76	5.85	8.36	16.7	25.1	33.4	41.8
.750	.963	1.20	2.41	3.61	5.42	8.43	12.0	24.1	36.1	48.2	60.2
.875	1.31	1.64	3.28	4.92	7.37	11.5	16.4	32.8	49.2	65.6	81.9
1.000	1.71	2.14	4.28	6.42	9.63	15.0	21.4	42.8	64.2	85.6	107
1.125	2.17	2.71	5.42	8.13	12.2	19.0	27.1	54.2	81.3	108	135
1.250	2.68	3.34	6.69	10.0	15.0	23.4	33.4	66.9	100	134	167
1.375	3.24	4.05	8.09	12.1	18.2	28.3	40.5	80.9	121	162	202
1.500	3.85	4.82	9.63	14.4	21.7	33.7	48.2	96.3	144	193	240

*(N) Near Field Length (inches in water).

Beam Spread Table

Table A-2: Beam spread angles for transducers

ELEMENT DIAMETER (INCHES)	FREQUENCY (MHz)										
	0.4	0.5	1.0	1.5	2.25	3.5	5.0	10.0	15.0	20.0	25.0
.125	71.5	55.8	26.8	17.9	11.9	7.80	4.58	2.75	1.53	1.38	.92
.250	34.0	27.1	13.3	8.95	5.96	3.90	2.75	1.38	.92	.69	.46
.375	22.5	17.9	8.87	5.96	3.97	2.60	1.83	.92	.61	.46	.31
.500	16.8	13.4	6.65	4.47	2.98	1.95	1.38	.69	.46	.34	.23
.625	13.4	10.7	5.32	3.58	2.38	1.56	1.10	.55	.37	.28	.18
.750	11.2	8.95	4.43	2.98	1.99	1.30	.98	.46	.31	.23	.15
.875	9.57	7.67	3.80	2.55	1.70	1.11	.79	.39	.26	.20	.13
1.000	8.37	6.71	3.32	2.23	1.49	.97	.69	.34	.23	.17	.11
1.125	7.44	5.96	2.95	1.99	1.32	.87	.61	.31	.20	.15	.10
1.250	6.70	5.36	2.66	1.79	1.19	.78	.55	.28	.18	.14	.09
1.375	6.09	4.88	2.42	1.63	1.08	.71	.50	.25	.17	.13	.08
1.500	5.58	4.47	2.22	1.49	.99	.65	.46	.23	.15	.11	.07

* Beam Spread angle (degrees) @ -6dB point (in water).

Transducer Specification 2.25 MHz - 1

Figure A-1: Centre Frequency 2.25 MHz

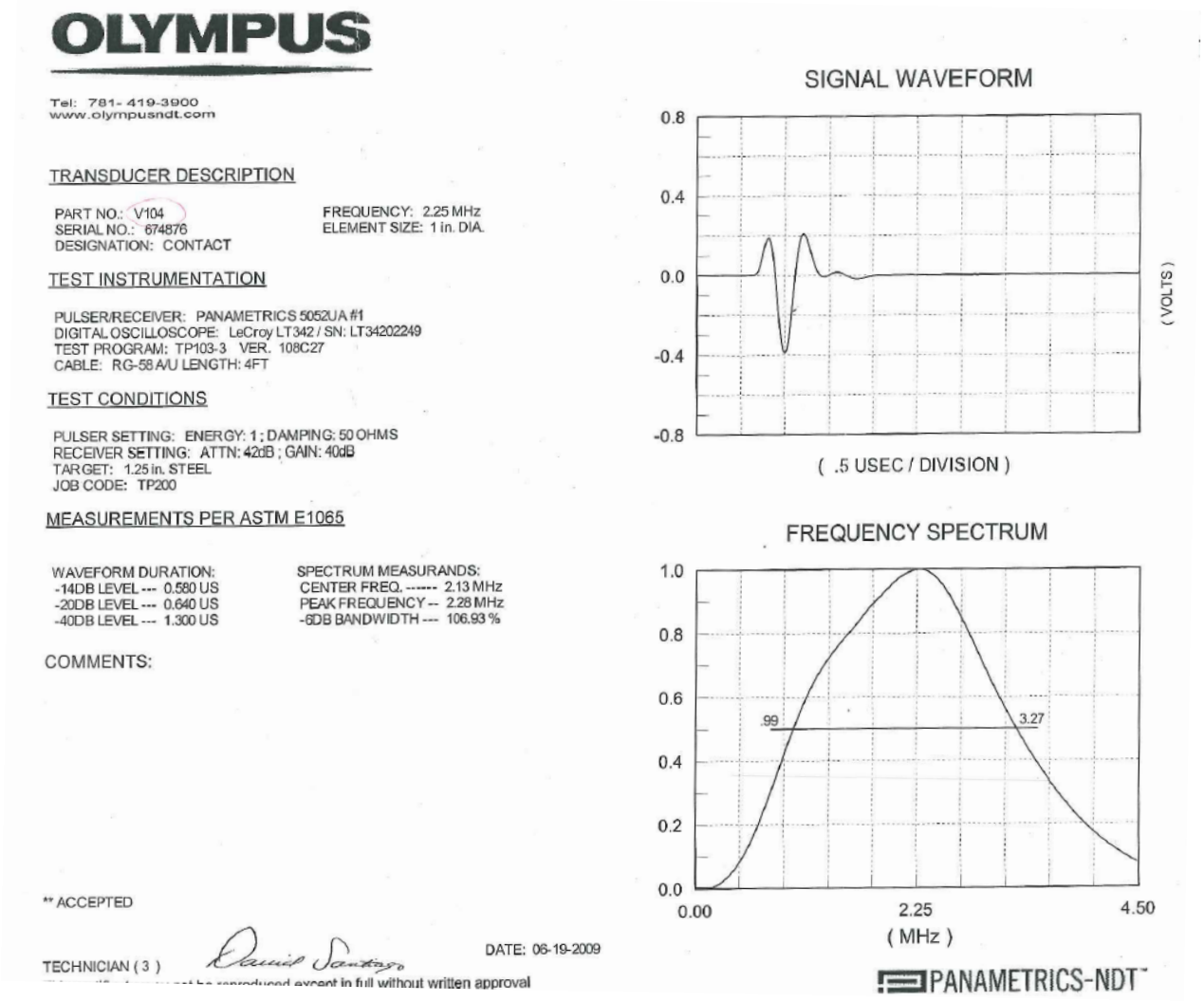

OLYMPUS

Tel: 781- 419-3900
www.olympusndt.com

TRANSDUCER DESCRIPTION

PART NO.: V104
SERIAL NO.: 674876
DESIGNATION: CONTACT

FREQUENCY: 2.25 MHz
ELEMENT SIZE: 1 in. DIA.

TEST INSTRUMENTATION

PULSER/RECEIVER: PANAMETRICS 5052UA #1
DIGITAL OSCILLOSCOPE: LeCroy LT342 / SN: LT34202249
TEST PROGRAM: TP103-3 VER. 108C27
CABLE: RG-58 A/U LENGTH: 4FT

TEST CONDITIONS

PULSER SETTING: ENERGY: 1 ; DAMPING: 50 OHMS
RECEIVER SETTING: ATTN: 42dB ; GAIN: 40dB
TARGET: 1.25 in. STEEL
JOB CODE: TP200

MEASUREMENTS PER ASTM E1065

WAVEFORM DURATION:
-14DB LEVEL --- 0.580 US
-20DB LEVEL --- 0.640 US
-40DB LEVEL --- 1.300 US

SPECTRUM MEASURANDS:
CENTER FREQ. ------ 2.13 MHz
PEAK FREQUENCY -- 2.28 MHz
-6DB BANDWIDTH --- 106.93 %

COMMENTS:

** ACCEPTED

TECHNICIAN (3) David Santiago DATE: 06-19-2009

SIGNAL WAVEFORM

0.8
0.4
0.0
-0.4
-0.8
(VOLTS)

(.5 USEC / DIVISION)

FREQUENCY SPECTRUM

1.0
0.8
0.6
0.4
0.2
0.0
.99
3.27
0.00
2.25
4.50
(MHz)

PANAMETRICS-NDT

2.25 MHz Transducer Specification - 2

Figure A-2 : Centre Frequency 2.25 MHz

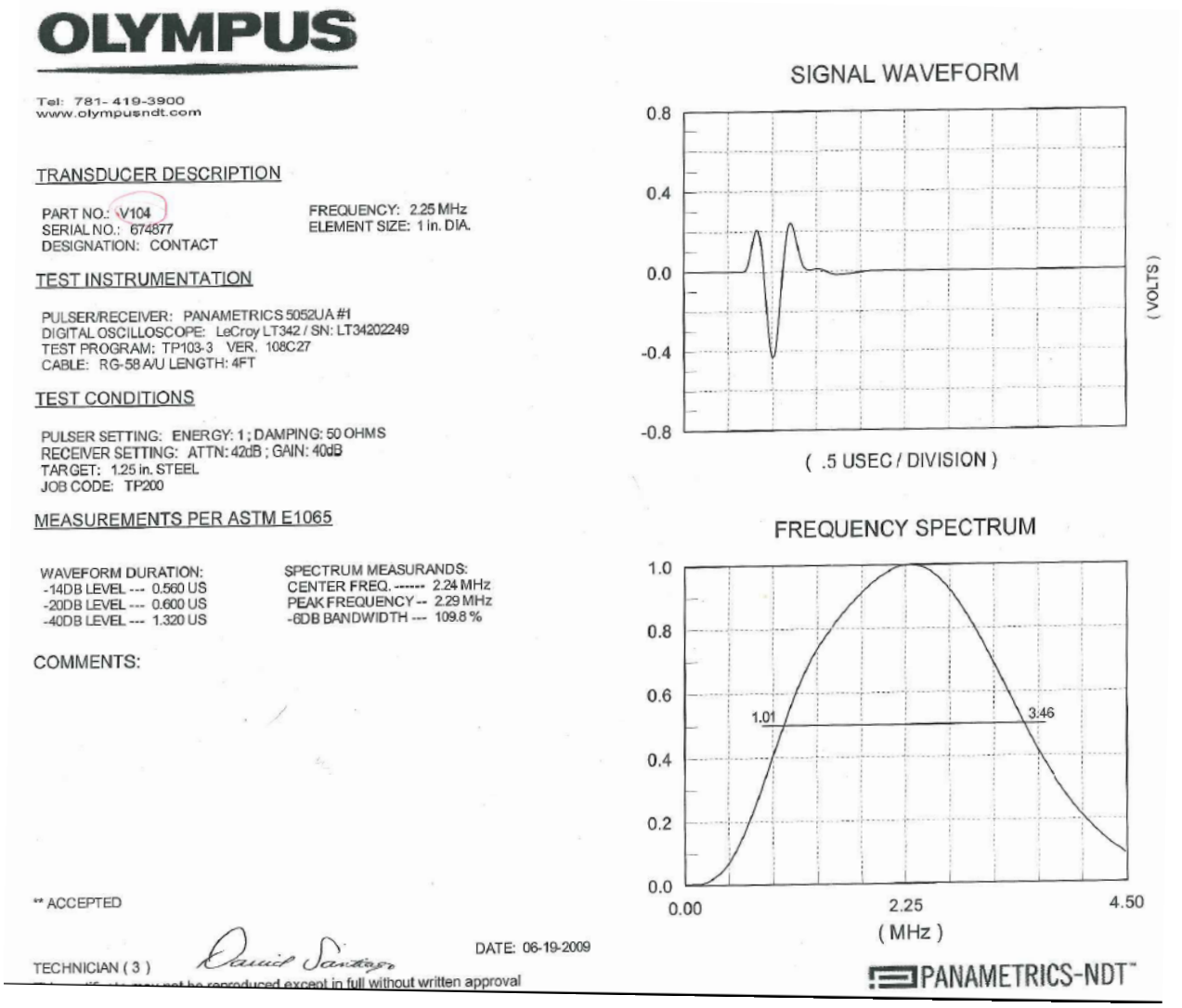

OLYMPUS

Tel: 781- 419-3900
www.olympusndt.com

TRANSDUCER DESCRIPTION

PART NO.: V104
SERIAL NO.: 674877
DESIGNATION: CONTACT

FREQUENCY: 2.25 MHz
ELEMENT SIZE: 1 in. DIA.

TEST INSTRUMENTATION

PULSER/RECEIVER: PANAMETRICS 5052UA #1
DIGITAL OSCILLOSCOPE: LeCroy LT342 / SN: LT34202249
TEST PROGRAM: TP103-3 VER. 108C27
CABLE: RG-58 A/U LENGTH: 4FT

TEST CONDITIONS

PULSER SETTING: ENERGY: 1 ; DAMPING: 50 OHMS
RECEIVER SETTING: ATTN: 42dB ; GAIN: 40dB
TARGET: 1.25 in. STEEL
JOB CODE: TP200

MEASUREMENTS PER ASTM E1065

WAVEFORM DURATION:
-14DB LEVEL --- 0.560 US
-20DB LEVEL --- 0.600 US
-40DB LEVEL --- 1.320 US

SPECTRUM MEASURANDS:
CENTER FREQ. ------ 2.24 MHz
PEAK FREQUENCY -- 2.29 MHz
-6DB BANDWIDTH --- 109.8 %

COMMENTS:

** ACCEPTED

TECHNICIAN (3) David Santiago DATE: 06-19-2009

SIGNAL WAVEFORM

0.8
0.4
0.0
-0.4
-0.8
(VOLTS)

(.5 USEC / DIVISION)

FREQUENCY SPECTRUM

1.0
0.8
0.6
0.4
0.2
0.0
1.01
3.46
0.00
2.25
4.50
(MHz)

PANAMETRICS-NDT

0.5 MHz Transducer Specification - 1

Figure A-3: Centre Frequency 0.5 MHz

OLYMPUS

Tel: 781-419-3900
www.olympusndt.com

TRANSDUCER DESCRIPTION

PART NO.: V101
SERIAL NO.: 700048
DESIGNATION: CONTACT

FREQUENCY: 0.50 MHz
ELEMENT SIZE: 1 in. DIA.

TEST INSTRUMENTATION

PULSER/RECEIVER: PANAMETRICS 5052UA #1
DIGITAL OSCILLOSCOPE: LeCroy LT342 / SN: LT34202249
TEST PROGRAM: TP103-3 VER. 109CGN
CABLE: RG-58 A/U LENGTH: 4FT

TEST CONDITIONS

PULSER SETTING: ENERGY: 4 ; DAMPING: 200 OHM
RECEIVER SETTING: ATTN: 44dB ; GAIN: 40dB
TARGET: 3.7 IN. COPPER
JOB CODE: TP200

MEASUREMENTS PER ASTM E1065

WAVEFORM DURATION:
-14DB LEVEL --- 2.080 US
-20DB LEVEL --- 2.200 US
-40DB LEVEL --- -17.080 US

SPECTRUM MEASURANDS:
CENTER FREQ. ------ 0.54 MHz
PEAK FREQUENCY -- 0.6 MHz
-6DB BANDWIDTH --- 103.55 %

COMMENTS:

** ACCEPTED

TECHNICIAN (3) David Santiago DATE: 03-17-2010

SIGNAL WAVEFORM

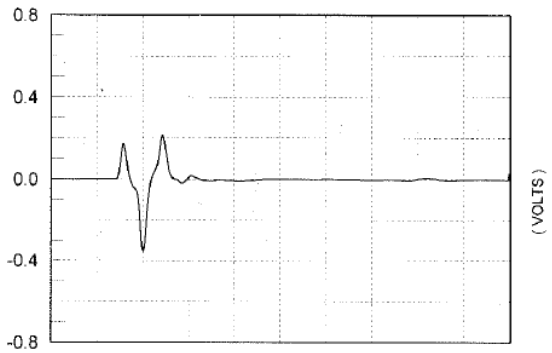

(2 USEC / DIVISION)

FREQUENCY SPECTRUM

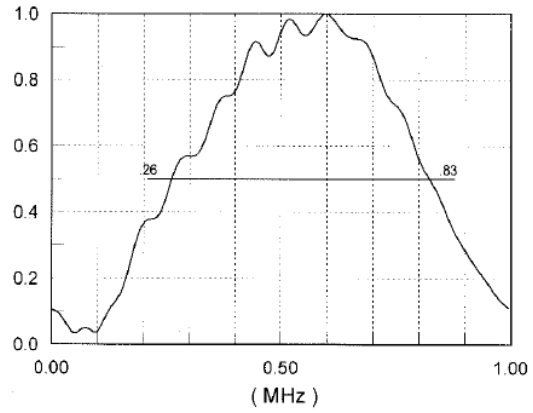

PANAMETRICS-NDT

0.5 MHz Transducer Specification - 2

Figure A-4: Centre Frequency 0.5 MHz

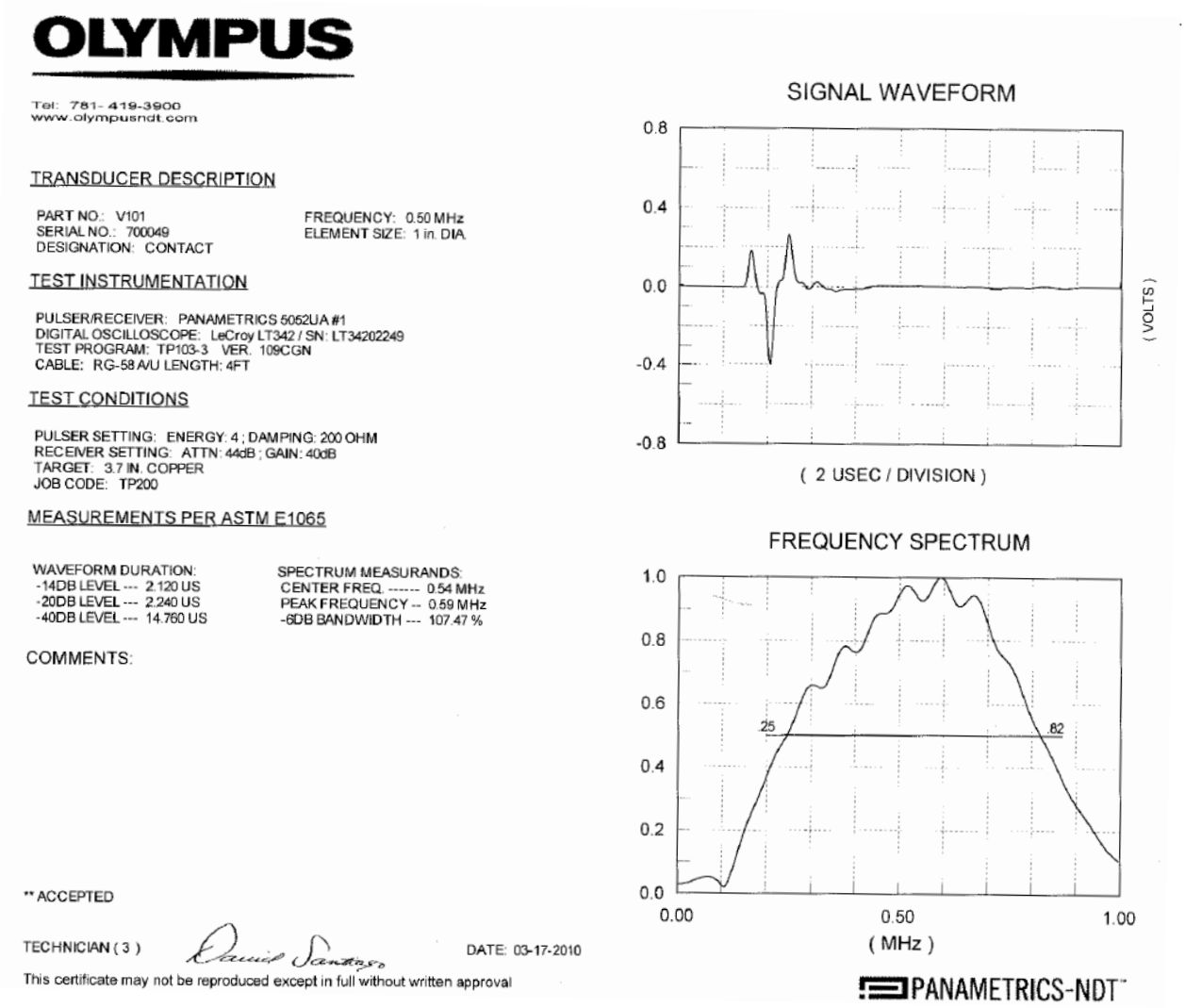

OLYMPUS

Tel: 781-419-3900
www.olympusndt.com

TRANSDUCER DESCRIPTION

PART NO.: V101
SERIAL NO.: 700049
DESIGNATION: CONTACT

FREQUENCY: 0.50 MHz
ELEMENT SIZE: 1 in. DIA.

TEST INSTRUMENTATION

PULSER/RECEIVER: PANAMETRICS 5052UA #1
DIGITAL OSCILLOSCOPE: LeCroy LT342 / SN: LT34202249
TEST PROGRAM: TP103-3 VER: 109CGN
CABLE: RG-58 A/U LENGTH: 4FT

TEST CONDITIONS

PULSER SETTING: ENERGY: 4 ; DAMPING: 200 OHM
RECEIVER SETTING: ATTN: 44dB ; GAIN: 40dB
TARGET: 3.7 IN. COPPER
JOB CODE: TP200

MEASUREMENTS PER ASTM E1065

WAVEFORM DURATION:
-14DB LEVEL --- 2.120 US
-20DB LEVEL --- 2.240 US
-40DB LEVEL --- 14.760 US

SPECTRUM MEASURANDS:
CENTER FREQ. ------ 0.54 MHz
PEAK FREQUENCY -- 0.59 MHz
-6DB BANDWIDTH --- 107.47 %

COMMENTS:

** ACCEPTED

TECHNICIAN (3)

DATE: 03-17-2010

SIGNAL WAVEFORM

0.8
0.4
0.0
-0.4
-0.8
(VOLTS)

(2 USEC / DIVISION)

FREQUENCY SPECTRUM

1.0
0.8
0.6
0.4
0.2
0.0
25
.82
0.00
0.50
1.00
(MHz)

PANAMETRICS-NDT

Appendix B - FFT Algorithm for Figures

MATLAB Main

```
fs=1000000000;
t0=xlsread('AL square all 2.5mm & angless.xls','trans','A2:A32769');
y0=xlsread('AL square all 2.5mm & angless.xls','trans','B2:B32769');
u0=xlsread('AL square all 2.5mm & angless.xls','trans','G2:G32769');
v0=xlsread('AL square all 2.5mm & angless.xls','trans','H2:H32769');
V0=fft(v0);
stem(abs(V0));
[V0,freq0] =positiveFFT(v0,fs);
plot(freq1,2*abs(aa1),'b');grid
```

Function for Taking Positive Components in the Frequency Domain

This can be done by assuming following syntax in the FFT MATLAB algorithm.

```
function [X,freq]=positiveFFT(x,Fs)
n=length(x); %get the number of points
N=2^nextpow2(n);
k=0:N-1;     %create a vector from 0 to N-1
T=N/Fs;      %get the frequency interval
freq=k/T;    %create the frequency range
X=fft(x)/N; % normalize the data
%only want the first half of the FFT, since it is redundant
cutOff = ceil(N/2);
%take only the first half of the spectrum
X = X(1:cutOff);
freq = freq(1:cutOff);
```

Function for Taking Centered both Positive and Negative Frequencies

```
function [X,freq]=centeredFFT(x,Fs)
```

```
%this is a custom function that helps in plotting the two-sided
spectrum
%x is the signal that is to be transformed
%Fs is the sampling rate
N=length(x);
%this part of the code generates that frequency axis
if mod(N,2)==0
k=-N/2:N/2-1; % N even
else
k=-(N-1)/2:(N-1)/2; % N odd
end
T=N/Fs;
freq=k/T;  %the frequency axis
%takes the fft of the signal, and adjusts the amplitude accordingly
X=fft(x)/N; % normalize the data
X=fftshift(X); %shifts the fft data so that it is centered
```

FFT Algorithm for Figure 2.10

```
f0=4;
fs=100;% sampling rate
ts = 1/Fs;
t = 0:ts:1-ts; % total time
xn = 1*sin (2*pi*f0*t);
L=length(xn)
N1=128; % no of samples taken
N2=256;% no of samples taken
N3=1024;% no of samples taken
n=0:N-1; %sample index for xn
% ts=1/fs; % sampling time interval
t1=(0:N1-1)*ts; % sampling period
t2=(0:N2-1)*ts; % sampling period
t3=(0:N3-1)*ts; % sampling period
Xk1=abs(fft(xn,N1)); % to get the frequency domain
```

```
Xk2=abs(fft(xn,N1)); % to get the frequency domain
Xk3=abs(fft(xn,N1)); % to get the frequency domain
k1=0:N1-1; % frequency index
k2=0:N2-1; % frequency index
k3=0:N3-1; % frequency index
freq1=(fs/N1)*k1; % mapping frequency range / frequency interval
freq2=(fs/N2)*k2; % mapping frequency range/ frequency interval
freq3=(fs/N3)*k3; % mapping frequency range/ frequency interval
Xk1=abs(fft(xn,N1))/L; %  FFT transformation and frequency domain
(amplitude spectrum)
Xk2=abs(fft(xn,N2))/L;  % FFT transformation and frequency domain
(amplitude spectrum)
Xk3=abs(fft(xn,N3))/L; % FFT transformation and frequency domain
(amplitude spectrum)
subplot(4,1,1) plot(fs*t,xn); hold on
xlabel('Time(Sec)'); ylabel('x(n)'); title('sampled sinusoid (x(n)');
legend('L=100,Fs=100 Sa/s');
subplot(4,1,2) plot(freq1,2*abs(Xk1)); hold on xlabel('frequency,
Hz'); ylabel('Amplitude');
title('128 FFT'); legend('N=128,k=n=0:N-1,L=100,Fs=100 Sa/s');
subplot(4,1,3) plot(freq2,2*abs(Xk2)); hold on
xlabel('frequency, Hz'); ylabel('Amplitude'); title('256 FFT');
legend('N=256,k=n=0:N-1,L=100,Fs=100 Sa/s');
subplot(4,1,4) plot(freq3,2*abs(Xk3));
xlabel('frequency, Hz');ylabel('Amplitude'); title('1024 FFT');
legend('N=1024,k=n=0:N-1,L=100,Fs=100 Sa/s'); hold off
```

FFT Algorithm for Figure 2.12

```
N1=16; % no of samples taken
N2=64;% no of samples taken
N3=512;% no of samples taken
n=0:N-1; %sample index for xn
ts=1/fs; % sampling time interval
```

```
t1=(0:N1-1)*ts; % sampling period
t2=(0:N2-1)*ts; % sampling period
t3=(0:N3-1)*ts; % sampling period
Xk1=abs(fft(v,N1)); % to get the frequency domain
Xk2=abs(fft(v,N1)); % to get the frequency domain
Xk3=abs(fft(v,N1)); % to get the frequency domain
k1=0:N1-1; % frequency index
k2=0:N2-1; % frequency index
k3=0:N3-1; % frequency index
freq1=(fs/N1)*k1; % mapping frequency range
freq2=(fs/N2)*k2; % mapping frequency range
freq3=(fs/N3)*k3; % mapping frequency range
VfreqzDomain1=abs(fft(v,N1))/L; % amplitude spectrum
VfreqzDomain2=abs(fft(v,N2))/L; % amplitude spectrum
VfreqzDomain3=abs(fft(v,N3))/L; % amplitude spectrum
subplot(4,1,1) stem(v);hold on
xlabel('Time(Sec)'); ylabel('x(n)'); title('sampled Discrte ponts
(x(n)'); legend('L=8,Fs=10Sa/s');
subplot(4,1,2) plot(freq1,abs(VfreqzDomain1)); grid; hold on
xlabel('frequency, Hz'); ylabel('Amplitude'); title('16 FFT');
legend('N=16,n=0:N-1,Fs=10Sa/s');
subplot(4,1,3) plot(freq2,abs(VfreqzDomain2));grid;hold on
xlabel('frequency, Hz');ylabel('Amplitude'); title('64 FFT');
legend('N=64,n=0:N-1,Fs=10Sa/s');
subplot(4,1,4) plot(freq3,abs(VfreqzDomain3));grid;
xlabel('frequency, Hz');ylabel('Amplitude'); title('512 FFT');
legend('N=512,n=0:N-1,Fs=10Sa/s'); hold of
```

Appendix C - Drawings for Test Specimens

Square Array Specimen

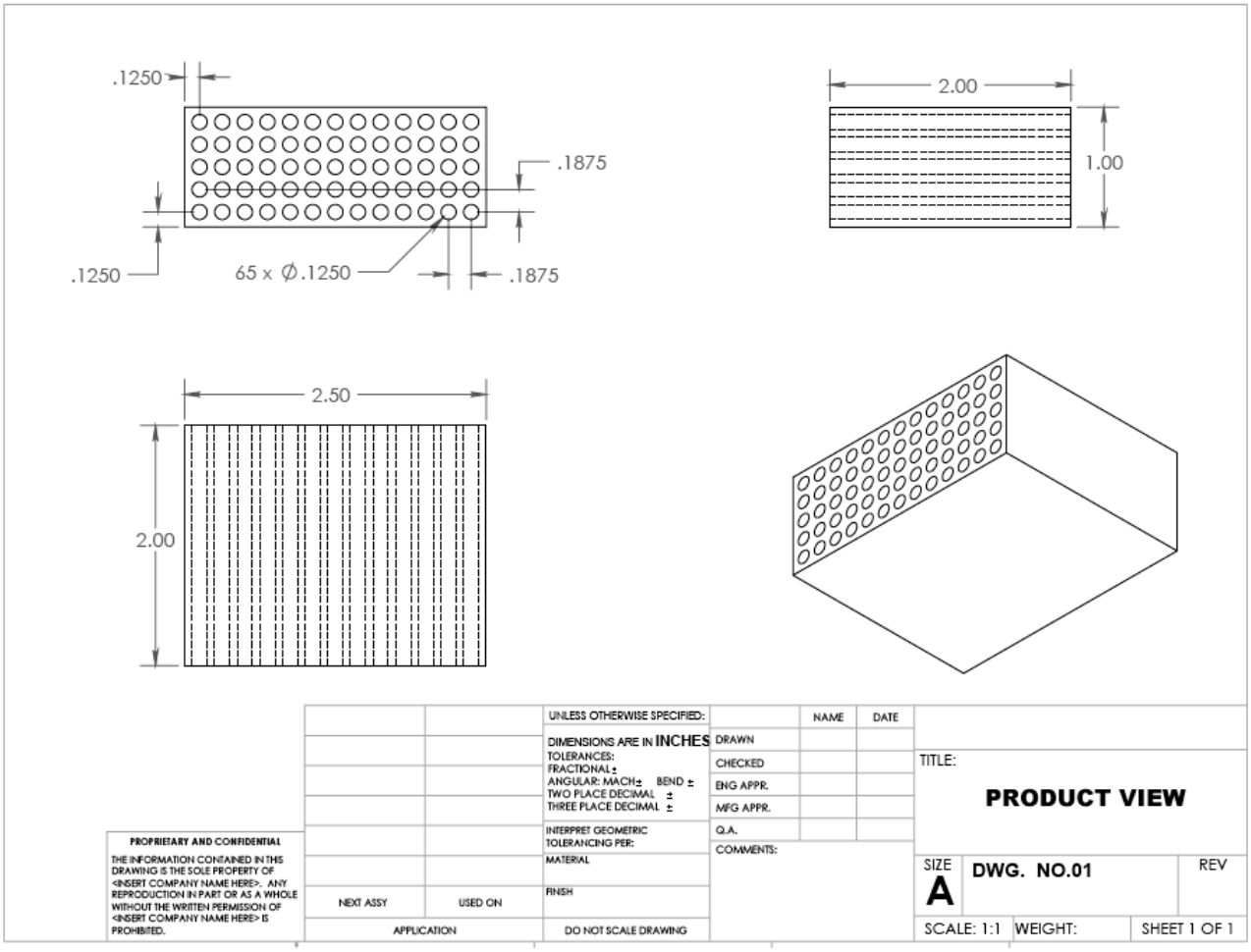

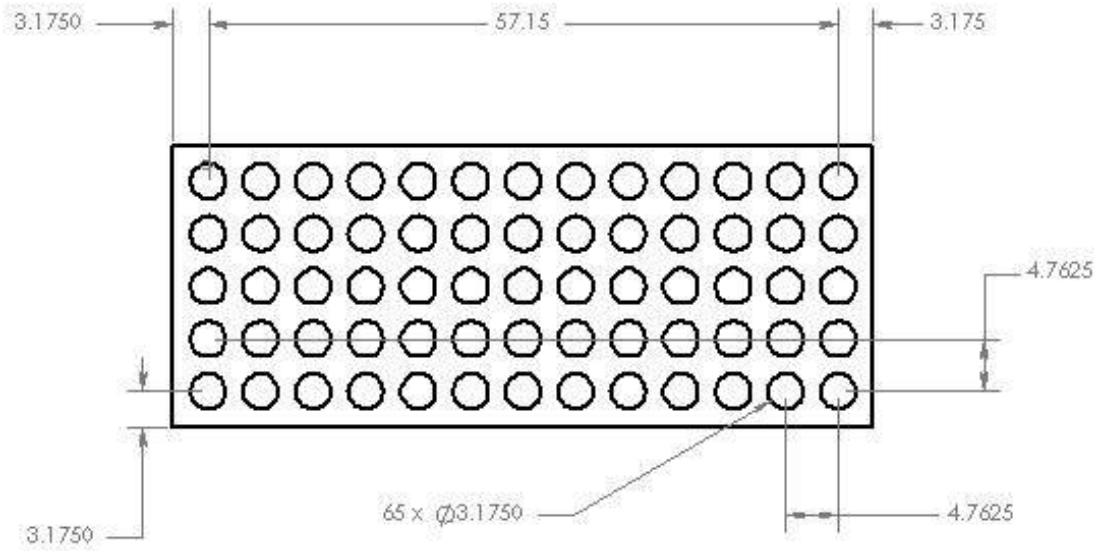

Triangular Array Specimen

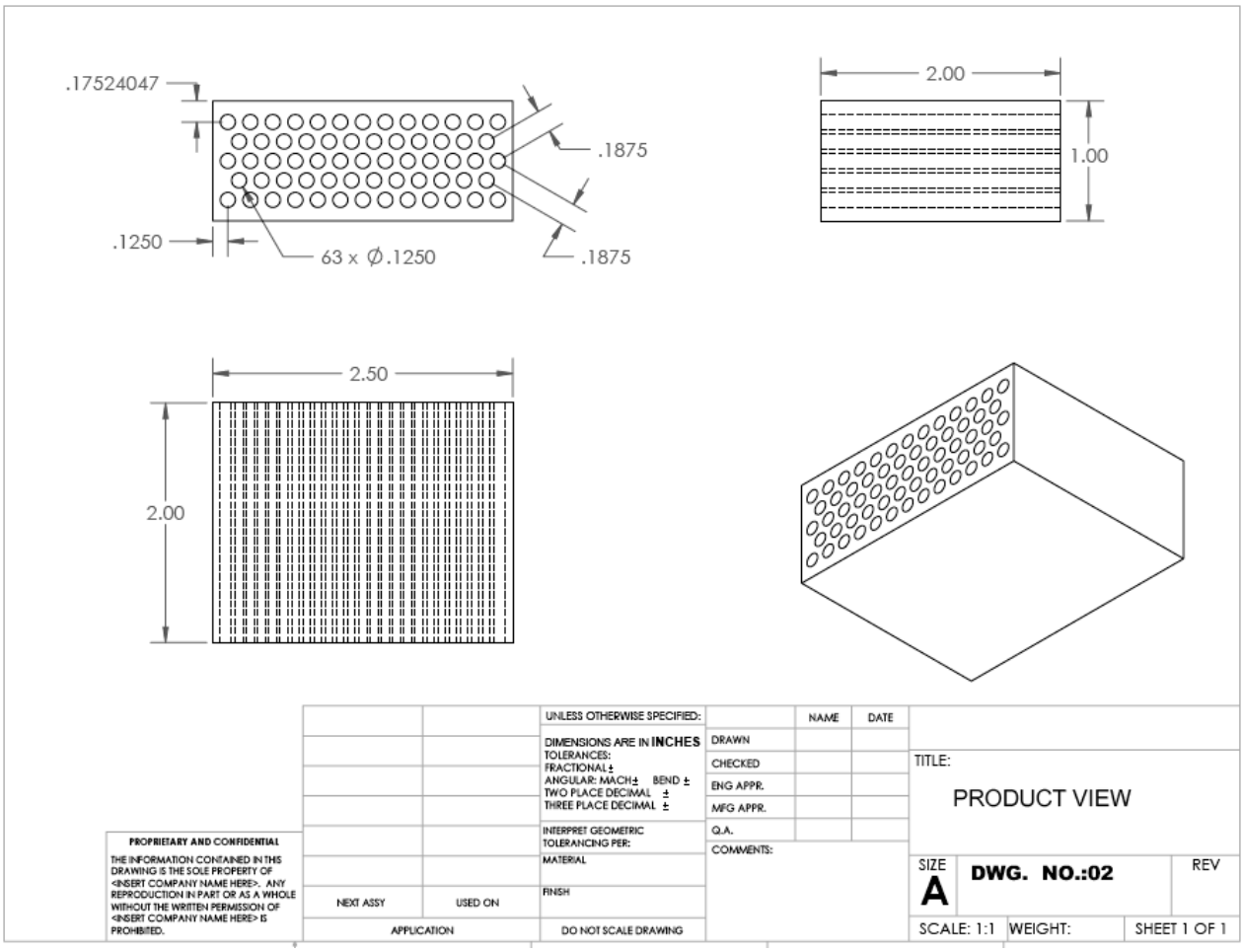

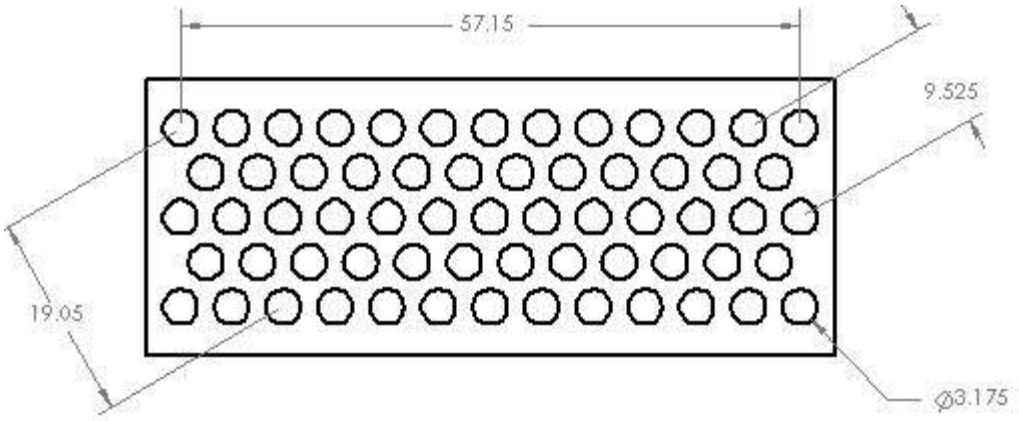

Rectangular Solid Specimen

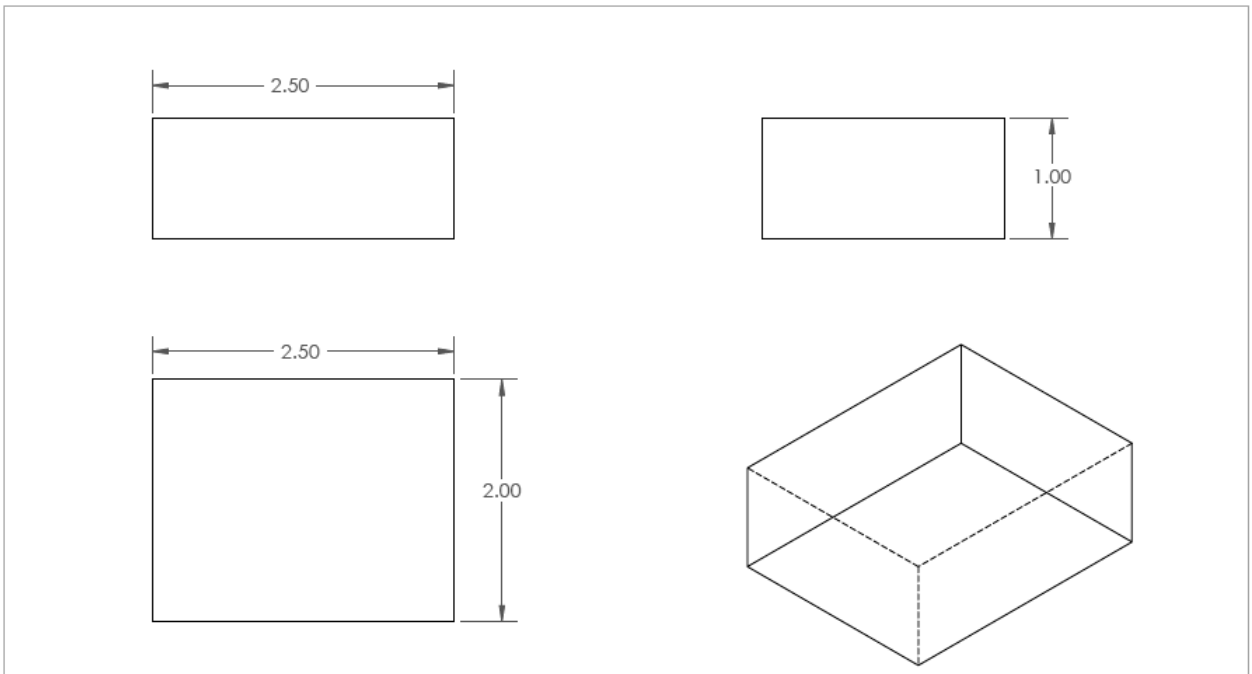

		UNLESS OTHERWISE SPECIFIED:		NAME	DATE
		DIMENSIONS ARE IN INCHES TOLERANCES: FRACTIONAL ± ANGULAR: MACH ± BEND ± TWO PLACE DECIMAL ± THREE PLACE DECIMAL ±	DRAWN		
			CHECKED		
			ENG APPR.		
			MFG APPR.		
		INTERPRET GEOMETRIC TOLERANCING PER:	Q.A.		
		MATERIAL	COMMENTS:		
NEXT ASSY	USED ON	FINISH			
APPLICATION		DO NOT SCALE DRAWING			

TITLE:

PRODUCT VIEW

SIZE	DWG. NO.:03	REV
A		
SCALE: 1:1	WEIGHT:	SHEET 1 OF 1